LIPID UTILIZATION OF *PSEUDOGYMNOASCUS DESTRUCTANS* AND ACCOMPANYING PHYSIOLOGICAL FACTORS THAT INFLUENCE WHITE-NOSE SYNDROME.

by

JOHN NEVILLE

Under the Direction of George Pierce, PhD

ABSTRACT

Pseudogymnoascus destructans is the causative agent of white-nose syndrome in bats and since its discovery in 2006 it is known to have caused the death of over 5.5 million bats in North America. As with all diseases there is a cycle that perpetuates the disease at the cost of the host's health. Currently, the majority of the research into this disease has been focused on the host organism. Therefore, in this research with the rational to further elucidate the complete disease cycle we concentrate on the pathogen with specific focus on its ability to utilize lipids found in bat wing sebum and in wing membranes as a substrate for growth and energy. *In vitro* growth experiments were conducted with the three most common fatty acids that comprise bat sebum, oleic, palmitic and stearic acid. None of the fatty acids were seen to have a significant difference in mean growth from the control group on SDA. Singularly, the control group, when growing on high nutrient content SDA media, was seen to produce an exudate. This exudate was analyzed and discovered to be fluorescent which is an important characteristic as UV trans-illumination is used as a diagnostic tool in the field. Additionally, as an accompaniment to the growth experiments bat wing explants from tri-color bats were fluorescently stained to visualize the difference in distribution of 16 and 18 carbon chain fatty acids in the wing membrane. Lastly, GC-MS analysis was conducted to determine what mVOCs are produced by *P. destructans* during growth on wing membrane tissue, during production of conidia and during production of exudate. High confidence compound identifications from the NIST spectral database were collected to create VOC profiles at these critical times in the disease cycle. Known fungal VOCs in published studies were compared to the GC-MS results to start understanding their possible function in the disease cycle and impact upon bat health. Which substrates contribute to the growth of *P. destructans* and the physiological changes that occur during growth are important to understanding the progressive impact *P. destructans* has on bat health through the course of the disease cycle.

INDEX WORDS: *P. destructans*, Lipid, Metabolism, Microscopy, White-nose syndrome, Fungus.

LIPID UTILIZATION OF *PSEUDOGYMNOASCUS DESTRUCTANS* AND ACCOMPANYING PHYSIOLOGICAL FACTORS THAT INFLUENCE WHITE-NOSE SYNDROME.

by

JOHN NEVILLE

A Dissertation Submitted in Partial Fulfillment of the Requirements for the Degree of

Doctor of Philosophy

in the College of Arts and Sciences

Georgia State University

2017

Copyright by
John Joseph Neville
2017

LIPID UTILIZATION OF *PSEUDOGYMNOASCUS DESTRUCTANS* AND ACCOMPANYING PHYSIOLOGICAL FACTORS THAT INFLUENCE WHITE-NOSE SYNDROME.

by

JOHN NEVILLE

Committee Chair: George Pierce

Committee: Sidney Crow, jr.

Robert Simmons

Eric Gilbert

Electronic Version Approved:

Office of Graduate Studies

College of Arts and Sciences

Georgia State University

December 2017

DEDICATION

I am dedicating this work to my wife, daughter, mother and father. Without their constant support I could not have achieved this work.

I am grateful to my wife for the time she has given me. She never hesitated or balked when I said I needed to stay late to do an experiment or when I would need to go in on a weekend to finish out my weeks work. When you have a young child and a pack of boisterous dogs at home giving up your time for someone else becomes an act of sainthood. Also, I am thankful for all the times she patiently listened to me talk about my work even though she is not nearly as excited about fungus as I am.

I want to thank my daughter for being a source of inspiration to me. You were always eager to see the images I took on the microscope and talk about "the tiny ugly germs." Your enthusiasm was infectious.

I want to thank my parents for their unwavering support through the years. From the times my dad drilled me on math flashcards to the completion of my dissertation you two have contributed in to my growth in more meaningful ways than I can list. Thank you.

ACKNOWLEDGEMENTS

I would like to thank my committee for their guidance.

I would like to thank Basically Bats Wildlife Conservation Society for their generous funding of my work.

I would like to thank Dr. Chris Cornelison for taking me into the Crow orphanage and his guidance, collaboration and support through my time in graduate school.

I would like to thank Dr. Kyle Gabriel for all of the fun collaborative work we did together.

I am very thankful for my friend and colleague Josh Renfroe. I couldn't have asked for a better person to share my office and ideas with.

I would like to thank Dr. Nang Thu Thu Kyaw for her assistance in completing the statistical portion of this work.

Thank you to the Trina Morris and Nikole Castleberry from the Georgia Department of Natural Resources. Without your generous help I never would have been able to get the bat samples I needed to complete this work.

Thank you to the US Forest Service for providing bat wings for portions of this research.

TABLE OF CONTENTS

ACKNOWLEDGEMENTS ..... **VI**

LIST OF TABLES ..... **X**

LIST OF FIGURES ..... **XI**

1 INTRODUCTION **1**

1.1 Purpose of the Study **1**

1.2 The genus of *Pseudogymnoascus* **3**

1.3 Proposed disease cycle of white-nose syndrome **4**

1.4 P. destructans transmission **5**

1.5 *P. destructans* infection **8**

1.6 *P. destructans* growth **11**

1.7 *P. destructans* reproduction **12**

1.8 *P. destructans* persistence on the host **13**

1.9 *P. destructans* persistence in the environment **13**

1.10 Connection between bats and lipids **14**

2 MATERIALS AND METHODS **17**

2.1 In vitro lipid growth **17**

2.2 LSCM Osbourne Cave **19**

2.3 LSCM Paulding Mine **23**

2.4 Big Brown Bat tissue **24**

2.5 GC-MS 27

3 RESULTS 29

3.1 *In vitro* growth of *P. destructans* on lipid media 29

3.1.1 Statistical analysis of growth 33

3.2 Osbourne Cave 35

3.3 Paulding Mine 41

3.4 Bat Fur 45

3.5 Big Brown Bat Tissue 50

3.6 Exudate 51

3.7 GC-MS exudate direct injection. 53

3.8 Compounds identified from SPME GC-MS analysis. 58

4 DISCUSSION 66

4.1 in vitro lipid growth experiments 66

4.2 LSCM of bat wing tissue 68

4.3 Bat fur 69

4.4 Exudate 70

4.5 GC-MS exudate 72

4.6 GC-MS SPME 73

REFERENCES 77

APPENDICES 86

Appendix A 86

Appendix A.1 SPME full compound lists. 92

LIST OF TABLES

Table 1 Confirmed WNS infected species with differential mortality..... 15

Table 2 Fatty acids used for in vitro growth experiments. 19

Table 3 Sample identification and staining scheme..... 20

Table 4 Sample identification and stains used. 23

Table 5 Table of Anova test results from SPSS..... 33

Table 6 P. destructans exudate GC-MS direct injection split runs. 53

Table 7 Classification and structure of compounds from P. destructans exudate. 54

Table 8 Acetic acid standard run. 57

Table 9 Compounds identified from SPME GC-MS analysis. 58

Table 10 Classification and structure of VOC compounds identified from SPME GC-MS. 59

LIST OF FIGURES

Figure 1 Lipase indicator media with P. destructans plug in induced R. rhodochrous anti-fungal co-culture assay. 2

Figure 2 White-nose syndrome disease cycle. 5

Figure 3 Neighbor-joining tree based on ecological and behavioral traits of bats from Europe and North America. 6

Figure 4 Mite with conidia attached. 7

Figure 5 Little Brown Bats in Salt Peter Cave KY. 8

Figure 6 Histological images of WNS infected bat tissue. 9

Figure 7 UV trans-illumination of bat wing. 10

Figure 8 Wide-field micrograph of P. destructans mycelia and conidia. 11

Figure 9 Enzyme indicator media inoculated with P. destructans. 12

Figure 10 P. destructans on Lipase enzyme indication media. 16

Figure 11 Equation for calculating mycelial area from an image. 18

Figure 12 Structure of Bodipy FL, D3821 probe. 21

Figure 13 Structure of Bodipy 500, D3823 probe. 21

Figure 14 ThermoFisher Fluorescence Spectraviewer for Bodipy 500 and DAPI stains. 22

Figure 15 ThermoFisher Fluorescence Spectraviewer for Bodipy FL and DAPI stains. 22

Figure 16 ThermoFisher Fluorescence Spectraviewer for Bodipy 500 and hoechst stains. 24

Figure 17 ThermoFisher Fluorescence Spectraviewer for Syto 9 and Propidium Iodide. 26

Figure 18 Sample of images used for radial mycelial growth. 29

Figure 19 Growth rate of P. destructans with varied quantities of D-glucose. 30

Figure 20 Mean radial growth of P. destructans on SDA. 30

Figure 21 Mean radial growth of P. destructans on oleic acid media. 31

Figure 22 Mean radial growth of P. destructans on palmitic acid media. 31

Figure 23 Mean radial growth of P. destructans on stearic acid media. 32

Figure 24 Comparison of P. destructans mean radial growth by media type. 32

Figure 25 Maximum intensity projection of Big Brown Bat wing tissue, sample 1. 35

Figure 26 Maximum intensity projection of Big Brown batwing tissue, sample 2. 36

Figure 27 Maximum intensity projection of Tri-color bat wing tissue, sample 1. 37

Figure 28 Maximum intensity projection of Tri-color bat wing tissue, sample 4. 38

Figure 29 Maximum intensity projection of Tri-color bat wing tissue, sample 5. 39

Figure 30 Maximum intensity projection of Tri-color wing tissue, sample 6. 40

Figure 31 Maximum intensity projection of Tri-color wing tissue, sample 6 from Paulding Mine. 41

Figure 32 Maximum intensity projection of Tri-color wing tissue, sample 7. 42

Figure 33 Maximum intensity projection of Tri-color wing tissue, sample 8. 43

Figure 34 Maximum intensity projection of Tri-color wing tissue, sample 9. 44

Figure 35 P. destructans isolate 71 growing on Big Brown Bat fur. 45

Figure 36 Big Brown bat fur inoculated with P. destructans isolate 71. 46

Figure 37 Big Brown Bat fur inoculated with P. destructans isolate 71. 47

Figure 38 Maximum intensity projection of Live/ dead staining of Big Brown Bat hair with P. destructans isolate 71. 48

Figure 39 Maximum intensity projection of Live/ dead staining of Big Brown Bat hair with P. destructans isolate 71. 49

Figure 40 Micrograph of Big Brown Bat wing tissue with visible P. destructans growth. 50

Figure 41 P. destructans on SDA visible spectrum image and UV excitation. 51

Figure 42 P. destructans grown on SDA under UV light source. 52

Figure 43 Exudate sample A chromatogram. 55

Figure 44 Exudate sample B chromatogram. 55

Figure 45 Exudate sample C chromatogram. 56

Figure 46 Exudate sample D chromatogram. 56

Figure 47 Acetic acid standard chromatogram. 57

Figure 48 Chromatogram for empty vial control, SPME. 62

Figure 49 Chromatogram for wing tissue control, SPME. 63

Figure 50 Chromatogram for P. destructans on Big Brown Bat wing, SPME. 63

Figure 51 Chromatogram for P. destructans producing exudate (sample B) on SDA, SPME. ... 64

Figure 52 Chromatogram for P. destructans heavy conidiation, SPME. 64

Figure 53 Section of Big Brown Bat wing with P. destructans growth used for GC-MS experiment. 65

Figure 54 Comparison of UV trans-illumination and in vitro imaging. 71

1 INTRODUCTION

1.1 Purpose of the Study

The fungal pathogen *Pseudogymnoascus destructans* is the causative agent of white-nose syndrome (WNS) in bats. WNS has been responsible for the death of over 7 million bats in the past 9 years and continues to devastate susceptible species. The disease now ranges from Canada to Georgia and has progressed westward to Washington (Batcon.org). Disease management is critical to stopping or slowing the spread of WNS and through the U.S. Fish and Wildlife service a working group has been created for this purpose (USFWS, 2016). Georgia State University's Applied and Environmental Microbiology group has implemented multiple treatments as disease management tools including the use of induced *R. rhodochrous* DAP 96253 as a contact independent anti-fungal biocontrol and the nebulizing of B-23 (Gabriel, 2017). While these methods have shown positive results in increased survivorship, all while not having a negative environmental impact, narrowly focusing on treatment and ignoring the rest of the disease cycle could hinder future work. Comprehensive and effective disease management requires developing an understanding of the full disease cycle which involves interplay between the host, the pathogen, and the environment.

Therefore, to accompany the ongoing investigation into treatment methodologies against WNS this work will focus on elucidating the portion of the disease cycle involving *P. destructans'* ability to grow on the host utilizing its lipid metabolism. As previous *in vitro* experiments at Georgia State have shown, *P. destructans* even when in a shared headspace with induced *R. rhodochrous* that is producing anti-fungal VOCs, extra-cellular lipases are still being produced and excreted. For *P. destructans* to continue the production of lipase in the presence of

anti-fungal volatiles it points to this enzymatic production as being a significant contributor to the organism's overall virulence.

Figure 1 Lipase indicator media with P. destructans plug in induced R. rhodochrous anti-fungal co-culture assay.

The above image shows a precipitate being produced on the media inoculated with a *P. destructans* plug indicating the presence and activity of a lipase enzyme. Conversely, the radial growth of *P. destructans* has been significantly inhibited. The orange organism is 5g wet weight of induced *R. rhodochrous* DAP 96253 fermentation paste.

From the strict viewpoint of enzyme production it is clear that *P. destructans* must have a negative health impact to a host organism. Correspondingly, *P. destructans* does not stand alone as a mammalian fungal skin infection. A functional comparison can be drawn between *P. destructans* and the pathogenic species in the genera of *Malassezia* and *Candida*, with the

common virulence factor that all three possess is being a lipophilic fungus that can cause significant skin infections (Park et al., 2013). All of these pathogens present with skin lesions and lead to further health complications in the host. The continued issues and history with *Malassezia* and *Candida* in the human and veterinary fields are an indicator that WNS infections are going to continue to be a serious problem and problem must be approached from multiple perspectives.

1.2 The genus of *Pseudogymnoascus*

The genus *Pseudogymnoascus* was of little significance prior to being associated with white-nose syndrome. In fact most of the information available today is only in the context of WNS. However, there are a few sources outside of this context and they illustrate the diversity and spread of this genus. A recent paper was published showing the presence of multiple species of *Pseudogymnoascus* sp. in the Antarctic, in an investigation into culturable fungi on the Fildes Peninsula (Ding et al., 2016). This research was precluded by the discovery of other *Pseudogymnoascus* sp. on the continent in 2015. The species were identified as being part of the genus due to their high percentage identity hits to *P. destructans* in the NCBI database (Santiago et al., 2015).

The organism *P. destructans*, since the attention brought to it by WNS, has been tracked across the globe. Researchers, focused on the organism as a wildlife pathogen, have positively identified *P. destructans* in France, Belgium, Netherlands, Germany, Hungary, Poland, Ukraine, Slovania, Croatia, Czech Republic, Latvia, Portugal, China and Russia (Pavlinic et al., 2015, Kuzal et al., 2016, Puechmaille et al, 2011, Wang et al., 2015, Paiva-Cardoso et al., 2014). It should be noted the study identifying *P. destructans* in China was based upon a 99% identity in

BLAST screenings and not on infected animals. During the Antarctic studies, a deviation of 1% was enough to discount the organism as being the species *P. destructans* and classify the found organisms just to the genus level in *Pseudogymnoascus*.

These instances do show the genus is much more pervasive in the world than was previously thought. Yet, *P. destructans* at this time is the only member of the genus identified in North America. For a long time, The North American continent was isolated from *P. destructans* leaving its ecology susceptible after introduction leading us to the problem we face today with high mortality events in multiple bat species.

1.3 Proposed disease cycle of white-nose syndrome

Current literature points to gaps in the state of understanding of the WNS disease cycle in all phases to the end that no one has proposed a disease cycle bringing together the entire body of work. With this in mind, the disease cycle in figure 2 is proposed and will be used to frame a context for this facet of WNS research. While this body of work will focus on the pathogen's physiology and accompanying factors that impact host health the incomplete understanding present in each portion of the disease cycle should be noted as to put the overall problem into context.

Figure 2 White-nose syndrome disease cycle.

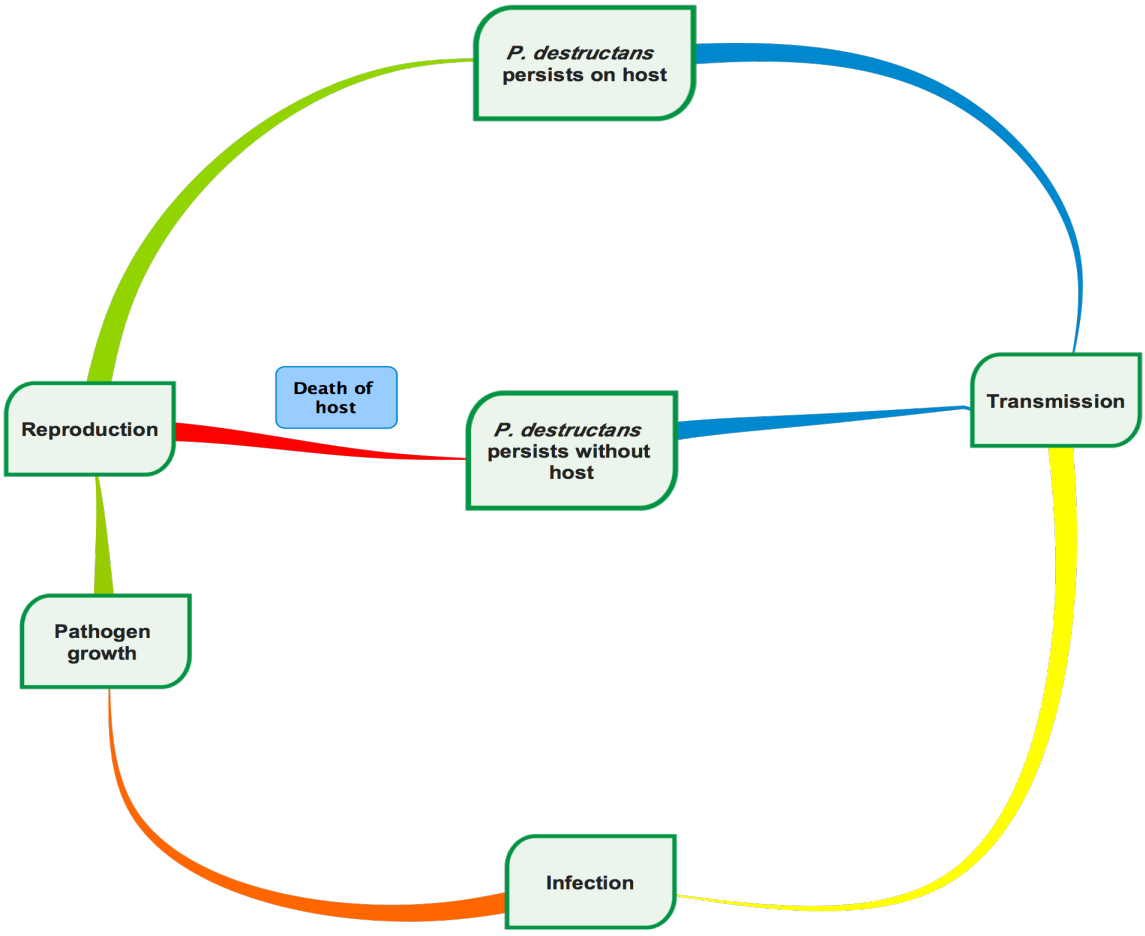

1.4 P. destructans transmission

One area of the disease cycle that is highly debated is the mode of transmission. Current hypotheses attempting to explain it include direct contact, environmental transmission, insect vectors, and behavioral traits of bats (Lucan et al., 2016, Zukal et al., 2014). The study by Zukal *et al.* approached transmission in a very different way attempting to combine phylogenetics and behavioral traits of North American and European bat species to produce a predictor of WNS infection. Initially, histopathology was used to confirm infections on sampled species.

Subsequently, a phylogenetic tree was constructed based upon 13 loci, combined with 11 behavior traits of the bat species using nearest neighbor-joining clustering in R. The data sets were combined to construct a tree to test the hypothesis of behavior being a predictor of WNS spread (Figure 3). As examination of the tree demonstrates, behavior characteristics do not show a clear correlative pattern of infection among bat species. With the final data set failing to provide a clear explanation of WNS transmission they fell back upon the blanket statement of all hibernating bats being at risk of contracting WNS. While this conclusion may at the surface appear to be an attempt to salvage an inconclusive study it brings forward how complex the transmission of WNS actually is.

Figure 3 Neighbor-joining tree based on ecological and behavioral traits of bats from Europe and North America.

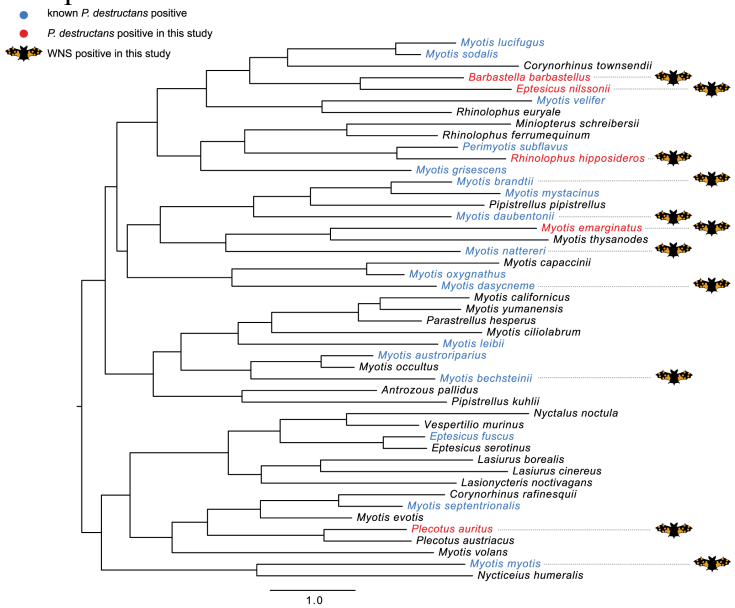

Wing mites, *Spinturnix myoti*, that are common on bats (genus *Myotis*) were determined by qPCR to harbor *P. destructans (*most likely as conidia). The study by Lucan et al. put forth the idea that mites are a vector for the spread of *P. destructans*. As Figure 4 shows, conidia can

and do easily adhere to mites. However, common sense should dictate that this is not the primary vector for transmission among infected bats.

Figure 4 Mite with conidia attached.

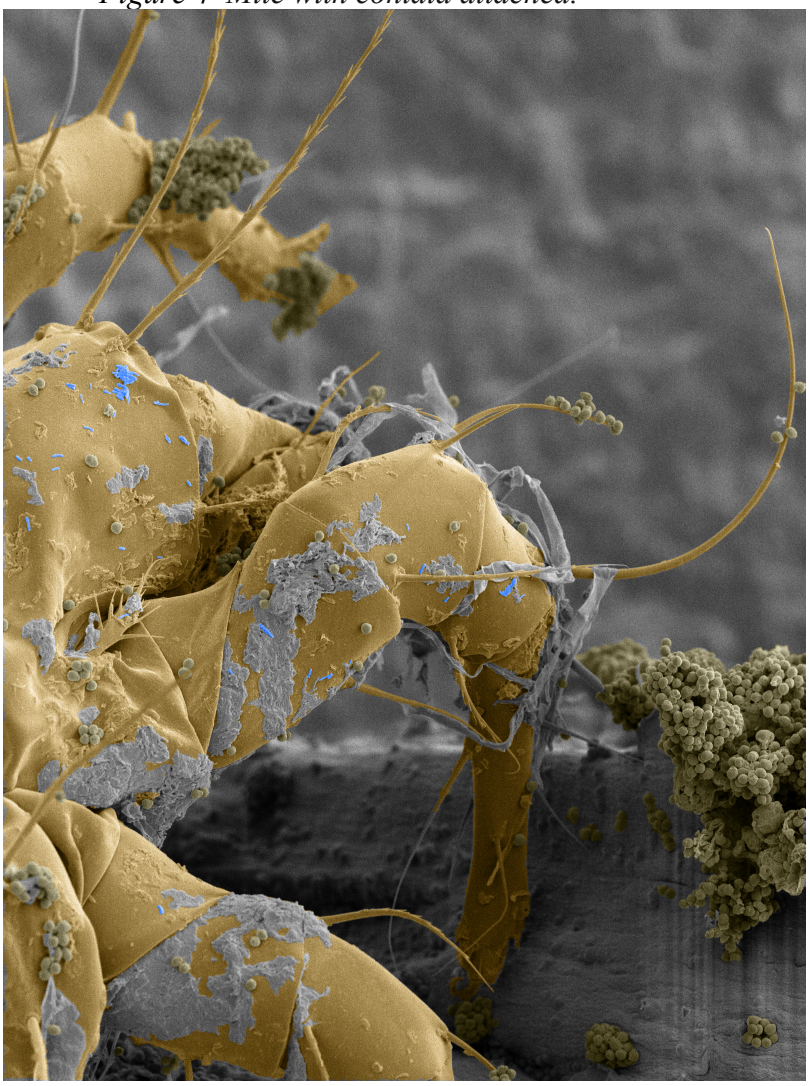

Transmission from host to host contact is the most likely scenario in which WNS is spread. Clustering species of bats have been shown to have high mortality rates. As Figure 5 shows, bats when clustered during torpor provide an almost confluent substrate to *P. destructans* to spread across.

Figure 5 Little Brown Bats in Salt Peter Cave KY.

1.5 *P. destructans* infection

In addition to transmission, physiological attributes of the host are obviously a strong variable in disease progression. The ability of the bat to heal from an infection is a major predictor of mortality. WNS has been shown to cause significant damage to wing membranes in addition to the muzzle (Voigt, 2013). Furthermore, studies with big brown bats (*Eptesicus fuscus)* have shown that wing membranes heal more slowly than tail membranes (Pollock et al., 2016). In parallel, the example of the fungal disease Chytridiomycosis in amphibians the presence of anti-fungal peptides secreted by the host, as well as a symbiosis with antagonistic bacteria, were identified on less-susceptible species and are being utilized to convey that protection to the most susceptible species (Rollins-Smith et al., 2005). Epidemiological studies

have shown a marked number of similarities between Chytridiomycosis and WNS disease progression furthering the idea that host factors in bats may drive decreased mortality in some species (Eskew et al., 2013). By understanding the host factors influencing differential susceptibility of bats to WNS, similar tools and approaches to control this devastating epidemic may emerge.

In the portion of the disease cycle focused on infection timely and accurate diagnosis is one of the main areas that currently has problems that impact the overall efforts in stopping WNS. Histology is a mainstay in the diagnosis of WNS infections allowing researchers to identify intercellular structures in the bat tissue that correspond to an infection and its severity.

Figure 6 Histological images of WNS infected bat tissue.

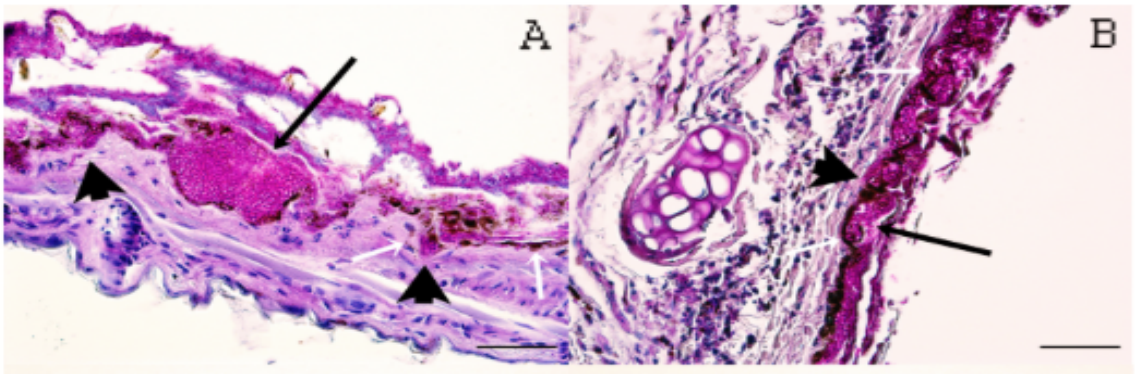

The above figure was adapted from Zukal et al. The black arrows indicate *P. destructans* mycelial invasion. White arrows are the dermis and epidermis interface.

However, identification through histology is highly invasive and requires biopsies or recovery of a body from a mortality event. Coupled with the length of time it takes for preparation and examination histology is a slow diagnostic method. Most determinations of infection are now done using qPCR (Muller et al., 2013). Swabbing of bat wings and muzzle are

enough to determine the presence of *P. destructans*. This method has a common downside with histology and that is the need for highly trained personnel and laboratory facilities. Moreover, the ease of field sampling followed by the lack facilities that can perform PCR has led to a backlog of identifications of infected individuals (personnel conversations).

The third most common method of identifying WNS infections is the use of UV trans-illumination on bat wings (Turner et al., 2014). This is a field expedient method used by field biologists and ecologists attempting to obtain a rapid diagnosis of infection. Figure 7 is an example of this method used on a bat during treatment field trials at Salt Peter Cave in Kentucky. There is a clear tear in the center of this animal's wing membrane but no discernable infection of WNS.

Figure 7 UV trans-illumination of bat wing.

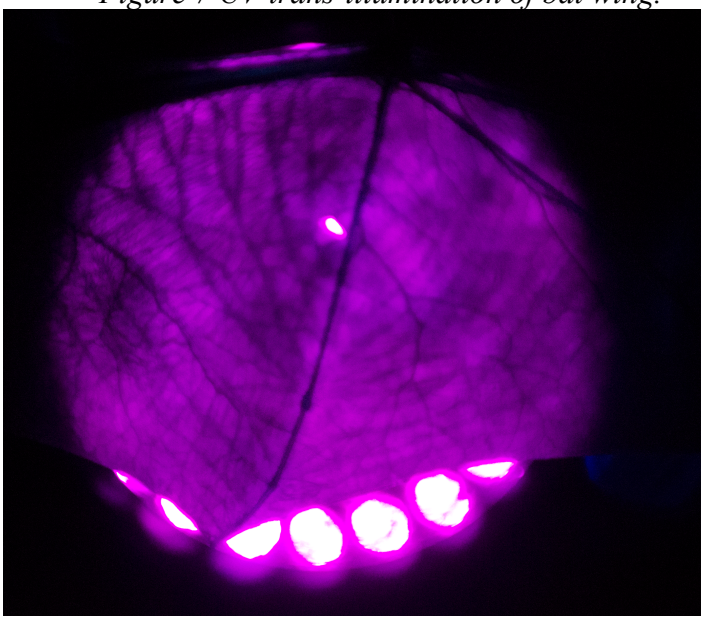

A lack of timely diagnosis of infection has hindered the progress of researchers studying WNS and wildlife biologists attempting to stop the spread of the disease.

1.6 *P. destructans* growth

P. destructans has a broad suite of enzymes it can produce enabling it to grow on a variety of substrates. These enzymes include acid phosphatase, alkaline phosphatase, N-acetyl-β-glucosaminidase, β- glucosidase, esterase, esterase lipase, lipase, leucine arylamidase, naphthol-AS-B1-phophohydrolase, and valine arylamidase, urease, and proteinases (Chaturvedi et al., 2010). There have been inconclusive reports of it also being able to produce a weak keratinase (Raudabaugh and Miller, 2013). Being a psychrophilic organism, *P. destructans* exhibits its best growth at 14^0C with moderate humidity. Growth of the organism is visualized as the lengthening and branching of white mycelia and frequently the production of curved condia.

Figure 8 Wide-field micrograph of P. destructans mycelia and conidia.

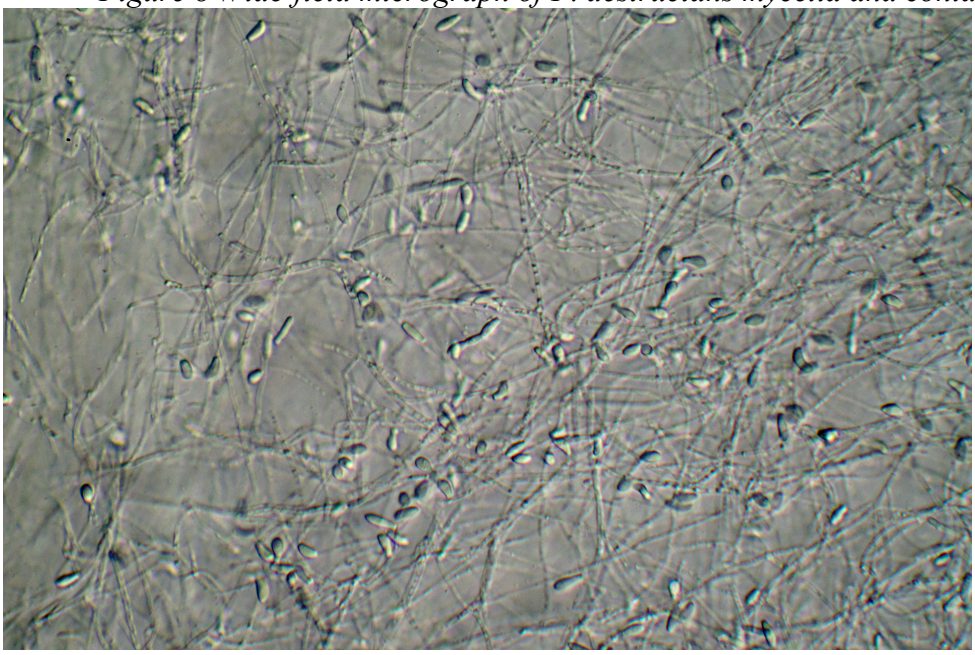

The above image was taken using a DIC-equipped microscope. The image is at 200x magnification.

Figure 9 Enzyme indicator media inoculated with P. destructans.

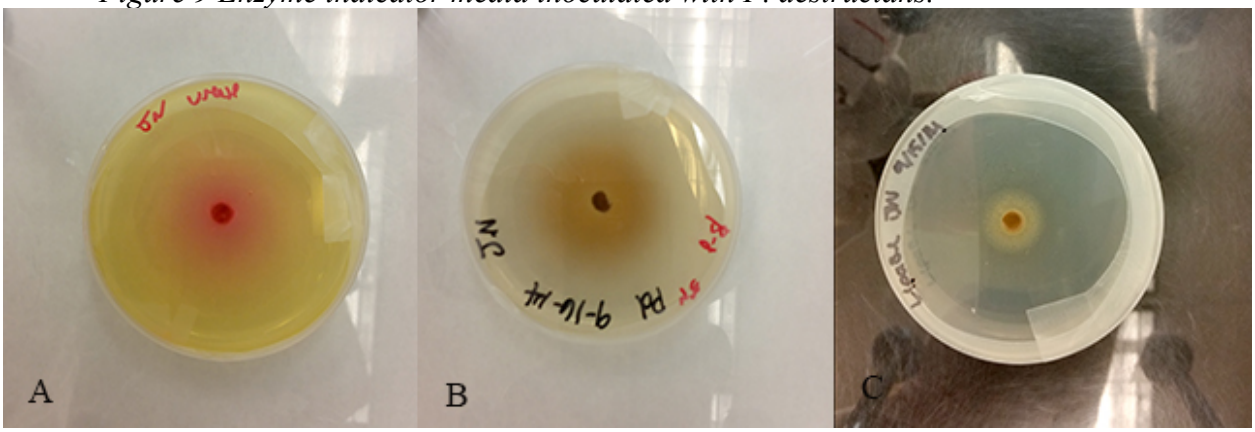

The above image is of enzyme indicator media used at Georgia State University in previous work in characterizing enzyme production during anti-fungal experiments. A) pink color change indicates urease production B) Brown color change indicates β- glucosidase production C) white precipitate indicates lipase production.

1.7 *P. destructans* reproduction

The isolates of *P. destructans* found in North America have been determined to be mono-clonal based upon whole genome sequencing of a multitude of isolates from North America (Rajkumar et al., 2011). The paper by Palmer et al. located the mating-type locus (MAT) in *P. destructans* and made the determination, using European isolates, that *P. destructans* is a heterothallic mating type. North American isolates in the wild and in vitro have only exhibited asexual reproduction.

The MAT in *P. destructans* are transcriptional regulators with the MAT1-1 being the precursor to the α-pheramone (ppg1) pathway. The MAT1-2 is hypothesized to regulate the G-coupled protein receptors that recongnize α-pheramone. While sexual reproduction has not been induced *in vitro* using the two mating types these are well characterized systems that are present

in model species (Bolker and Kahmann, 1993). Presumably, as with many microorganisms the ideal culture conditions have yet to be met. With thorough molecular based research being conducted on *P. destructans* analysis of mVOCs being produced under various conditions could yield pertinent information.

1.8 *P. destructans* persistence on the host

A discussion of *P. destructans* persisting on the host leads back to transmission. There are no studies to date of whether mycelia remains viable on the host through the summer when the animals are active and non-immunosuppressed. However, this is not necessary for persistence. A dormant but viable propagule is all that is necessary for the organism to persist and begin to grow and reproduce again once the bat goes back into torpor. Alternatively, a viable conidium could be passed onto a new host and propagated on it or introduced into a new hibernacula.

While it is conjecture, this line of reasoning is supported by studies that have shown bats that use above ground hibernation sites are not as susceptible to WNS while disease progression data shows WNS has progressed throughout species that do hibernate in caves and mines (Fenton, 2012). *P. destructans*, being a psychrophilic organism, having conidia reintroduced to a cool humid environment would once again begin to germinate and grow.

1.9 *P. destructans* persistence in the environment

After the death of the host bat *P. destructans,* unlike many pathogens, easily persists in the environment. In fact, a dead host becomes a high nutrient substrate for growth and

reproduction. An infection that causes death, followed by utilization of the dead host for energetic requirements solidly puts *P. destructans* into classification as a necrotroph.

The enzyme production of *P. destructans* imparts its ability to persist in the environment independently. It is known to produce acid phosphatase, alkaline phosphatase, N-acetyl- β-glucosaminidase, β- glucosidase, esterase, esterase lipase, lipase, leucine arylamidase, naphthol-AS-B1-phophohydrolase, and vailine arylamidase, urease, and proteinases (Chaturvedi et al., 2010).

1.10 Connection between bats and lipids

While there clearly are gaps in many areas of the disease cycle, this work focuses on what may be the least understood part of the disease cycle. Therefore, this research aims to expand our knowledge of growth while focusing on *P. destructans* lipid metabolism and the relationship it has to the heterogeneous lipid content of bat wing membranes. Since 2007 WNS has been positively identified on 12 species of hibernating bat, although the development of WNS and significant mortality has only been observed in 7 of these species as shown in Table 1 (Batcon.org). Currently the reason for this differential susceptibility is unknown, although examples from other invasive fungal infections would indicate that host factors and the pathogens response to them are the predominant influence on susceptibility (Mendes-Giannini et al., 2000). Consequently, field biologists working with WNS infected bats have noted, bat species that secrete larger amounts of sebum appear to be less susceptible to WNS (personal conversations).

Table 1 Confirmed WNS infected species with differential mortality.

Infected with high	**Infected with low**
Eptesicus fuscus	*Myotis austroriparius*
Myotisyotis leibii	*Lasionycteris noctivagans*
Myotis grisescens	*Corynorhinus townsendii virginianus*
Myotis lucifugus	*Lasiurus borealis*
Myotis sodalis	*Corynorhinus rafinesquii*
Myotis septentrionalis	
Perimyotis subflaus	

With respect to the pathogen, previous studies have enumerated a variety of exo-enzymes produced by *P.destructans* with the implication that they may have an impact on disease progression (Chaturvedi et al., 2010, Reynolds and Barton, 2014). Of particular interest to researchers are proteases and lipases that would be key in degrading bat wing tissues, and initiating the deep tissue invasion characteristic of WNS (Pannkuk et al., 2015). As with other fungal pathogens, understanding a virulence factor and any host factors that combat them are of paramount importance. Previous work at Georgia State University has focused on confirming the production of specific exo-enzymes and their activity when exposed to anti-microbial compounds (Unpublished data). Figure 4 is taken from that study confirming the production of lipase by *P. destructans* using a lipase differential media. Consequently, with lipase production being a known virulence factor it is hypothesized that this putative virulence factor is the primary reason *P. destructans* exhibits rapid growth and persistence in instances of fatal and non-fatal infections.

Figure 10 P. destructans on Lipase enzyme indication media.

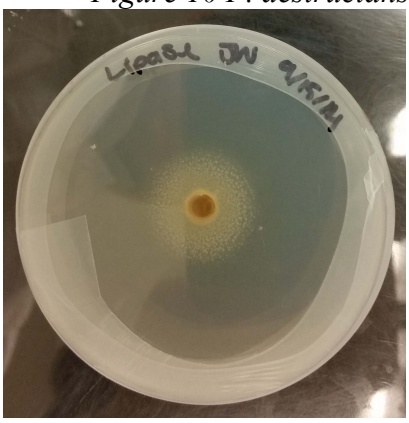

The above figure shows *P. destructans* plug inserted into media that forms a precipitate when active lipase enzymes are present. The photo was taken 7 days post-inoculation.

Furthermore, research into bat sebum has provided a lipid profile that is species specific highlighting the variable composition from one species to another. The work by Pannkuk et al. investigated the composition of wing sebum across bat species. Their work showed 16:0, 18:0 and 18:1 carbon chain fatty acids are the most prevalent across the 13 species sampled. The quantities of each type of fatty acid varied from species to species. This factor of variable lipid composition across species brings forth the idea that bat wing sebum and tissue when viewed as a nutrient substrate can possible influence the growth rate of *P. destructans*.

Therefore, it is hypothesized, based upon the known enzymatic capabilities of *P. destructans* and the continued propagation of WNS in bats, that the lipid content of sebum and wing tissue can act as a suitable growth substrate. Furthermore, the high number of mortality events has shown an infection of WNS in bats is predominantly fatal. Consequently, the ability of *P. destructans* to sustain a high growth rate and undergo reproduction by solely utilizing lipids will indicated lipid utilization is a virulence factor of *P. destructans* with serious impact upon the disease cycle.

2 MATERIALS AND METHODS

2.1 In vitro lipid growth

A defined media originally formulated for *Aspergillus nidulans* growth studies was chosen for its performance in supporting mycological growth and the ease of substituting carbon sources (Kafer, 1977). The media was comprised of 50 ml of a 20x sodium salts solution (10.4g KCl, 10.4g $MgSO_4$•&H_2O, 30.4g KH_2PO_4, 74.5g NH_4Cl, 1 L DI H_2O), 1 mL of trace elements (2.2g $ZnSO_4$•$7H_2O$, 1.1g H_3BO_3, 0.5g $MnCl_2$•$4H_2O$, 0.5g $FeSO_4$•$7H_2O$, 0.16g $CoCl_2$•$6H_2O$, 0.16g $CuSO_4$•$5H_2O$, 0.11g $(NH_4)_6Mo_7O_{24}$•$4H_2O$,5.0g Na_4EDTA per 100 ml pH to 6.5 using KOH), 10g D-glucose, 15g Agar, volume adjusted to 1 L using DI H_2O. The pH was adjusted to ~6.5 and autoclaved for 20 minutes. All 100mm x 15mm petri plates (Fisherbrand) were poured at a 25 ml volume.

The first set of media made followed the above protocol except varied quantities of D-glucose were used at 5g, 10g, or 15g. *P. destructans* cultures from glycerol stocks were grown on Sabouraud Dextrose Agar (Difco) plates at 14^0C until confluent lawns were present. 6 mm diameter transfer tubes (Spectrum Labs) were used to cut plugs from the *P. destructans* lawns. The plugs were placed in equal sized holes in the center of the Aspergillus media and incubated at 14^0C for 30 days. Cultures of each variant were grown in triplicate. The growth rate of *P. destructans* on each plate was calculated and averaged for each glucose concentration variant.

The growth rate was determined by taking images throughout the duration of the experiment by placing the petri plate in a stand that held a cell phone approximately 19 cm above. The first image taken during each series was of a ruler placed at the same height as the surface of the agar in the petri plate. This image was used as calibration by allowing the pixel-

to-meter ratio to be determined. This accounted for any variations in height and camera phone used from one series of images to the next (Gabriel, 2017).

The measurement of the area of mycelial growth was done in Adobe Photoshop CS6. The magnetic lasso tool was used to highlight the perimeter of mycelial growth and select the area inside. An area measurement was then given in number of pixels. This measurement was converted into cm^2 using the equation in Figure 10.

Figure 11 Equation for calculating mycelial area from an image.

$$\left(\frac{Number\ of\ pixels\ in\ area}{Number\ of\ pixels\ per\ cm}\right)^2 = Area\ of\ mycelium\ in\ cm^2$$

The area of mycelial growth in cm^2 was entered in Microsoft excel and used to plot the growth rate over time. The determination of growth rate was determined the same way for all variations of the Aspergillus media.

A media series was formulated based on the three fatty acids that have been shown to be the most prevalent in bat wing tissue and sebum were substituted for the D- glucose in the Aspergillus media. The quantities used were at an equal amount of carbon to that contained in 5g of D-glucose, which was determined to be the optimum concentration for *P. destructans in vitro* growth. The sodium salts versions of the fatty acids were used due to a higher flash point, enabling autoclaving, and better solubility.

Table 2 Fatty acids used for in vitro growth experiments.

Fatty acid and carbon chain length.	Palmitic acid sodium salt (Acros Organics), 16:0	Sodium stearate (TCI), 18:0	Sodium oleate (Stream Chemicals), 18:1
Mass with equal carbon content to 5g of D-glucose.	2.89g	2.81g	2.81g

After autoclaving the media was placed on a stirring hot plate and the temperature of the media was kept above the melting point of the fatty acid it contained with constant stirring thereby allowing an equal distribution of the fatty acid in each petri plate.

P. destructans was also grown on SDA and the aspergillus media without a carbon source as positive and negative controls. The growth rates were determined and plotted using the same methodology as the fatty acid growth series.

2.2 LSCM Osbourne Cave

Wing biopsies were taken from six tri-color bats (*Perimyotis subflavus)* located in Osbourne Cave at Blacks Bluff Preserve in Floyd County, Georgia. The biopsies were taken using a 4 mm^2 circular core sampling tool (Electron Microscopy Sciences) on an area of the wing within 5 cm of the body and between visible veins. The outstretched wing was held against a cutting mat while the core sampling tool was being used. The mat and core sampling tool were cleaned with 70% ethanol between samples. Three males and three females were sampled.

The samples were immediately placed in a 2.5% glutaraldehyde .1 M sodium cacodylate solution. The samples were kept on ice overnight. The samples were then rinsed with a 1% glycine sodium cacodylate solution 3 times spanning 24 hours and with agitation at 150 rpm. Samples were broken separated into two groups for staining with either Bodipy 500 or Bodipy FL and DAPI (table X). Samples 2 and 3 were frozen for future use.

Table 3 Sample identification and staining scheme.

Sample ID #	**Wing**	**Sex**	**Visible WNS infection**	**Stain**
1	Left	F	No	Bodipy 500
2	Left	F	Yes	N/A
3	Left	M	No	N/A
4	Left	F	No	Bodipy FL
5	Left	M	No	Bodipy 500
6	Right	M	No	Bodipy FL
1 BB	Left	unknown	No	Bodipy 500
2 BB	Left	unknown	No	Bodipy FL

Fluorescent stains specific to membrane lipids were used to label the cells of the wing explants, providing visualization of lipid quantity and regional localization. Bodipy is a fatty acid analog that can localize in the membrane due to the lack of an ionic charge. The Bodipy D3821 structure makes it equivalent to a C-16 fatty acid and the structure of D3823 makes it equivalent to a C-18 fatty acid (Thermofisher, 2017, Johnson, 1991).

Figure 12 Structure of Bodipy FL, D3821 probe.

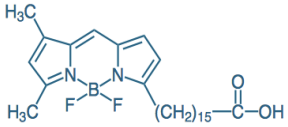

BODIPY® FL C_{16} D3821 (4,4-Difluoro-5,7-Dimethyl-4-Bora-3a,4a-Diaza-*s*-Indacene-3-Hexadecanoic Acid).

Figure 13 Structure of Bodipy 500, D3823 probe.

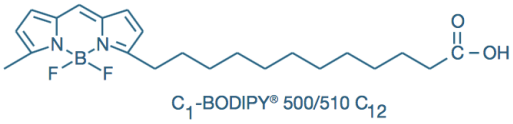

Two 6 mm^2 circular samples were taken from a big brown bat (*Eptesicus fuscus)* wing that was frozen and was being stored at -80^{0}C. Samples were fixed in a 2.5% glutaraldehyde .1 M sodium cacodylate solution and then rinsed with a 1% glycine .1 M sodium cacodylate solution 3 times spanning 24 hours and with agitation at 150 rpm. One sample was stained with Bodipy 500 and one with Bodipy FL. Both samples were stained with DAPI.

Images were taken using a Carl Zeiss LSM 780 laser scanning confocal microscope. The laser and PMT settings were initially determined using the ThermoFisher Fluorescence Spectraviewer online tool (ThermoFisher.com). Figures 13 and 14 show the excitation and emission profiles for the fluorescent stains used. Based upon the profiles for the stains used the

405 and 488 lasers were selected. Two tracks were used for the ease of separating data gained from the separate fluorophores. Laser and PMT power were adjusted independently from one image to another based upon visual optimization and were not standardized for quantification.

Figure 14 ThermoFisher Fluorescence Spectraviewer for Bodipy 500 and DAPI stains.

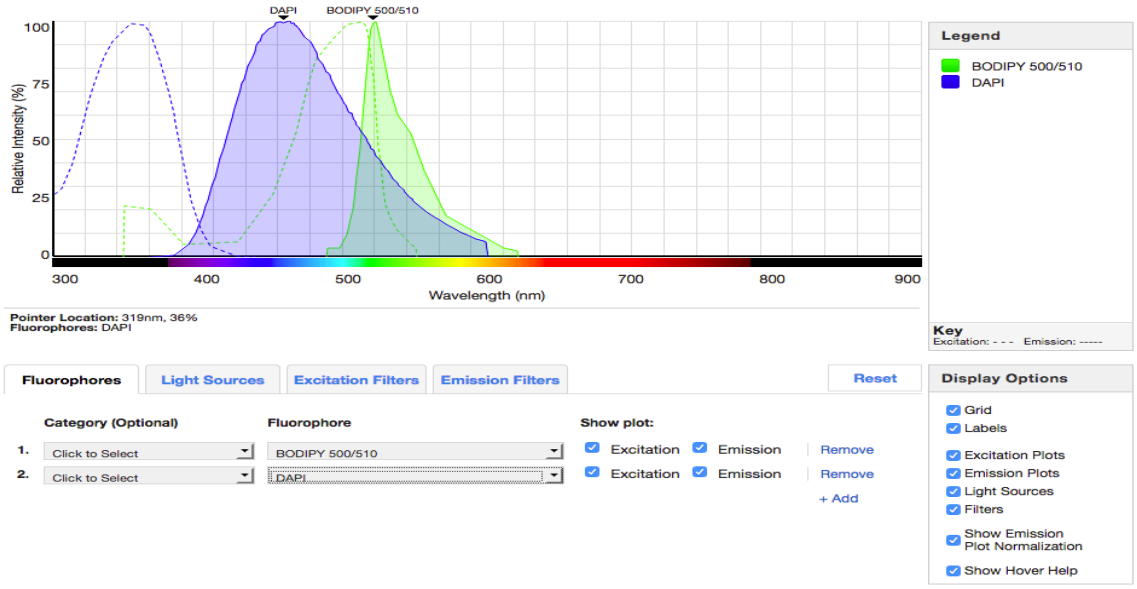

Figure 15 ThermoFisher Fluorescence Spectraviewer for Bodipy FL and DAPI stains.

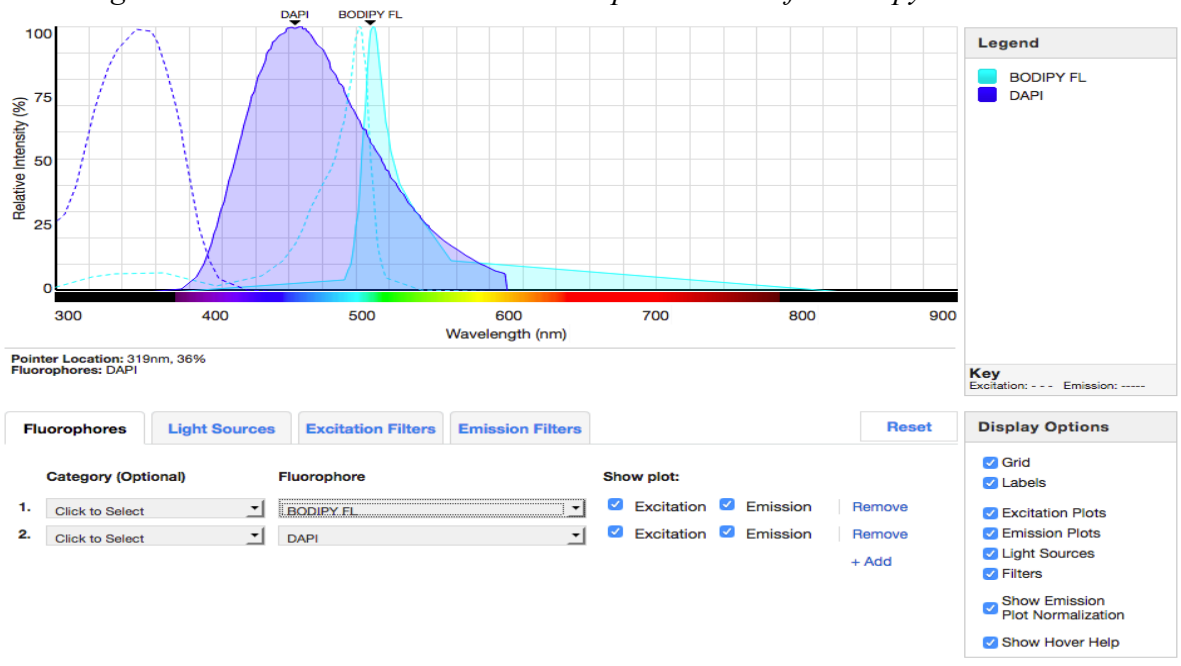

Images obtained were collected as z-stacks and were processed into either maximum intensity projection or 3D renderings with an adjustment on the y axis with the purpose of visualizing the composite size of the z plane. All images were post-processed using Adobe Photoshop CS6 where a histogram stretch and gamma adjustment was performed.

2.3 LSCM Paulding Mine

Four Tri-color bats (*Eptesicus fuscus)* were sampled using the same methodology as in Osbourne Cave. Two of the bats were male and two were female. The biopsy samples were placed into .1 M sodium cacodylate solution and placed on ice. Samples were not fixed and were stained within 6 hours of excision. The samples were stained with either Bodipy 500 or Bodipy FL and all samples were stained with Hoechst as detailed in table 4.

Table 4 Sample identification and stains used.

Sample ID #	**Wing**	**Sex**	**Visible WNS infection**	**Stain**
6	Right	Female	No	Bodipy 500
7	Right	Male	Yes	Bodipy 500
8	Left	Female	No	Bodipy FL
9	Left	Male	No	Bodipy FL

Figure 16 ThermoFisher Fluorescence Spectraviewer for Bodipy 500 and hoechst stains.

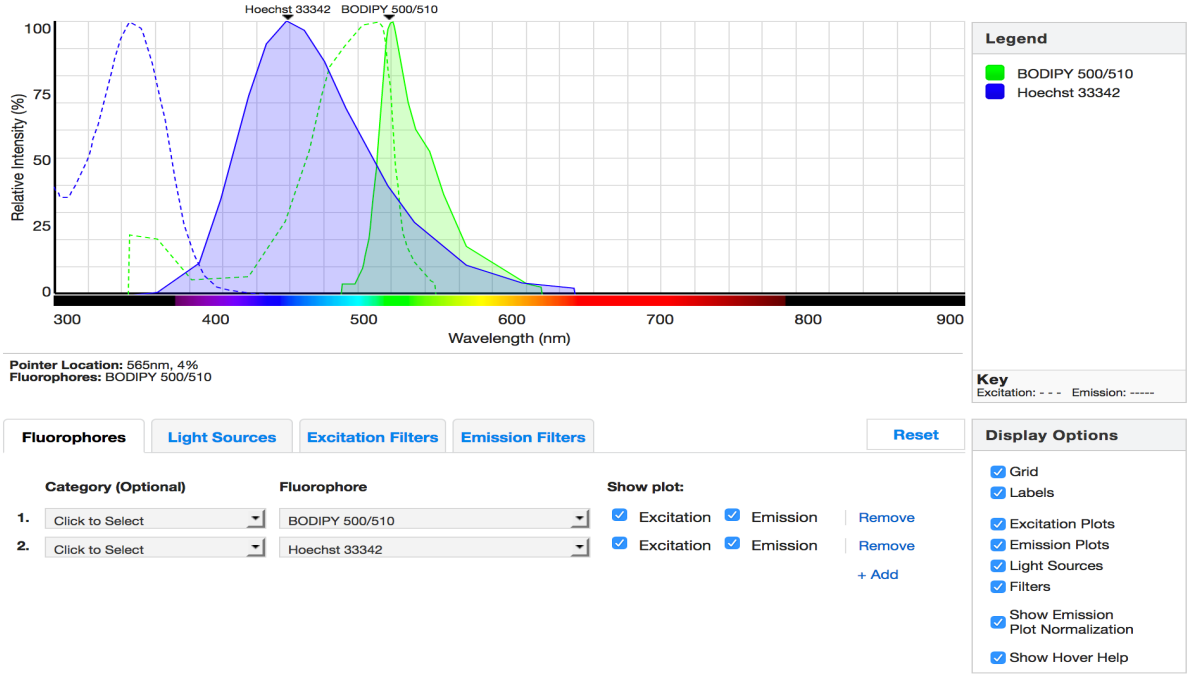

Images obtained were collected as z-stacks and were processed into maximum intensity projection. Furthermore, some images were obtained using the addition of transmitted light. All images were post-processed using Adobe Photoshop CS6 where a histogram stretch and gamma adjustment was performed.

2.4 Big Brown Bat tissue

Sections from a pair of frozen big brown bat (*Eptesicus fuscus*) wings were used for *in vitro* growth experiments of *P. destuctans*. Samples included wing tissue and fur. The samples were pinned in petri dishes and inoculated using a cotton swab that was rubbed across an area of a *P. destructans* 71 isolate culture that was grown on SDA media and incubated at 14 ^{0}C and was exhibiting heavy conidiation. The plates were wrapped in parafilm and incubated at 14 ^{0}C for 60 days.

A few hairs visibly infected with *P. destructans* were removed from the fur for examination by bright-field microscopy. They were imaged using a Nikon E800 compound microscope equipped with differential interference contrast optics. The images were acquired using a Zeiss axiocam and corresponding software. Stacked images were processed with Helicon Focus (Helicon Soft). All images were post-processed with Adobe Photoshop performing a histogram stretch and gamma adjustment.

Prior to processing for scanning electron microscopy, the fur sample was examined using a Meiji stereoscope and imaged with a Canon T3 DSLR using Canon software. All images were post-processed with Adobe Photoshop performing a histogram stretch and gamma adjustment.

Samples that were examined using scanning electron microscopy (SEM) were fixed using a 2.5% glutaraldehyde .1 M sodium cacodylate solution at 4^0C overnight. The samples were washed three times using a .1M sodium cacodylate solution. The samples were placed in a 1% osmium tetroxide solution for 3 hours and then washed three times using a .1M sodium cacodylate solution. The samples were then dehydrated through a gradient of acetone solutions (30%, 50%, 70%, 90%, 95%, 100%, 100%). The samples were then critical point dried. After full dehydration, the samples were mounted on aluminum studs (Electron Microscopy Sciences) using carbon tape and sputter coated in gold.

A small amount of hair inoculated with *P. destructans* was taken from the fur, and was placed in a 2% glucose PBS solution. Fluorescent stains were added to determine viability of the organism. The Life Technologies bacterial live/dead staining kit containing Syto 9 and Propidium iodide was used as directed by manufacturer's protocols for fluorescent imaging (ThermoFisher, 2004). Additionally, calcafluor white MR2 (Sigma Aldrich)at a 25mM

concentration was added. The hair was mounted on a glass slide using mounting media from the Live/Dead stain kit.

The hair was imaged using a Carl Zeiss LSM780 laser scanning confocal microscope (LSCM). The imaging parameters were set using the ThermoFisher Spectra viewer that shows excitation and emission parameters for the selected fluorophores (Figure 16). The spectra viewer does not contain calcofluor white (EX/EM 405/450) information. However, it is present as a preset configuration on the LSCM.

Figure 17 ThermoFisher Fluorescence Spectraviewer for Syto 9 and Propidium Iodide.

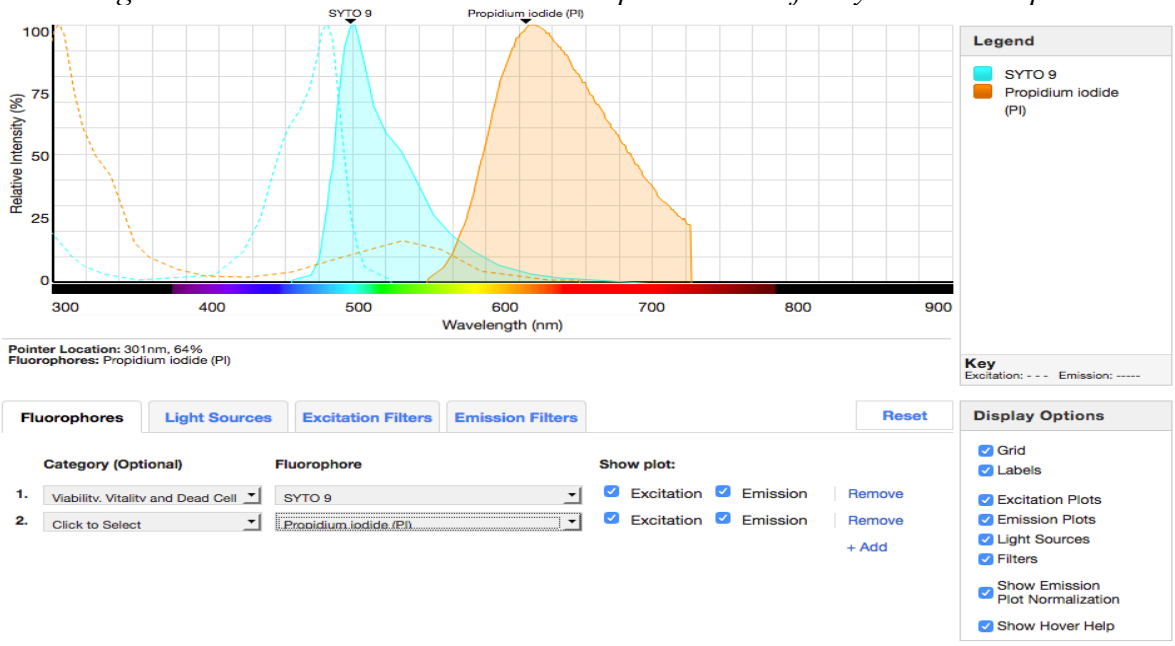

The section of fur examined using SEM was fixed using osmium tetroxide vapors for 24 hours to preserve the adhered *P. destructans*. After fixation, the sample was mounted on an aluminum stud using carbon tape and then sputter coated in gold.

Images were taken on a Tescan Vega 3 LMU scanning electron microscope. All samples were imaged a 5 KV at varying scanning rates and resolutions based upon visual optimization. All

images were post processed using Adobe Photoshop CS6 for a histogram stretch and gamma adjustment.

2.5 GC-MS

P. destructans 71 was grown on a defined Aspergillus media with glucose as the carbon source until a confluent lawn was present. A $5mm^2$ circular plug was removed from the lawn and transferred to SDA plates. The cultures were grown for 43 days to the point where a visible exudate was seen on top of the mycelia (Figure 17).

1 µl samples of the exudate were taken and direct injected in the Agilent 7980a GC-MS. The inlet was set at 250^0C with a split ration of 5:1 at 5mL/min. An Agilent Hp5-Ms column (30mx250µmx0.25µm) was used starting at 35^0C – 39^0C ramped at 3^0C/min and held for 2 minutes and ramped from 39^0C to 55^0C at 2^0C/min and from 55^0C to 250^0C at 3^0C/min. The detector range was 35-450 m/z.

A Supelco 65 µm PDMS/DVB fused silica 24 Ga solid-phase micro extraction (SPME) fiber was prepared per manufacturers protocols (CITE Supelco). A 10 mm^2 circular plug of *P. destructans* (sample B) on SDA agar that had visible exudate on the mycelia was excised and placed in a 22 cc Supelco screw top vial that had been stored at 14^0C. The SPME fiber was exposed to the shared headspace with the sample for 24 hours at 14^0C. The SPME fiber was run on the Agilent 7890a GC-MS using the same parameters as the direct injection exudate samples. The same collection and analysis procedures, but without a split flow at the inlet, were used for samples of *P. destructans* isolate 71 exhibiting heavily conidiation, bat wing tissue and an empty vial.

Analysis of compound spectra for identification was performed using the deconvolution or the integration algorithms in the Agilent Masshunter software. Compounds not automatically identified in the Masshunter software were identified using the National Institute of Standards ARDMIS software.

P. destructans cultures were UV illuminated using a Mic-Fi digital stereoscope. Micrographs of the exudate were taken using the Mic-Fi stereoscope. Images of the mycelia with the exudate were taken using a Samsung Galaxy S7. A histogram stretch and gamma adjustment were performed on the images using Adobe Photoshop.

3 RESULTS

3.1 *In vitro* growth of *P. destructans* on lipid media

The initial growth experiments focused on finding an optimum carbon concentration for growth of *P. destructans*. Defined media plates containing either 5g, 10g, or 15g of D-glucose were used.

Figure 18 Sample of images used for radial mycelial growth.

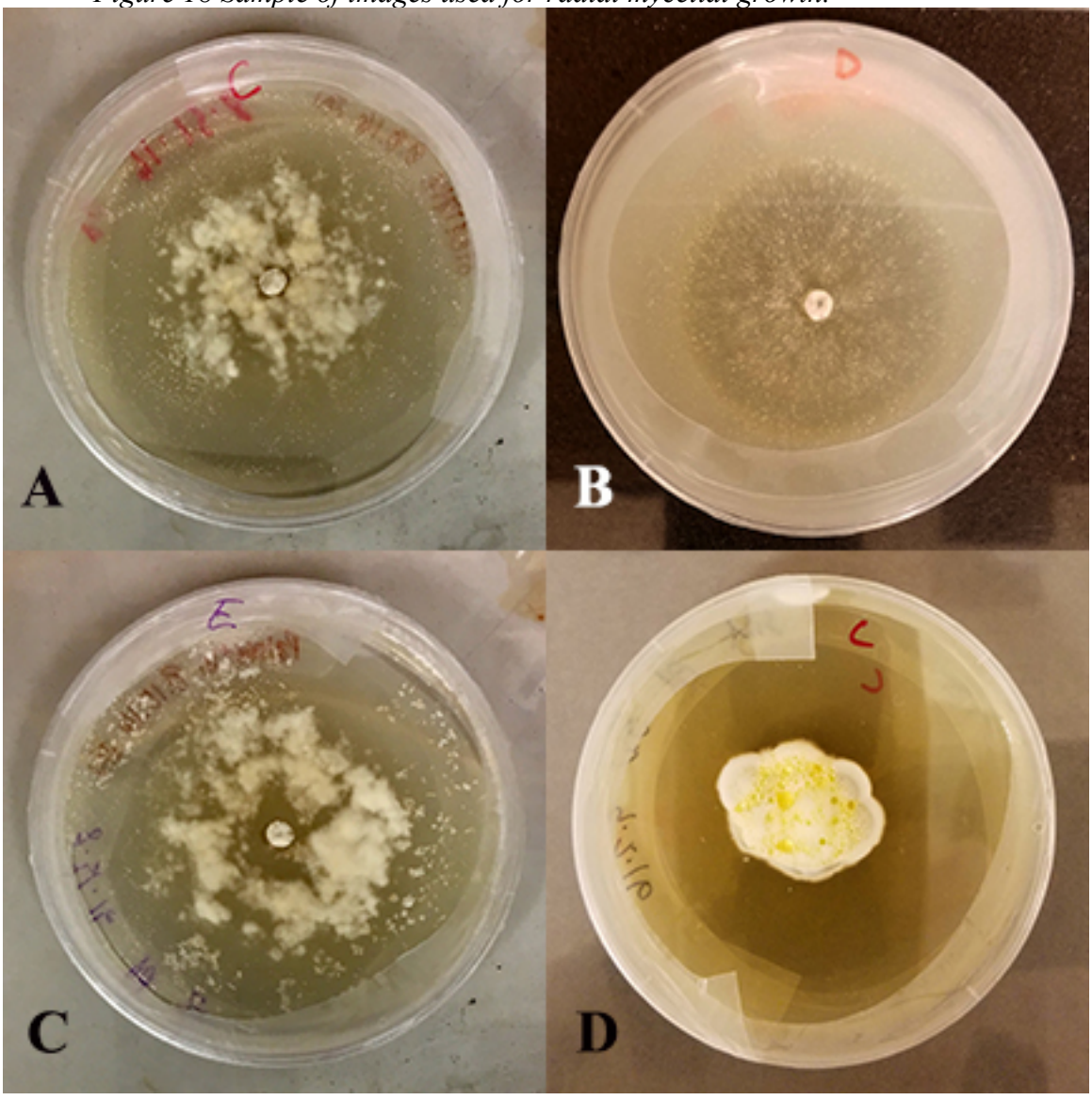

A) Stearic acid B) Oleic acid C) Palmitic acid D) SDA

Figure 19 Growth rate of P. destructans *with varied quantities of D-glucose.*

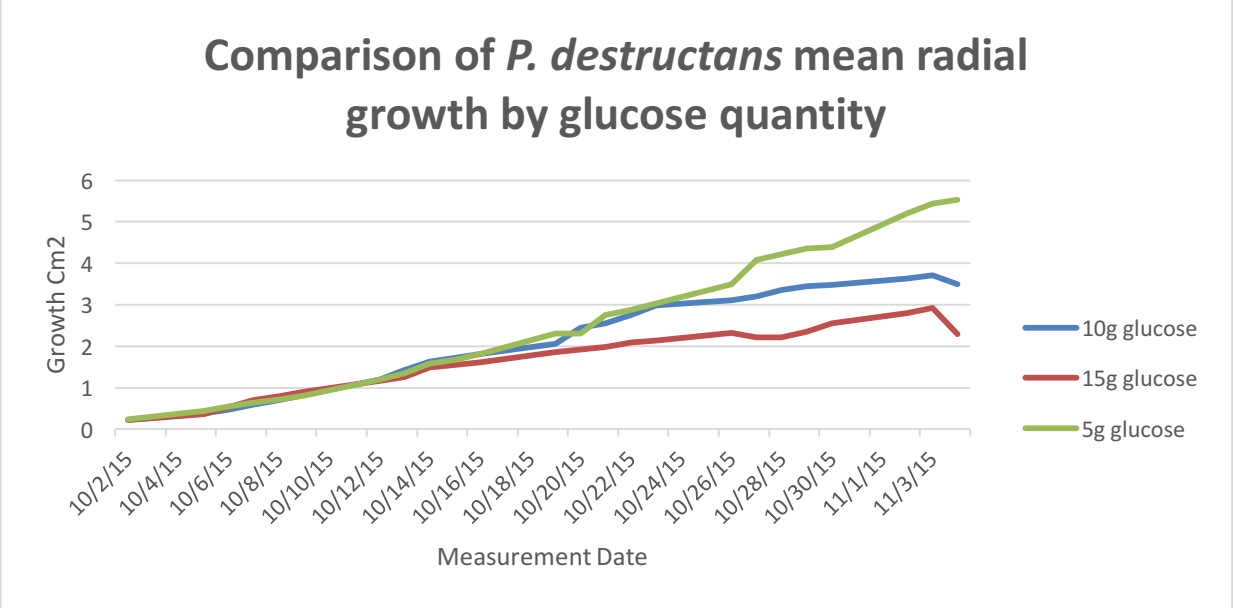

The below graphs show the mean growth of *P. destructans* over a 70 day period incubated at 14^0C.

Figure 20 Mean radial growth of P. destructans on SDA.

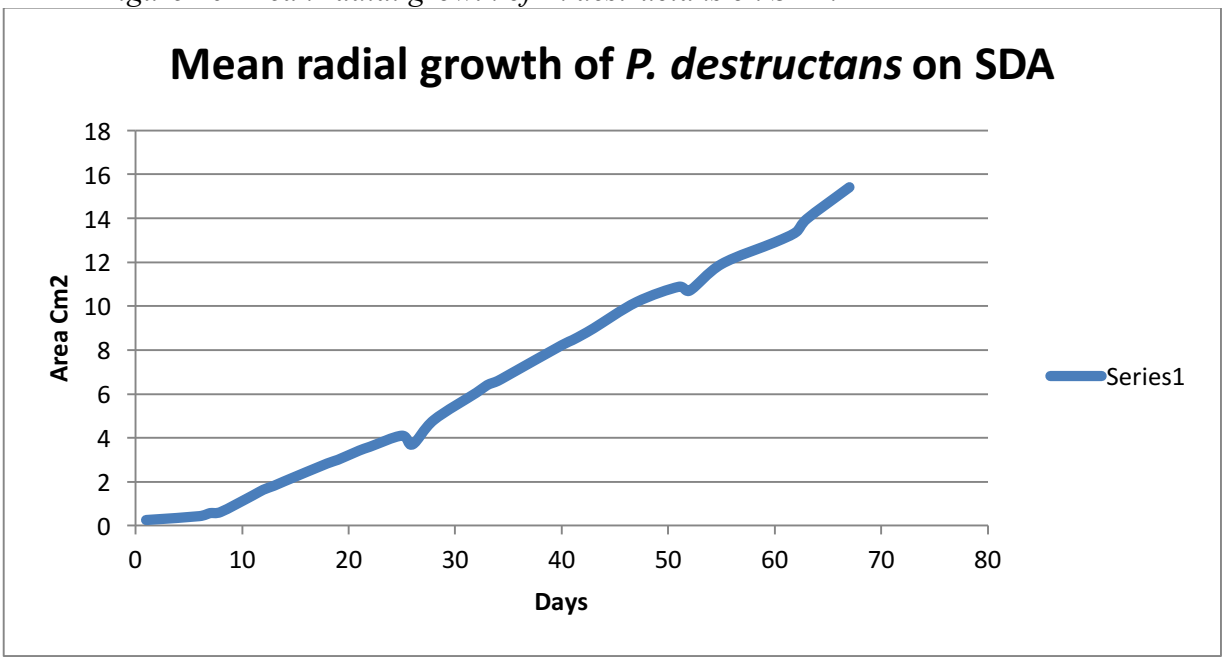

Figure 21 Mean radial growth of P. destructans on oleic acid media.

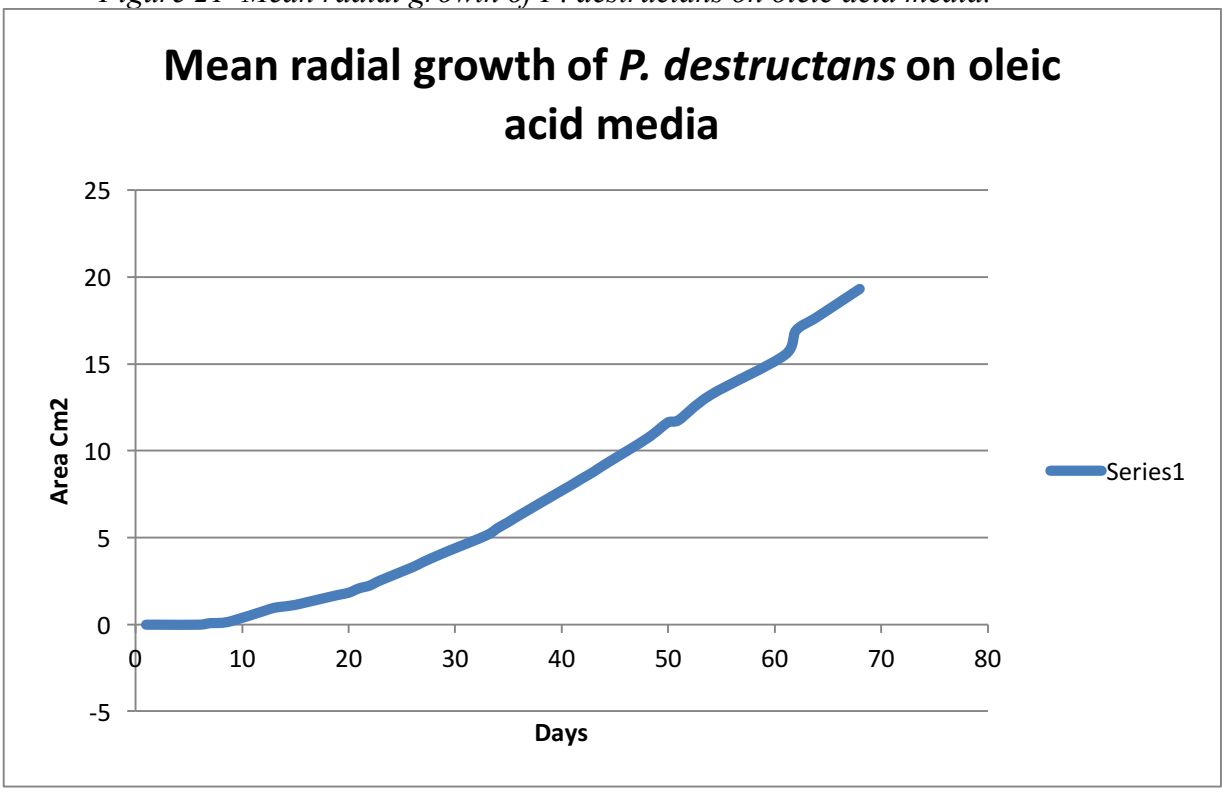

Figure 22 Mean radial growth of P. destructans on palmitic acid media.

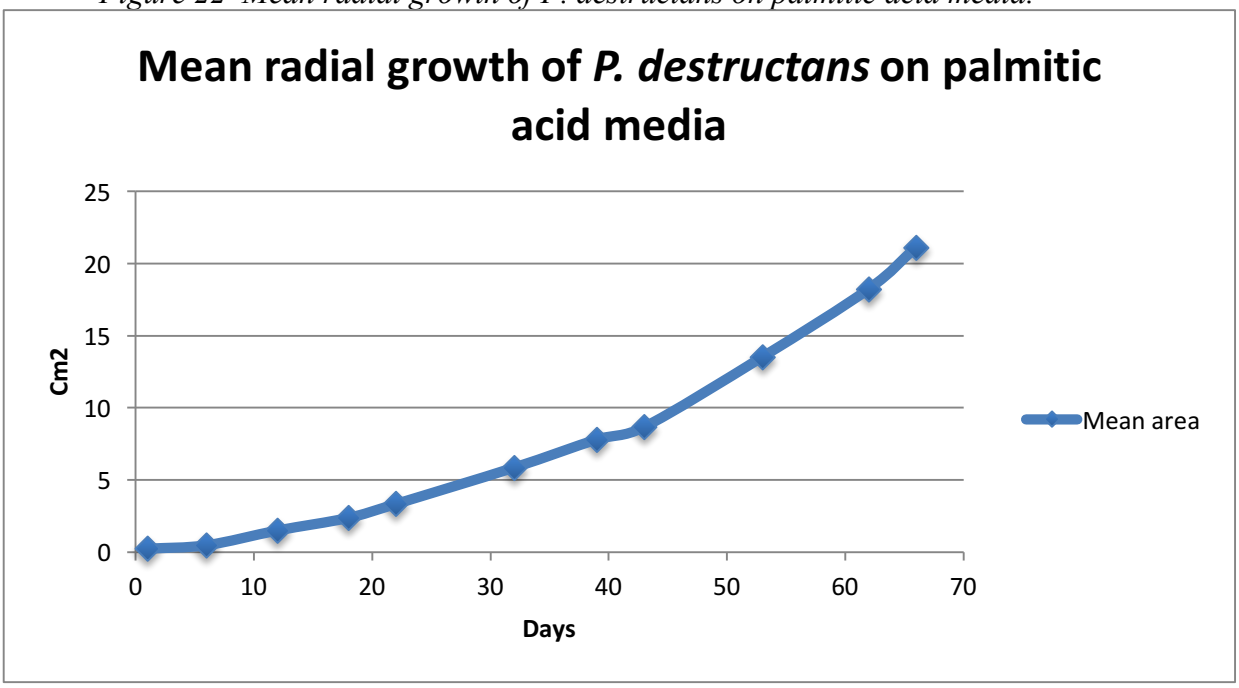

Figure 23 Mean radial growth of P. destructans on stearic acid media.

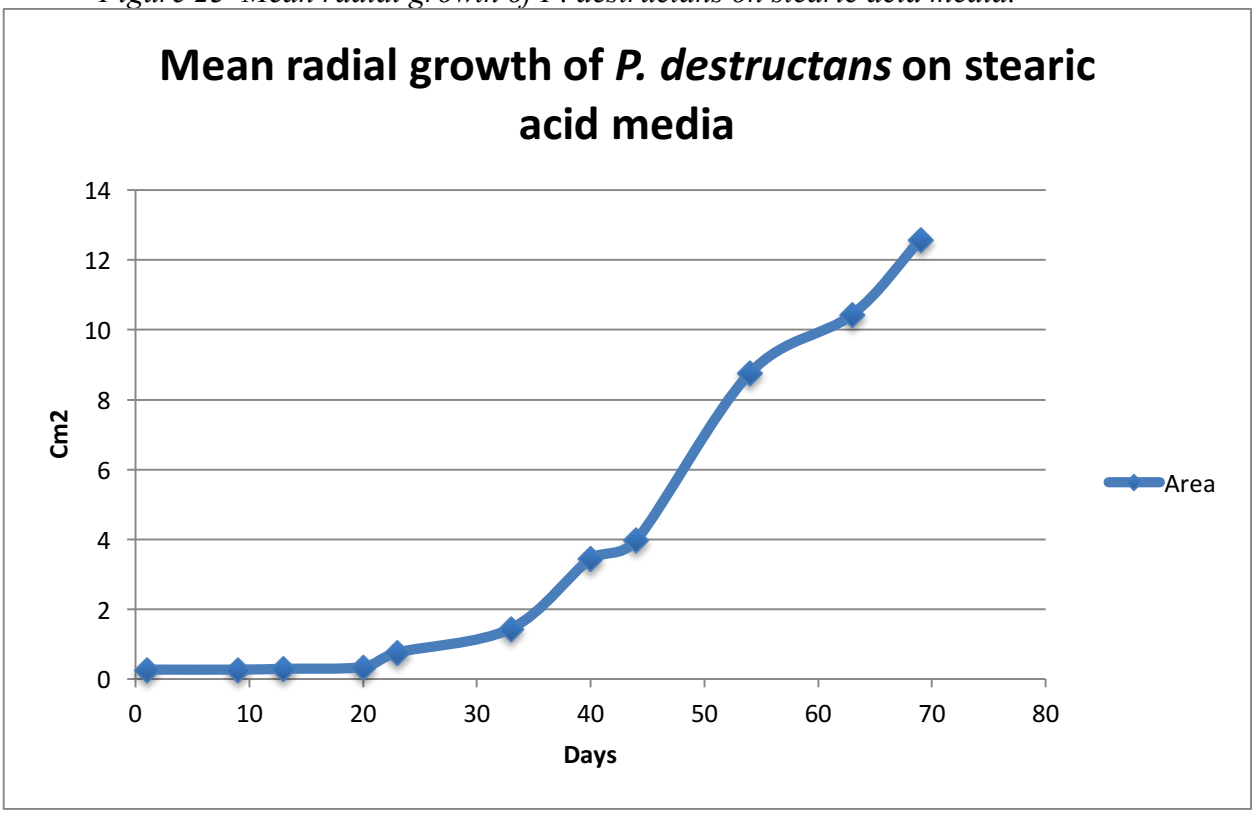

Figure 24 Comparison of P. destructans mean radial growth by media type.

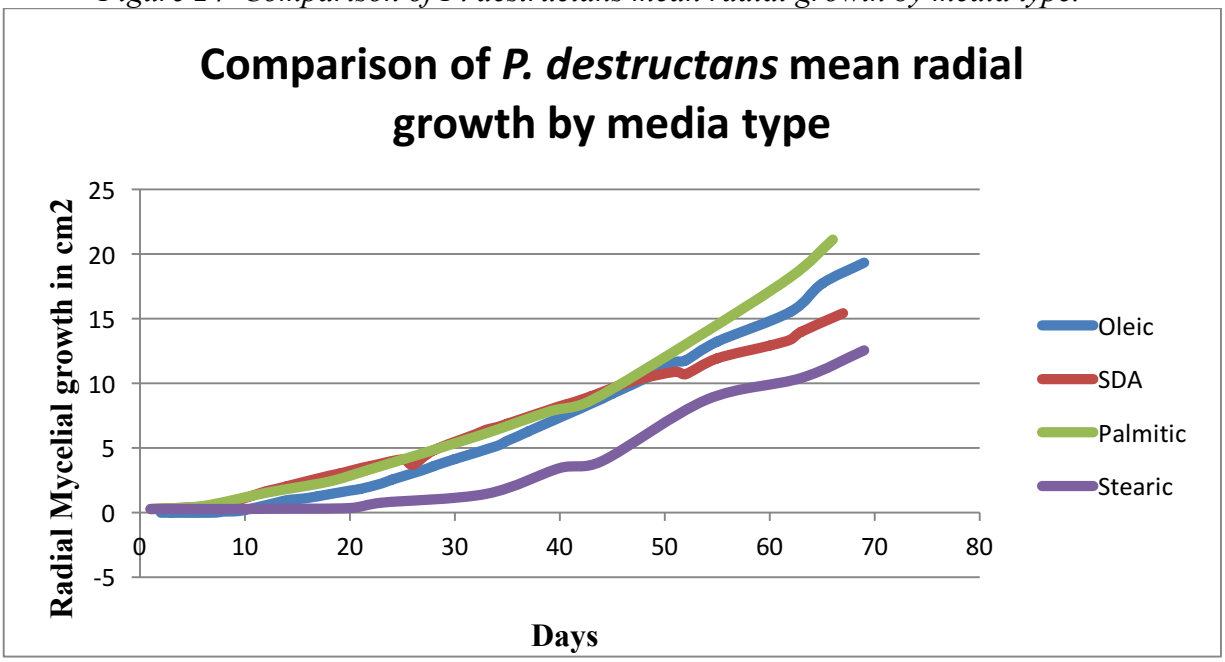

The above graph is a comparison of the mean growth rates of each type of media tested against the control of SDA. Stearic acid, the longest chain saturated fatty acid (18:0) was seen to have the least amount of growth over the duration of the experiment. The unsaturated 18c chain, Oleic had a greater amount of growth. Palmitic acid, the shortest chain fatty acid (16:0) was seen to have the most growth even more than that of the SDA control.

3.1.1 Statistical analysis of growth

An Anova and Tukeys statistical test was run on the overall mean growth of each media type to measure if there was a statistical difference between the growth of the groups using SPSS (IBM). As table 5 shows there was not a significant difference in growth between any of the fatty acid groups and the SDA group. There was only a statistically relevant difference between the mean growth of *P. destructans* on the palmitic and stearic media.

Table 5 Table of Anova test results from SPSS.

		Mean			**95% confidence interval**	
(i)Media	**(J)Media**	**Difference (i-J)**	**Std. Error**	**Sig.**	**Lower Bound**	**Upper Bound**
SDA	Oleic	-3.900	2.703	.489	-11.466	3.667
	Palmitic	-5.693	2.703	.185	-13.2596	1.874
	Stearic	2.848	2.703	.721	-4.719	10.414
Oleic	SDA	3.900	2.703	.489	-3.667	11.466
	Palmitic	-1.793	2.703	.910	-9.360	5.773

	Stearic	6.747	2.703	.091	-.819	14.314
Palmitic	SDA	5.693	2.703	.185	-1.874	13.259
	Oleic	1.793	2.703	.910	-5.773	9.360
	Stearic	8.541	2.703	.023	.974	16.107
Stearic	SDA	-2.848	2.703	.721	-10.414	4.719
	Oleic	-6.747	2.703	.091	-14.314	.819
	Palmitic	-8.541	2.703	.023	-16.107	-.974

3.2 Osbourne Cave

Figure 25 Maximum intensity projection of Big Brown Bat wing tissue, sample 1.

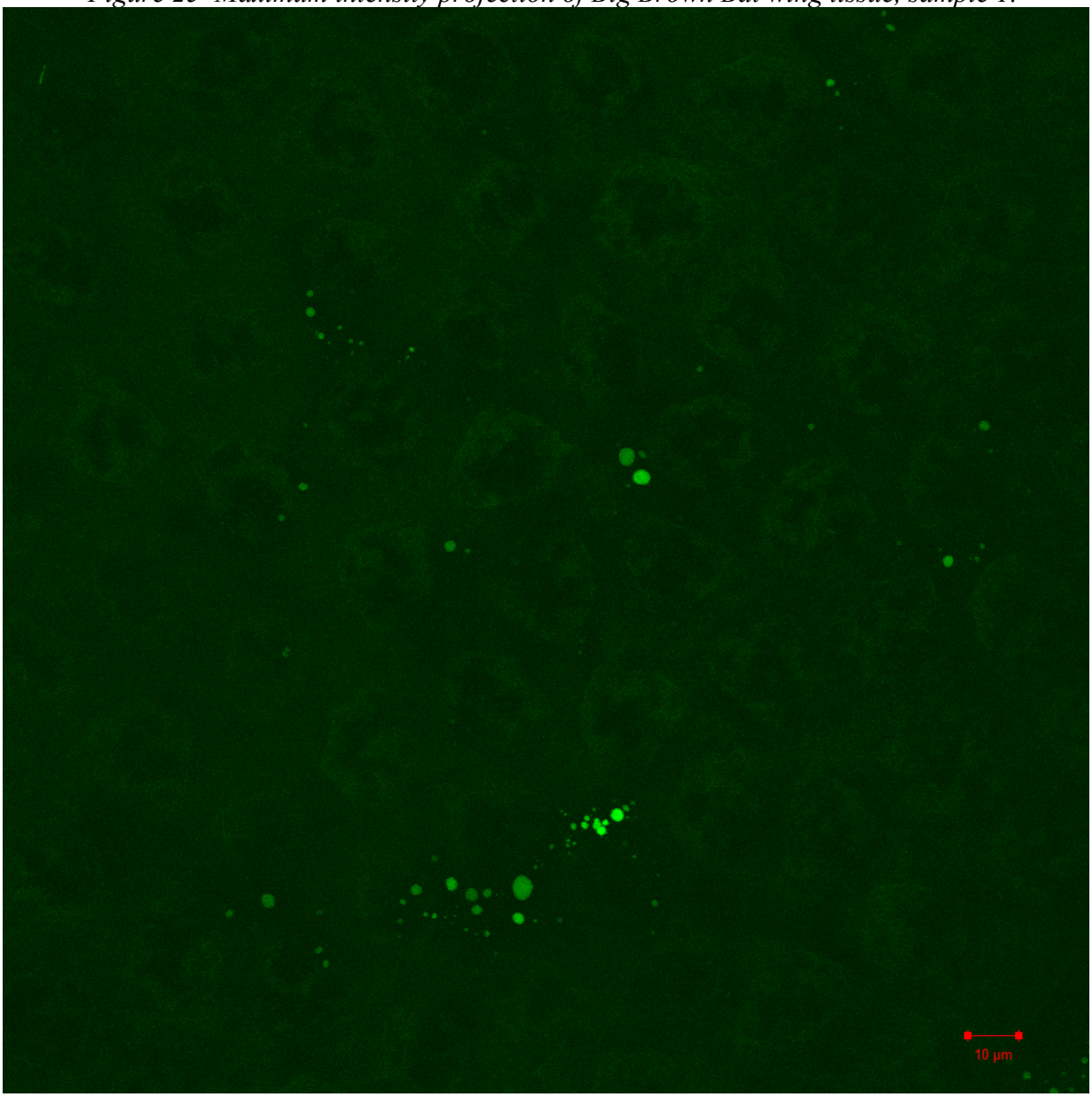

The above image of sample 1 from a Big Brown bat was stained with Bodipy 500. The image is at 40x.

Figure 26 Maximum intensity projection of Big Brown batwing tissue, sample 2.

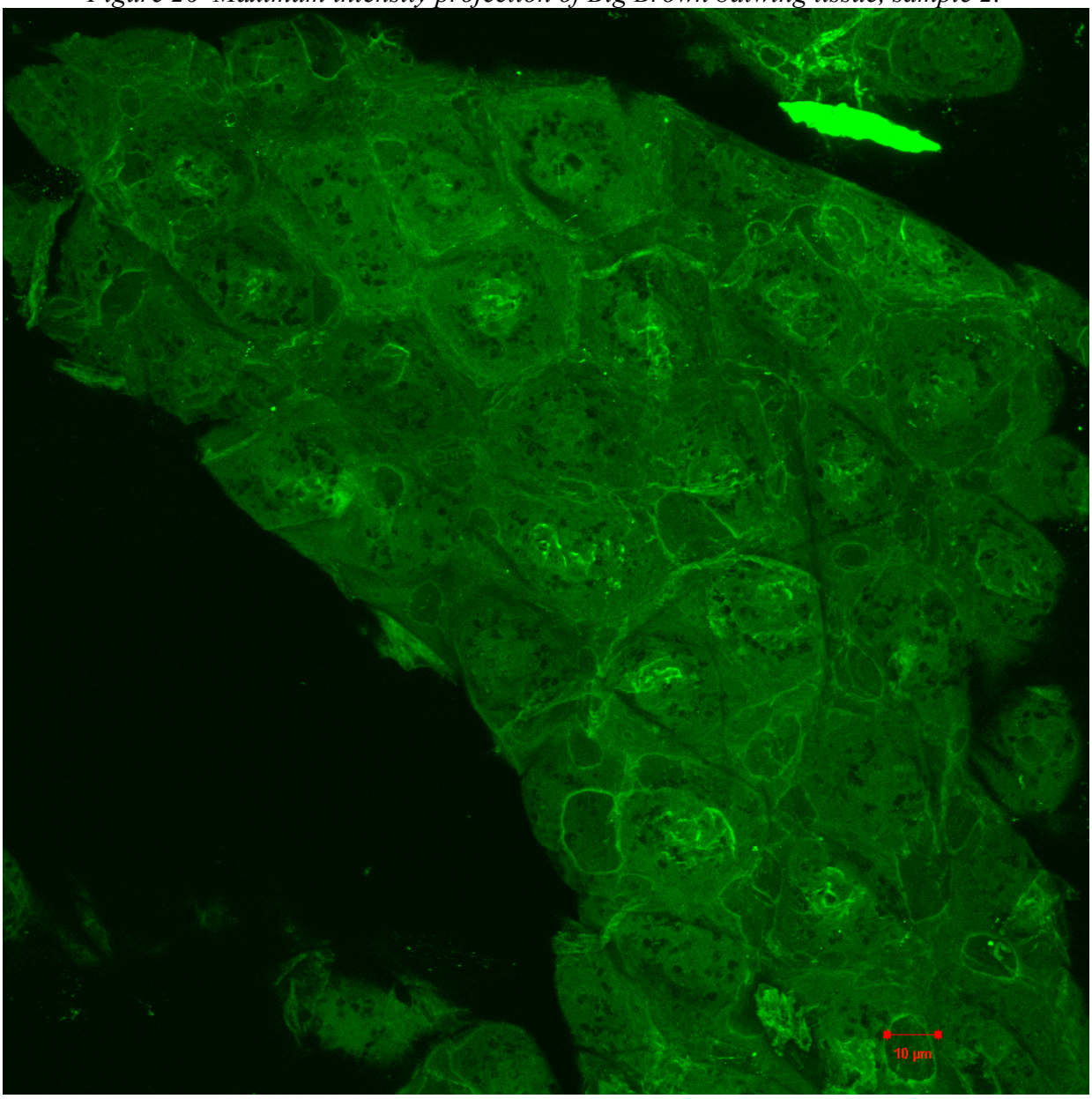

The above image of sample 2 is from a Big Brown bat and was stained with Bodipy FL. The image was taken at 40x magnification.

Figure 27 Maximum intensity projection of Tri-color bat wing tissue, sample 1.

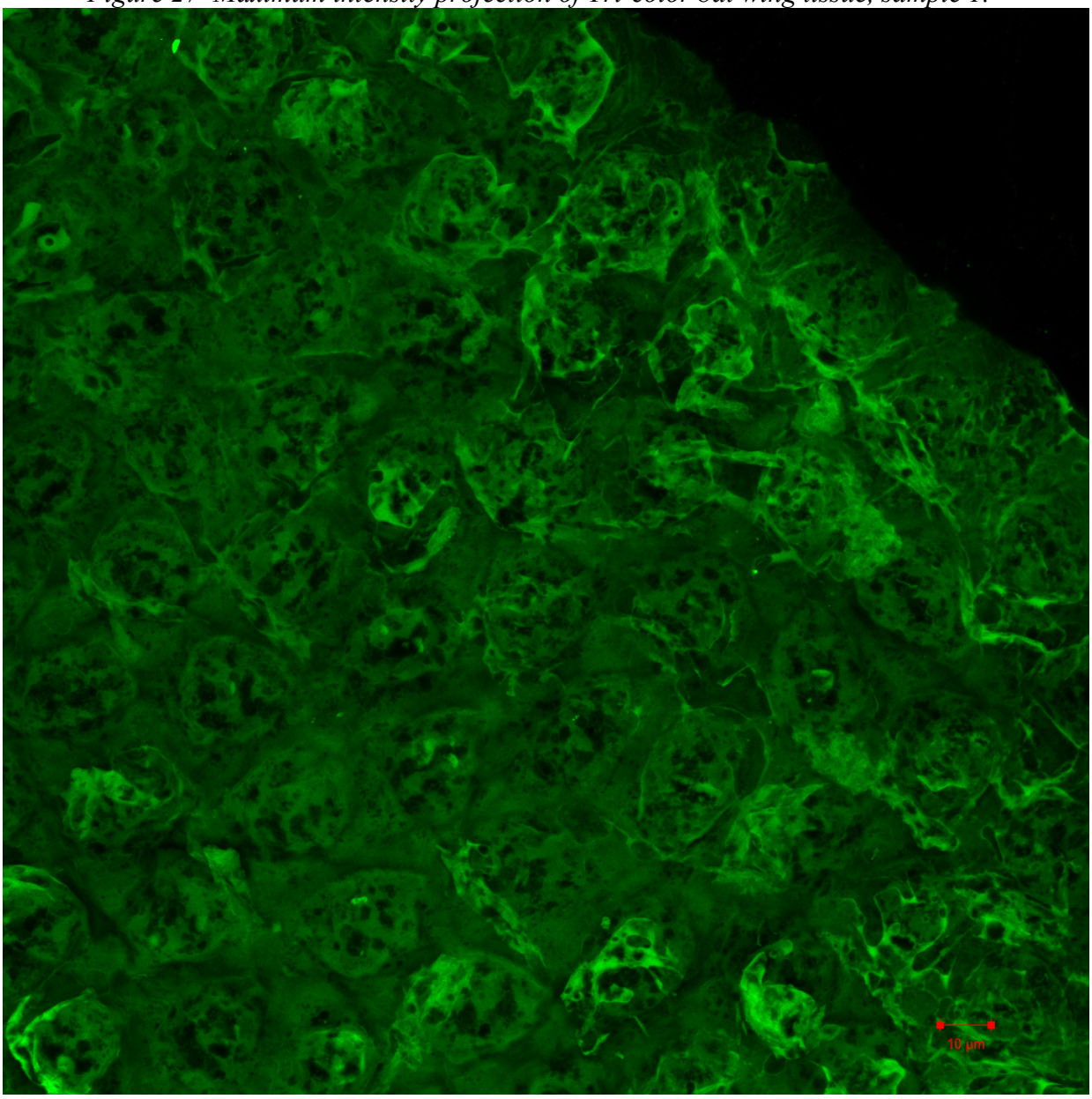

The above image of sample 1 from a tri-color bat is stained with Bodipy 500. The above image was taken at 40x magnification.

Figure 28 Maximum intensity projection of Tri-color bat wing tissue, sample 4.

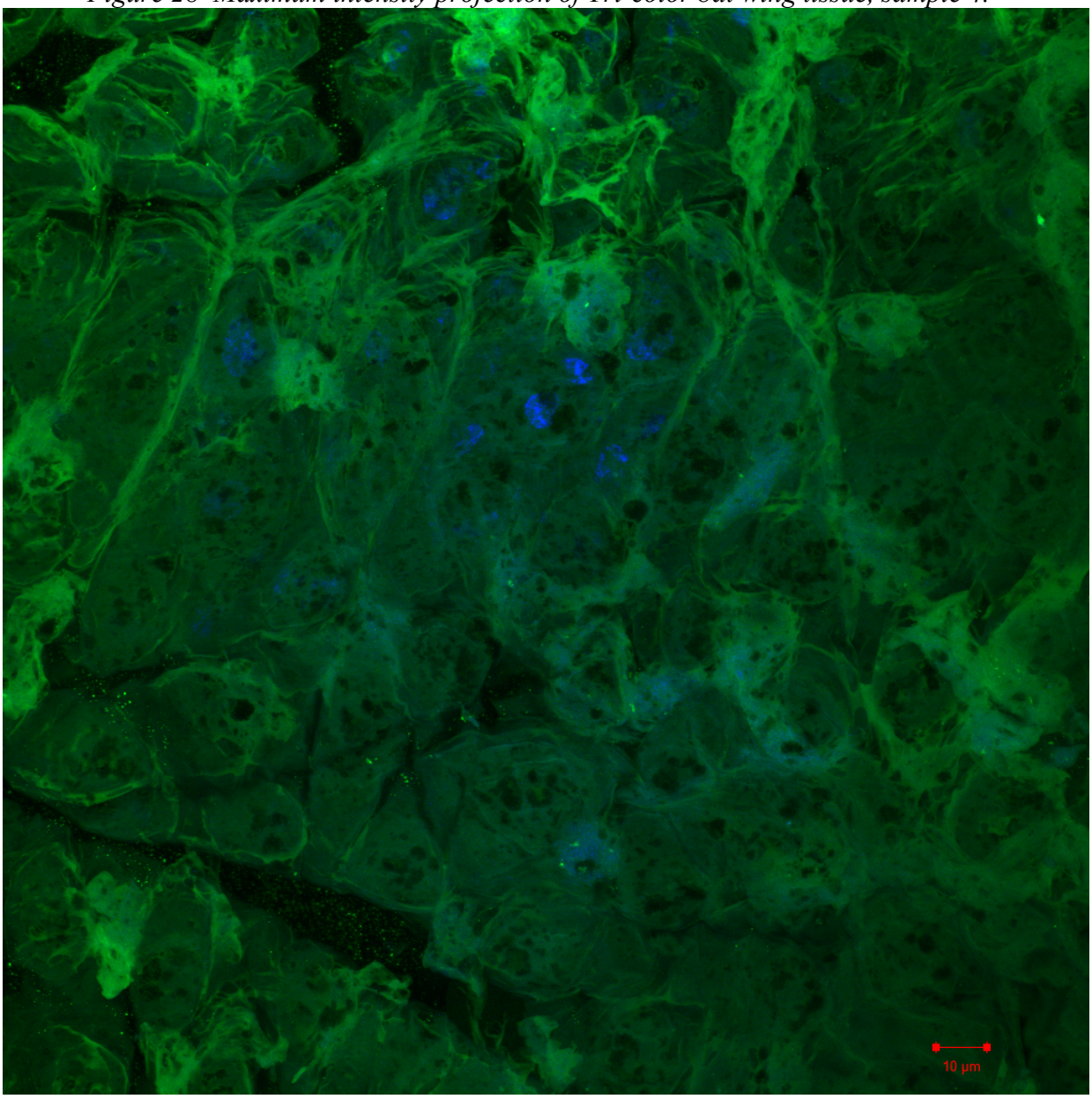

The above image of sample 4 from a tri-color bat is stained with Bodipy FL and DAPI. The above image was taken at 40x magnification.

Figure 29 Maximum intensity projection of Tri-color bat wing tissue, sample 5.

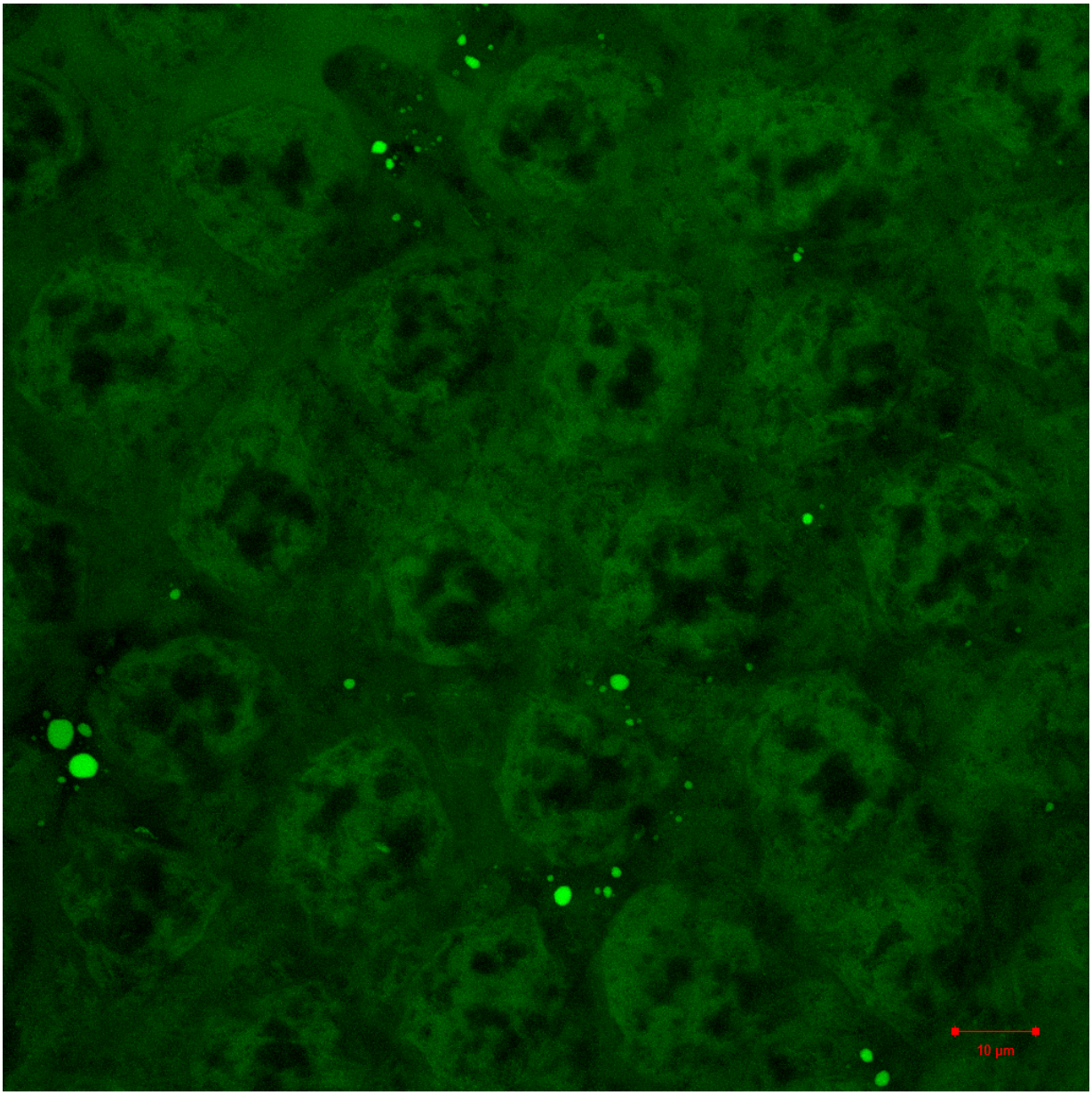

The above image of sample 5 from a tri-color bat is stained with Bodipy 500. The above image was taken at 63x magnification.

Figure 30 Maximum intensity projection of Tri-color wing tissue, sample 6.

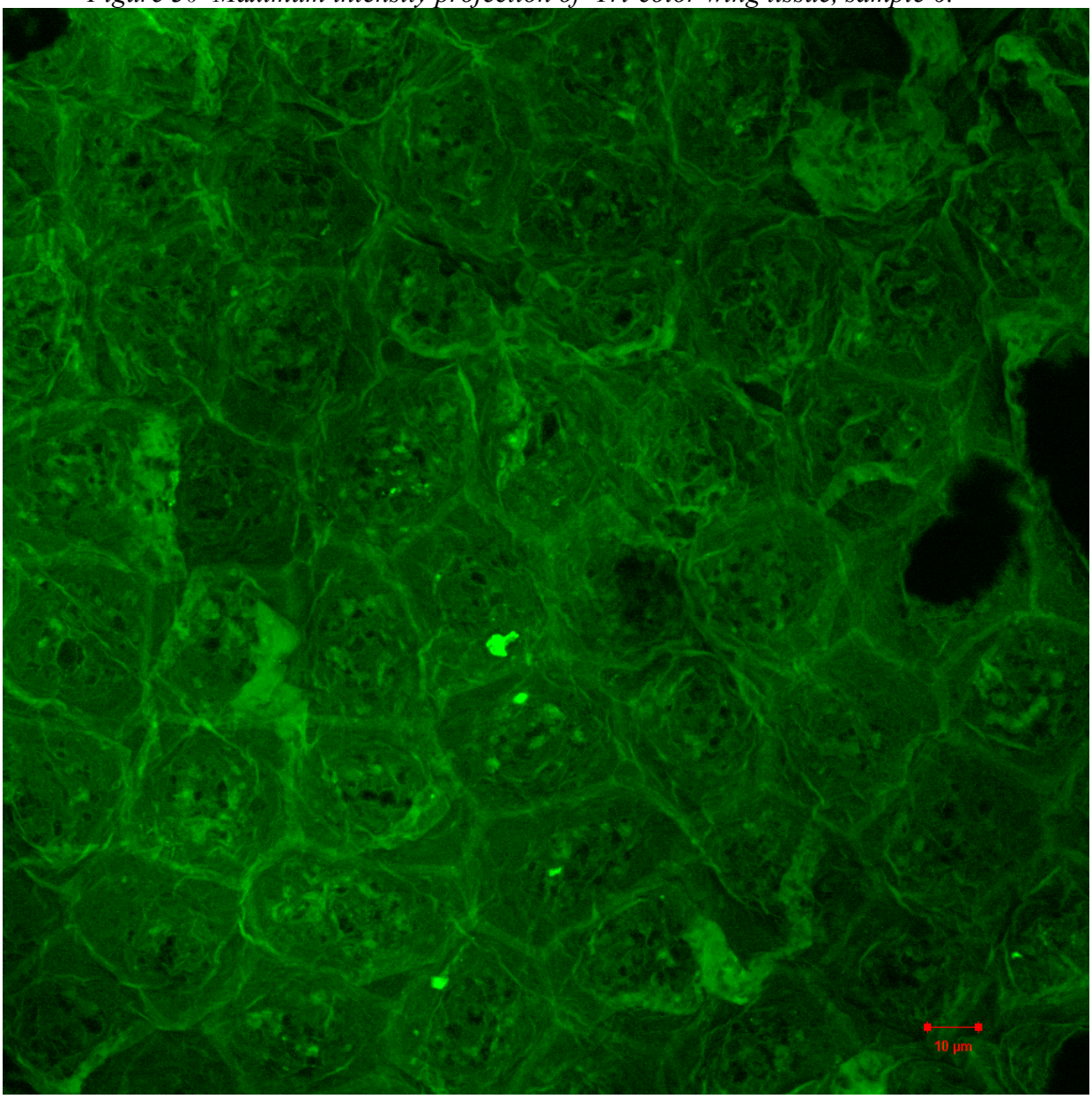

The above image of sample 6 from a tri-color bat is stained with Bodipy FL. The above image was taken at 40x magnification.

In all of the samples there is a noticeable difference in the areas that do not stain when Bodipy 500 is used in comparison with FL. The centers of the cells don't stain with Bodipy 500

as they are seen to do with FL. This indicates the presence of C-16 fatty acids at the center of the cells in the wing membrane and a lack of C-18.

3.3 Paulding Mine

Figure 31 Maximum intensity projection of Tri-color wing tissue, sample 6 from Paulding Mine.

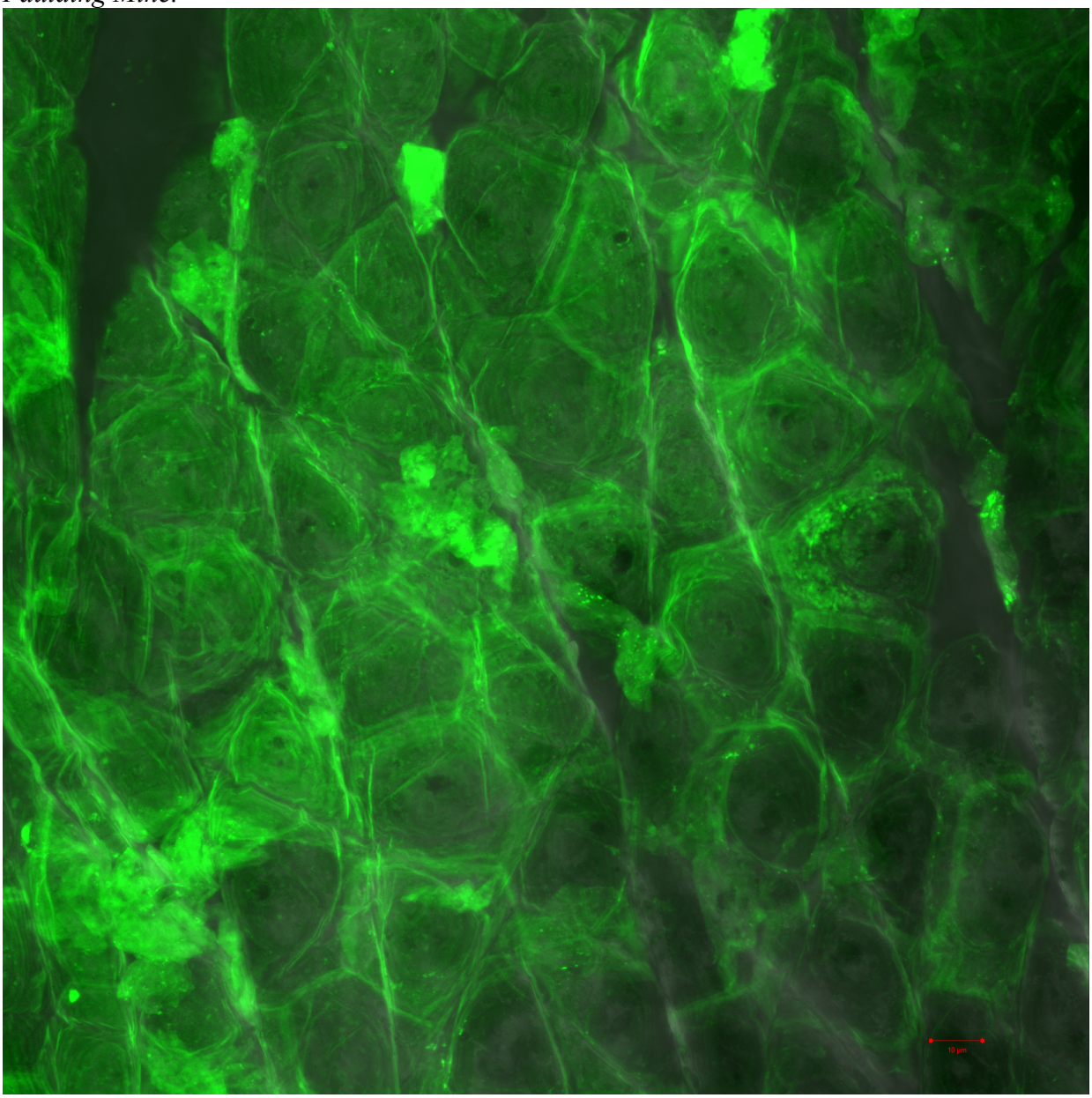

Figure 32 Maximum intensity projection of Tri-color wing tissue, sample 7.

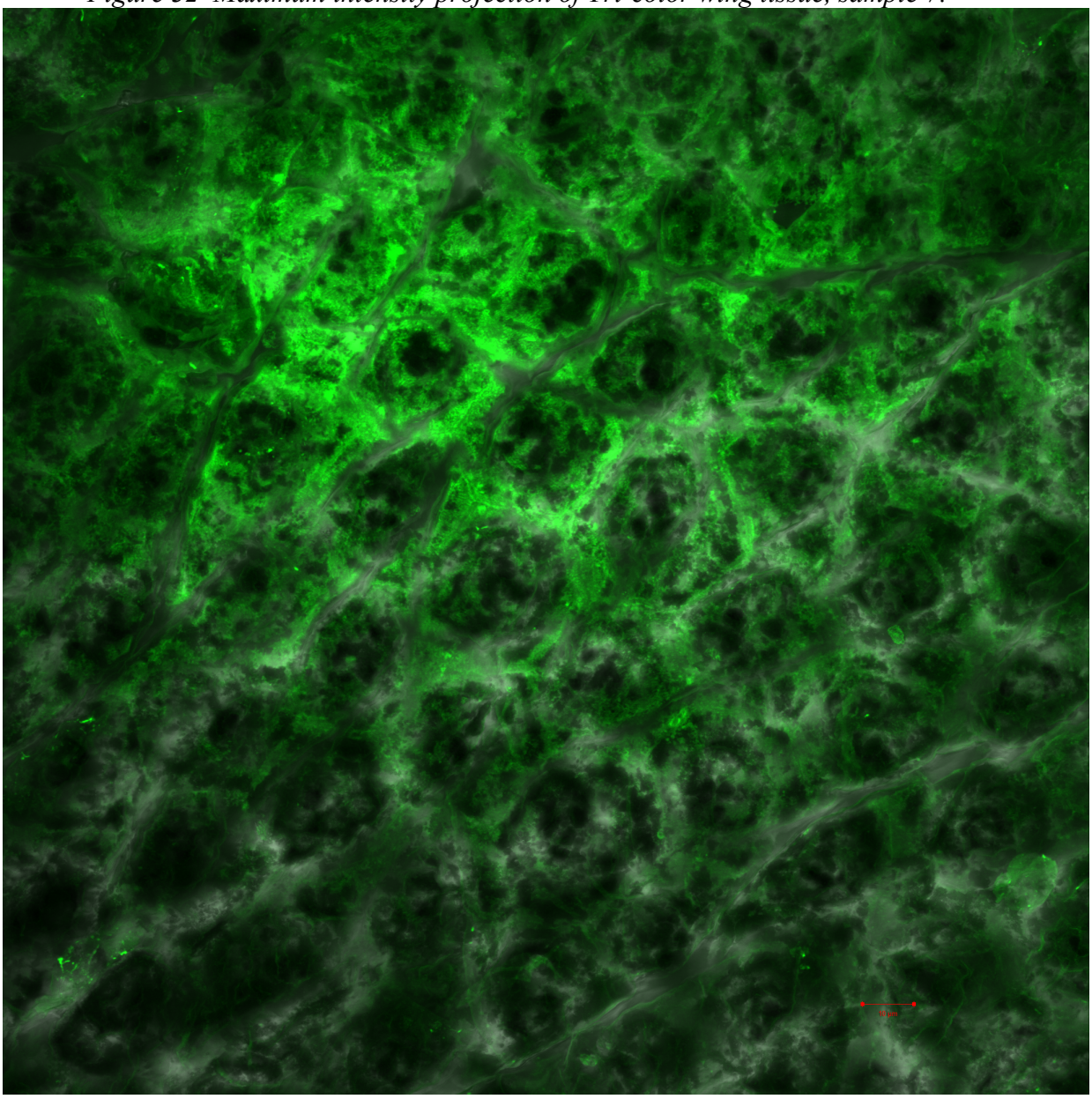

Figure 33 Maximum intensity projection of Tri-color wing tissue, sample 8.

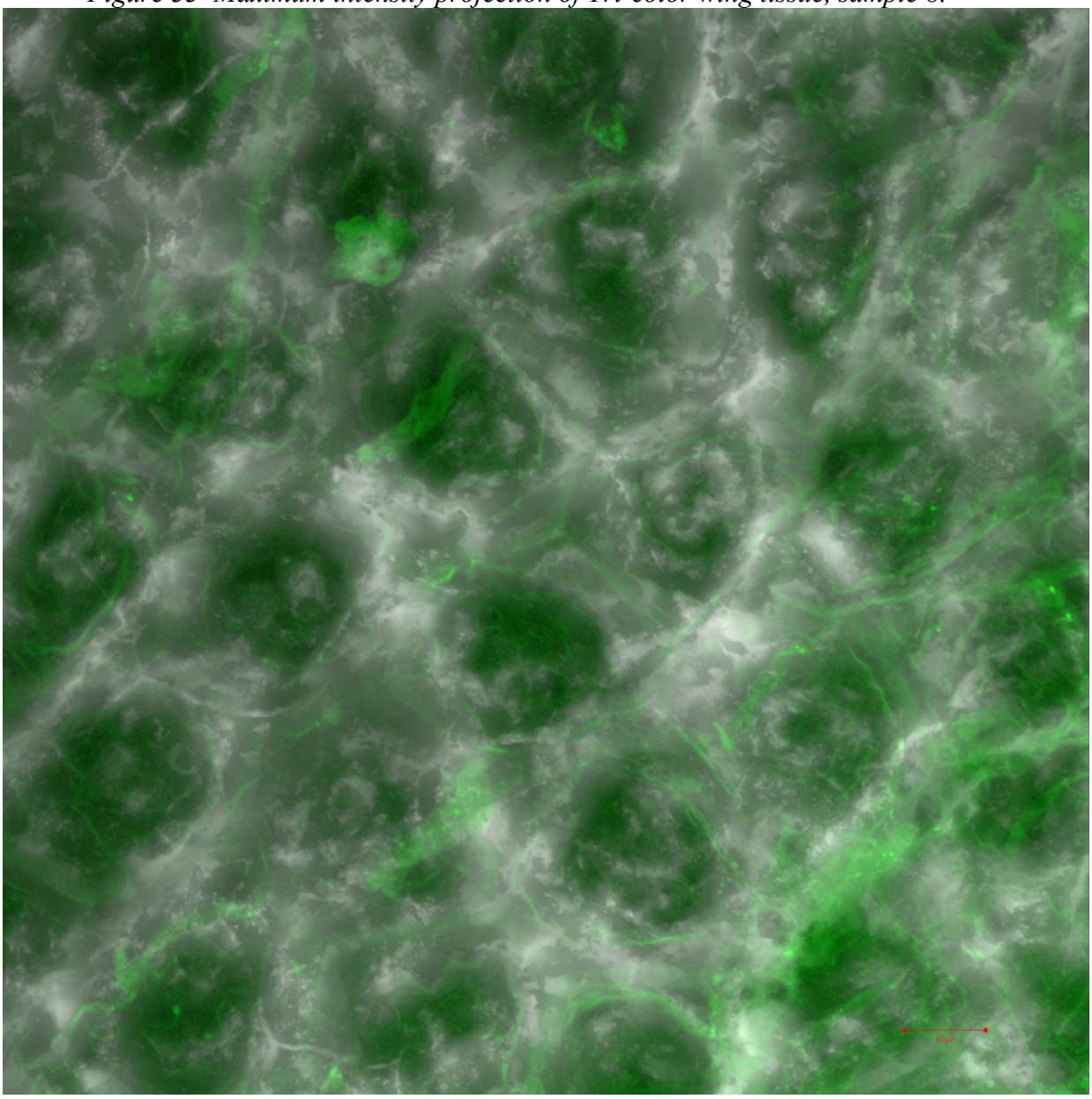

Figure 34 Maximum intensity projection of Tri-color wing tissue, sample 9.

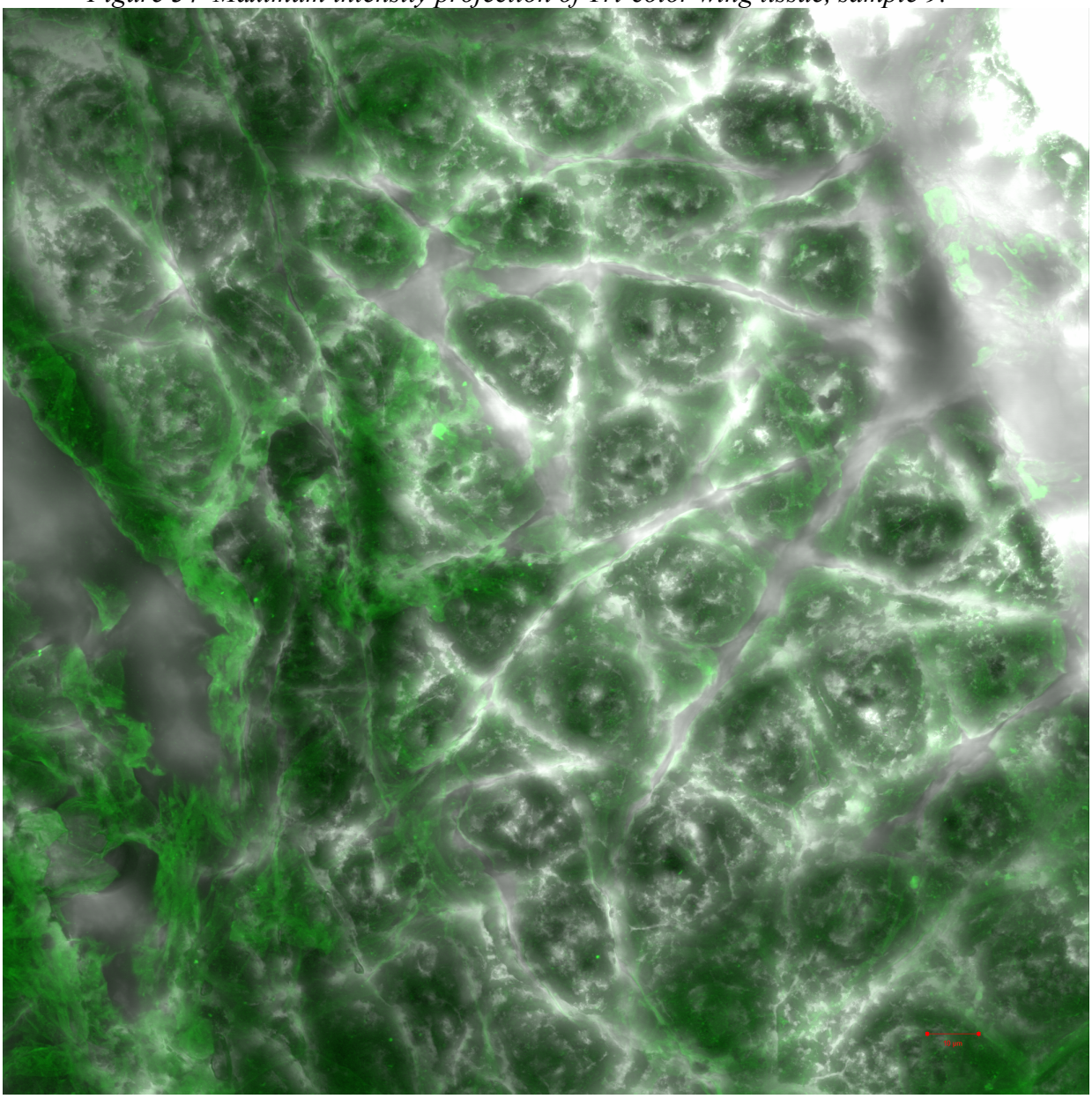

3.4 Bat Fur

Figure 35 P. destructans *isolate 71 growing on Big Brown Bat fur.*

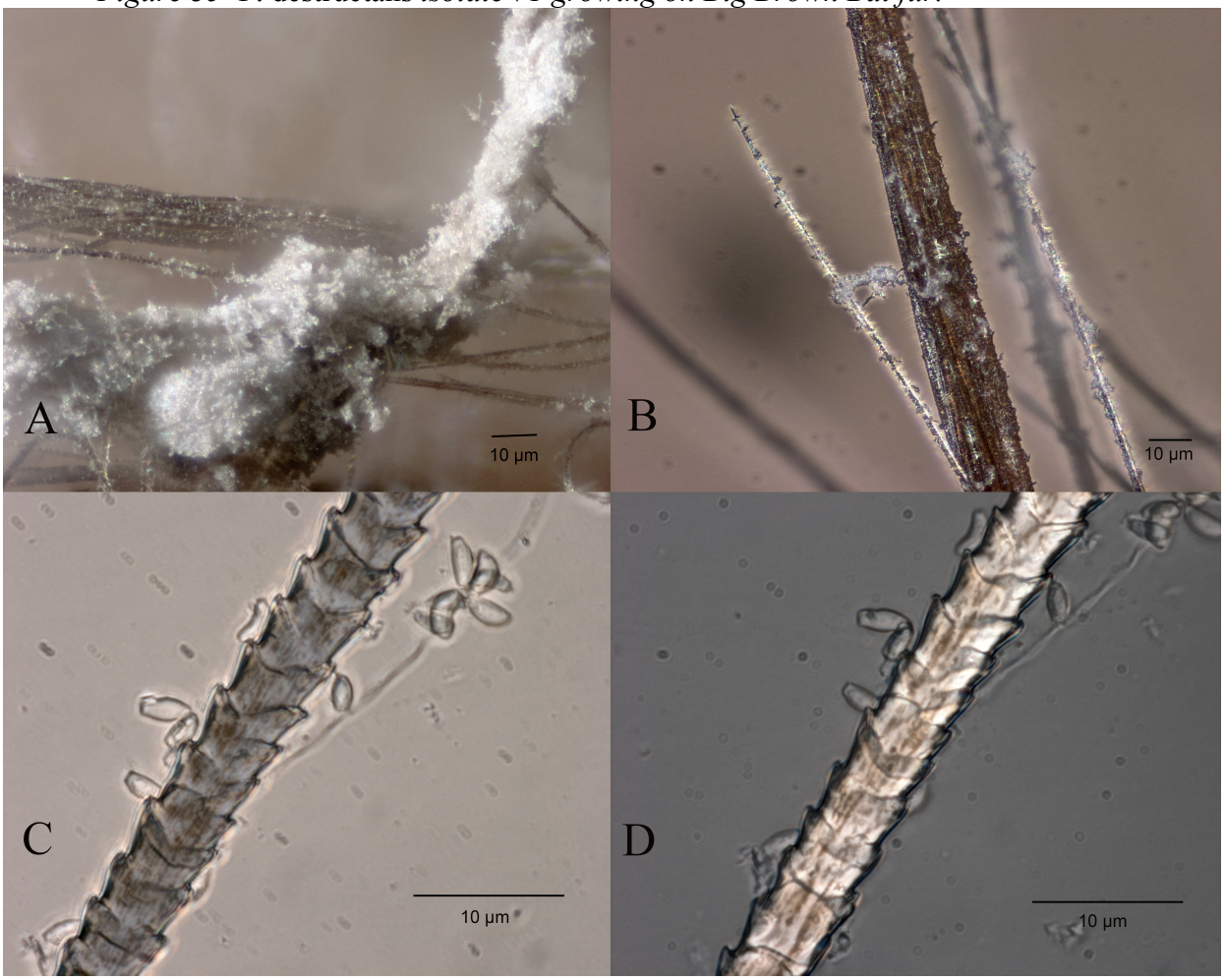

Images A and B are at 400x magnification. They show heavy growth of *P. destructans* on Big Brown Bat hair. Images C and D are slide mounted and imaged at 1000X magnification. They show *P. destructans* mycelia wrapping around an individual Big Brown Bat hair. Notably, the mycelia do not appear to penetrate the hair.

Figure 36 Big Brown bat fur inoculated with P. destructans *isolate 71.*

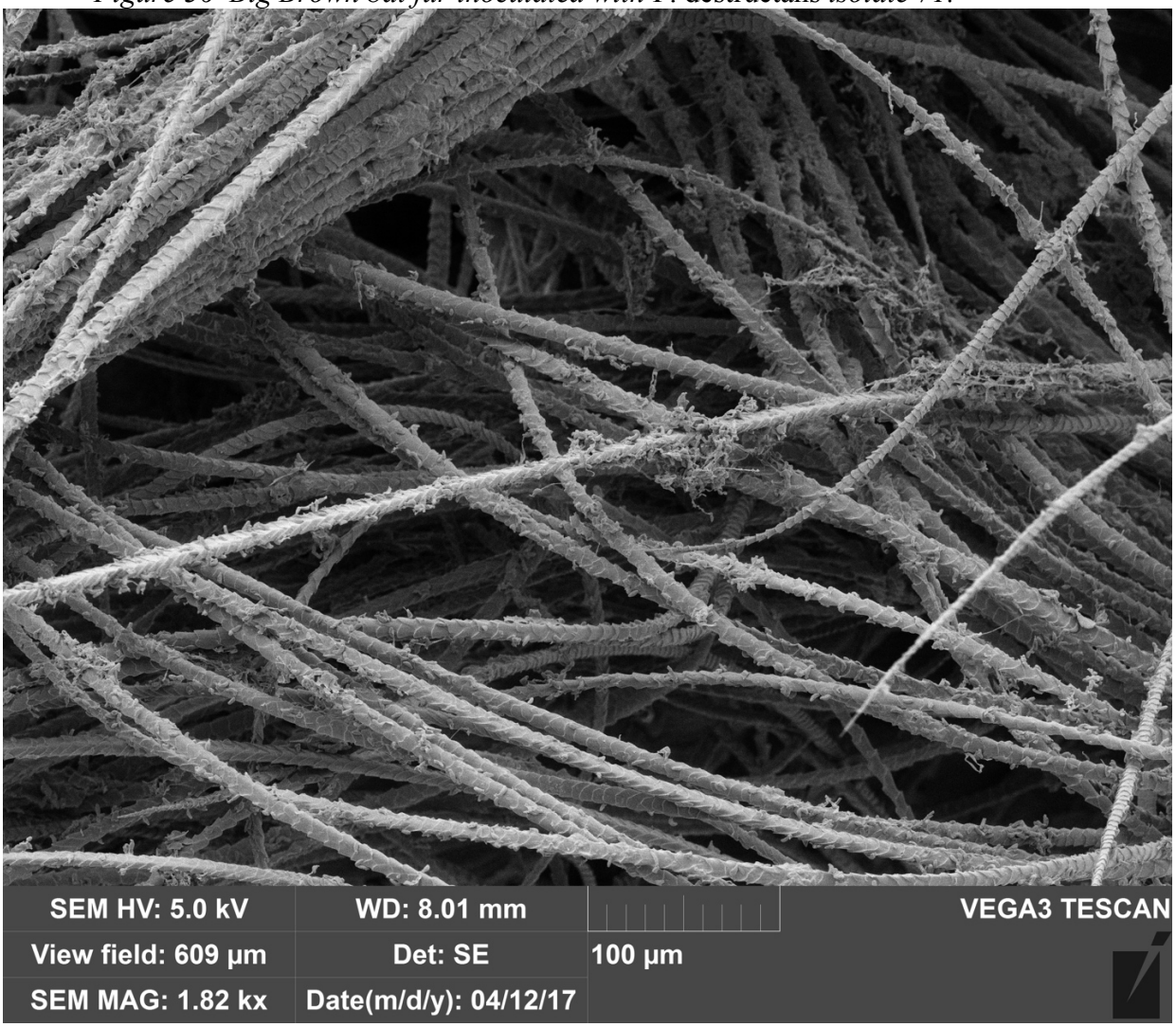

Figure 37 Big Brown Bat fur inoculated with P. destructans *isolate 71.*

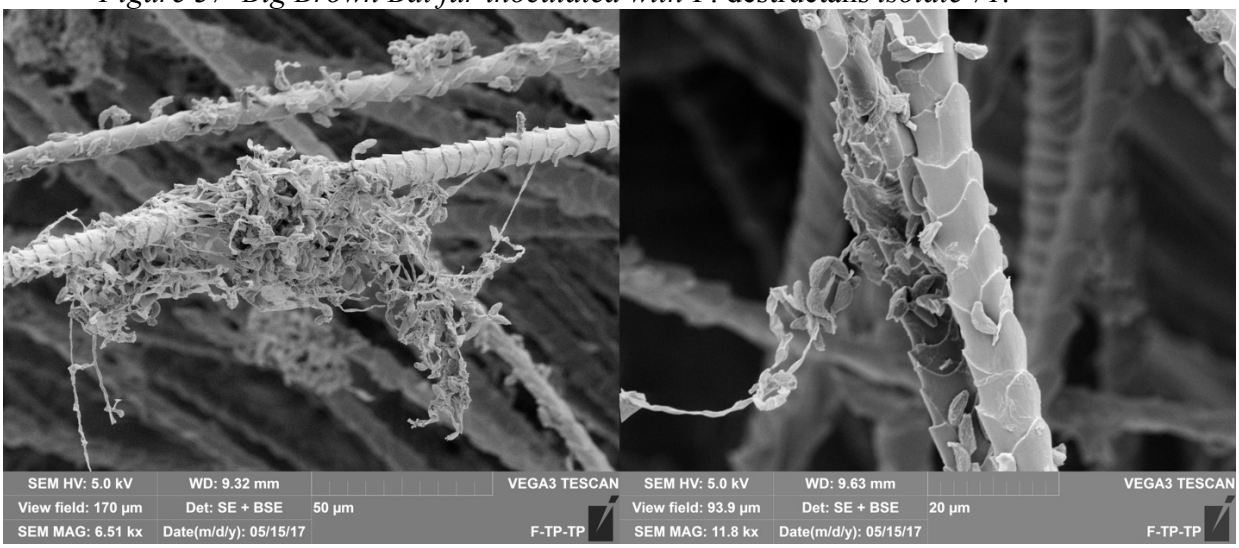

Figure 36 shows a magnification progression of *P. destructans* growing on Big Brown Bat hair. This hair sample was from an animal that had never been in contact with *P. destructans* prior to *in vitro* inoculation. The mycelia twists around the individual hairs without any sign of penetration. The growth and conidiation is pronounced enough to make the determination that there is a nutrient source for the fungus on the hair.

Figure 38 Maximum intensity projection of Live/ dead staining of Big Brown Bat hair with P. destructans *isolate 71.*

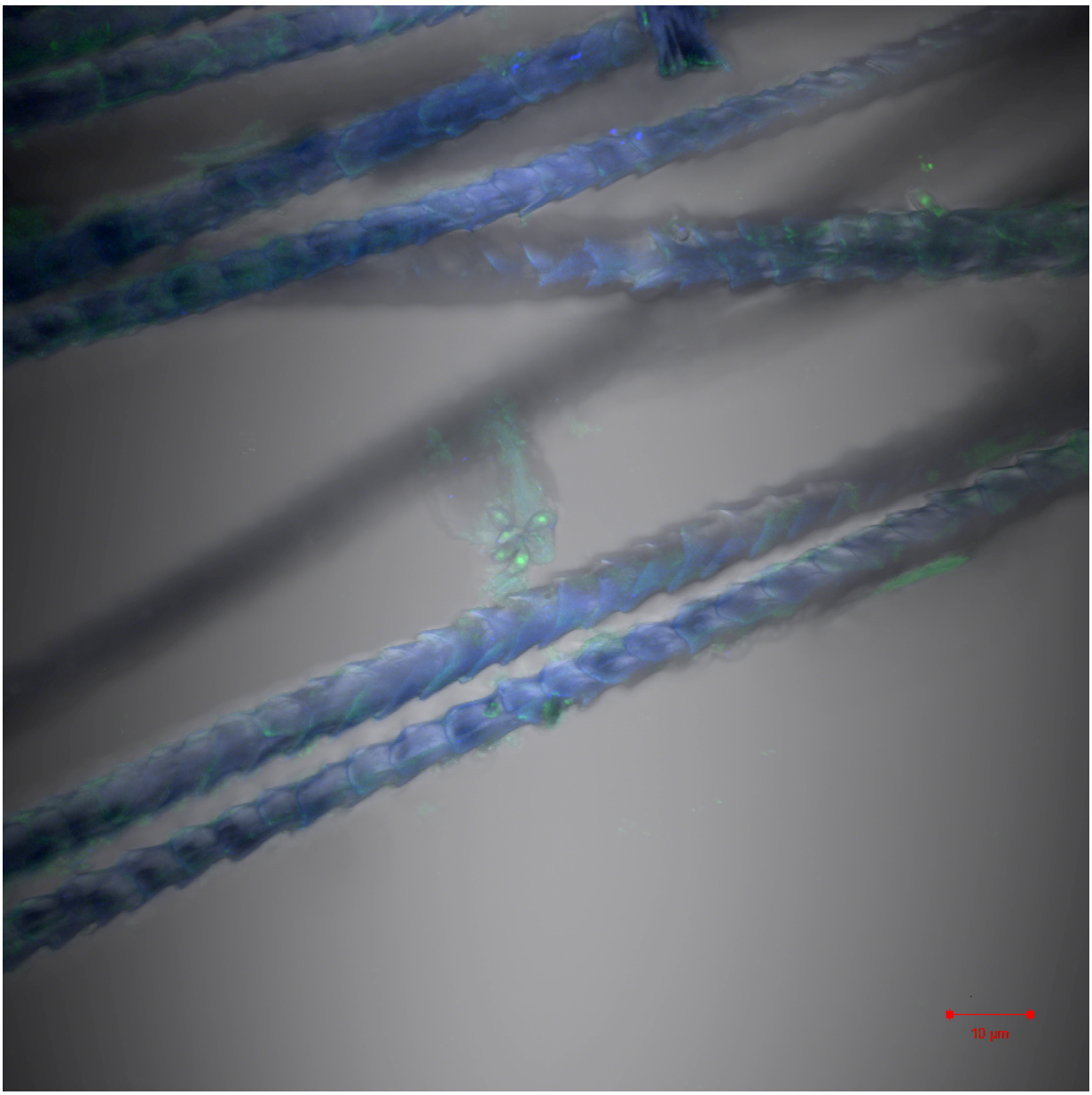

Figure 39 Maximum intensity projection of Live/ dead staining of Big Brown Bat hair with P. destructans *isolate 71.*

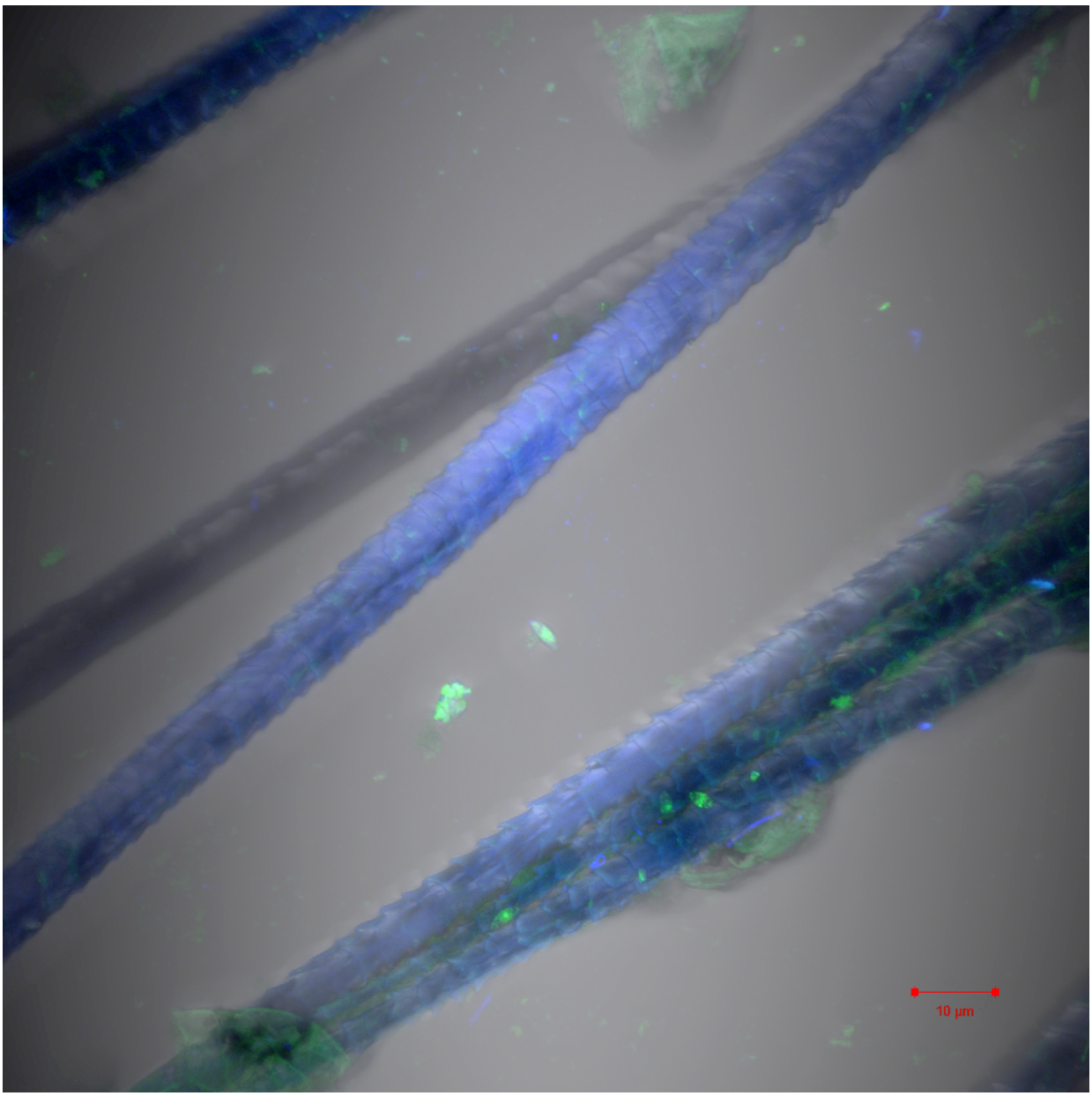

A small portion of the fur from the Big Brown Bat was taken with the purpose of determining if the *P. destructans* present was alive or dead. The calcofluor white stain used gives the bat hair the blue fluorescence. The green fluorescence is from the Syto 9 staining, indicated a live organism. It can clearly be seen where the live mycelia are wrapped around the

edges of the hair. Additionally, the conidia with intense green centers give a clear indication of being viable. As with many of the other images of *P. destructans* growing on bat hair there is no indicator of mycelial penetration into the hair.

3.5 Big Brown Bat Tissue

Figure 40 Micrograph of Big Brown Bat wing tissue with visible P. destructans *growth.*

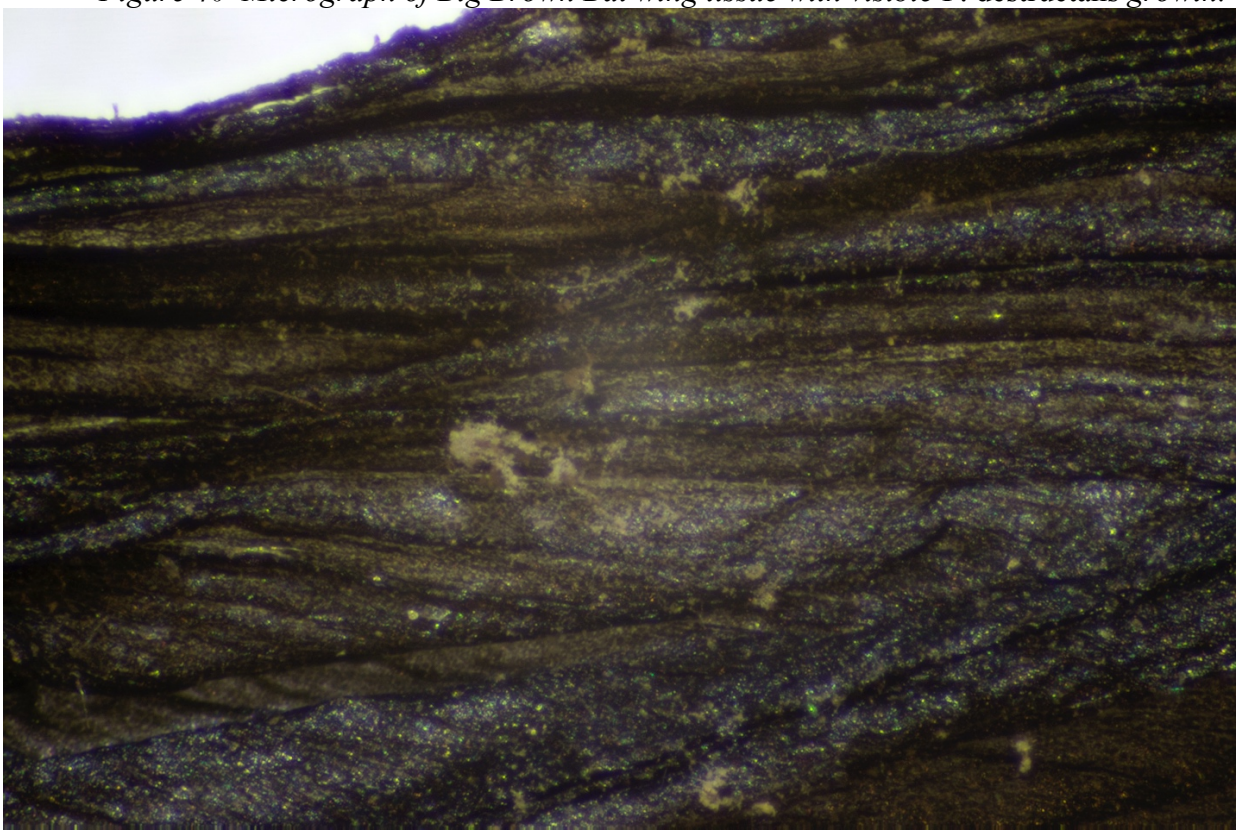

Figure 39 shows Visible *P. destructans* growth on the surface of the wing tissue.

3.6 Exudate

Figure 41 P. destructans *on SDA visible spectrum image and UV excitation.*

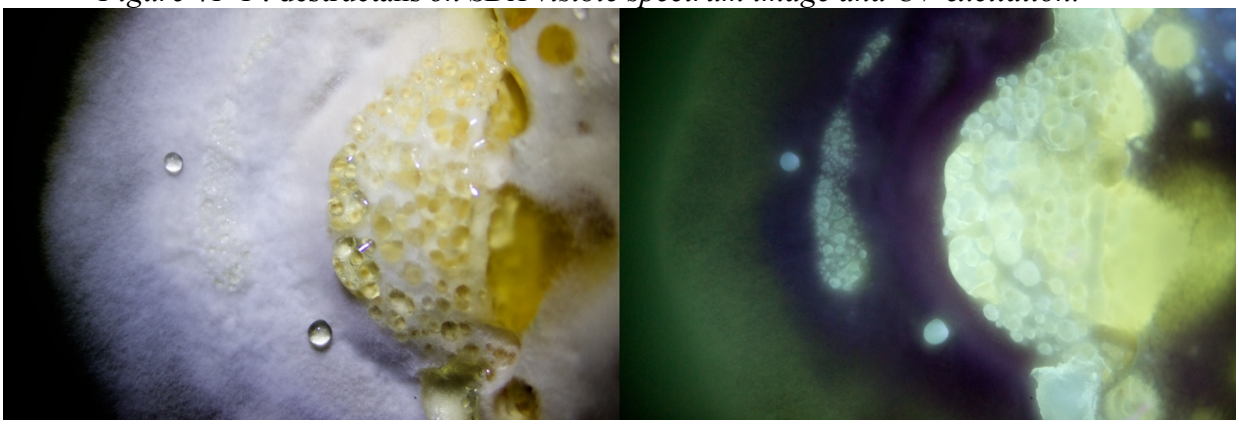

These images were taken with a stereoscope using visible illumination (A) and UV illumination.

The *P. destructans* 71 isolate was grown on SDA plates as a positive control for the lipid growth experiments. During the course of the cultures growth it was observed that an amber colored liquid was accumulating on the top of the characteristic white mycelia and is believed to be an exudate. The first observation of the exudate occurred at 26 days post plug transfer from the limited nutrient media plate used for initial growth. During UV light illumination it was seen that the areas with heavy exudate accumulation fluoresced in the spectrum of 500 to 600 nm. The mycelia appeared to have mild fluorescence but after further examination it is determined to most likely be mild reflectance of the UV light source.

Figure 42 P. destructans *grown on SDA under UV light source.*

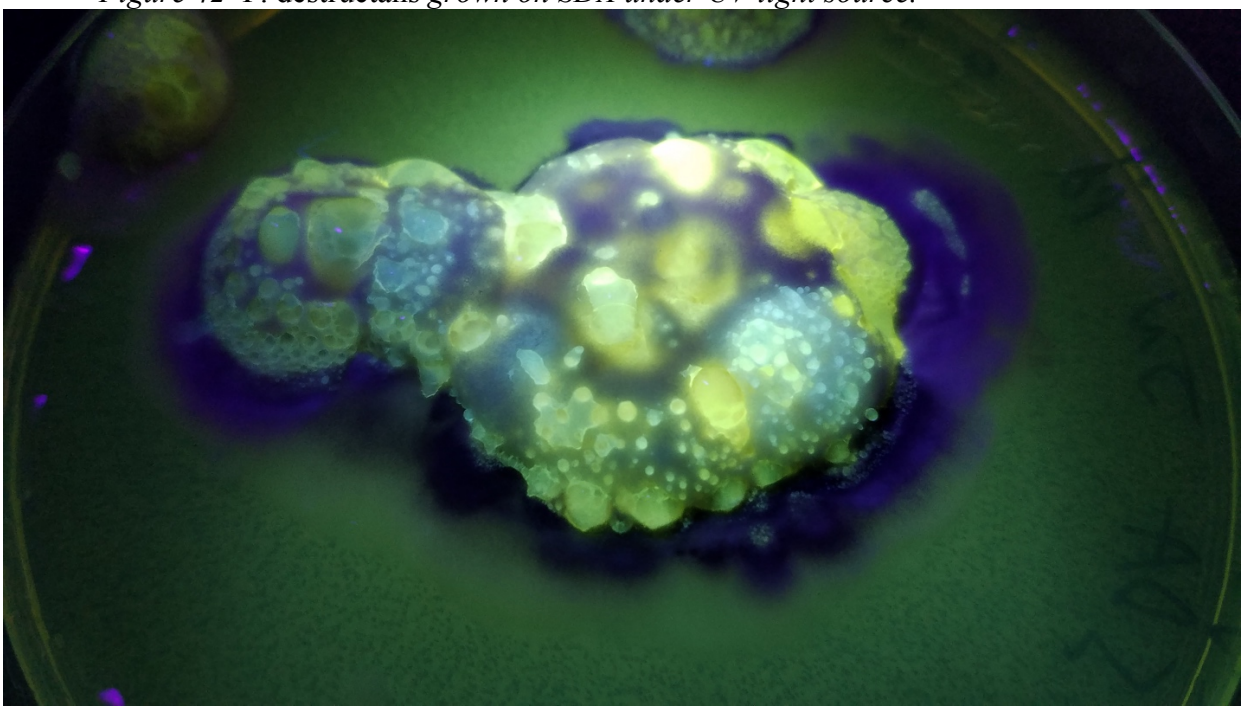

3.7 GC-MS exudate direct injection.

Table 6 P. destructans exudate GC-MS direct injection split runs.

Compound Name	**Sample A – RT/% identity**	**Sample B – RT/% identity**	**Sample C – RT/% identity**	**Sample D – RT/% identity**
Methylamine,N,N-dimethyl-	1.57/ 86.64	1.63/ 87.65	NP	1.7/ 92.39
Acetic acid	3.12/ 93.66	3.33/ 95.57	3.25/ 84.6	3.99/ 96.72
Acetic acid, methyl ester	3.66/ 86.41	3.86/ 81.38	3.78/ 61.8	4.47/ 86.44
Dehydromevalonic lactone	20.19/ 90.2	20.2/ 91.14	20.18/ 92.6	24.5/ 92.26
n-Hexadecanoic acid	51.5/ 58.10	51.51/ 83.23	NP	NP
Octadecanoic acid	57.61/ 69.3	57.6/ 63.9	NP	NP

NP – Not Present in this sample.

Table 6 shows compounds with high confidence identifications as part of the exudate through direct injection GC-MS. These samples were run on split mode thereby only allowing the higher concentration compounds to make it to the column. The deconvolution algorithm of the Agilent Masshunter software was used to aid in identifying peaks. This table concentrates on compounds that were seen in multiple samples and were examined using the same methodology. A comprehensive table of identified compounds from each sample is in the appendix.

Table 7 Classification and structure of compounds from P. destructans exudate.

Compound Name	**Compound Classification**	**Structure**
Methylamine,N,N-dimethyl-	Amine	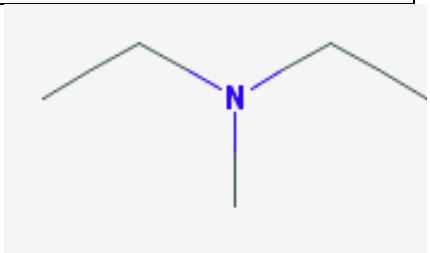
Acetic acid	esters	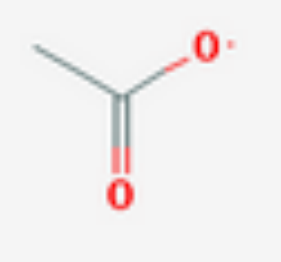
Acetic acid, methyl ester	esters	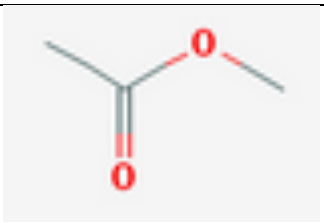
Dehydromevalonic lactone		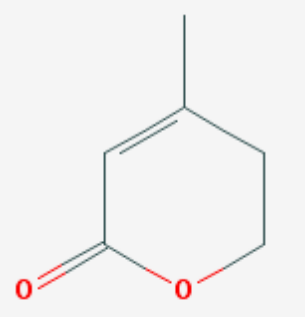
n-Hexadecanoic acid	Acids	

Octadecanoic acid	Benzenoids	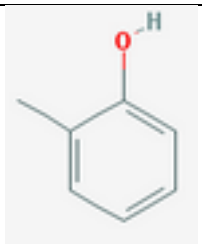

Figure 43 Exudate sample A chromatogram.

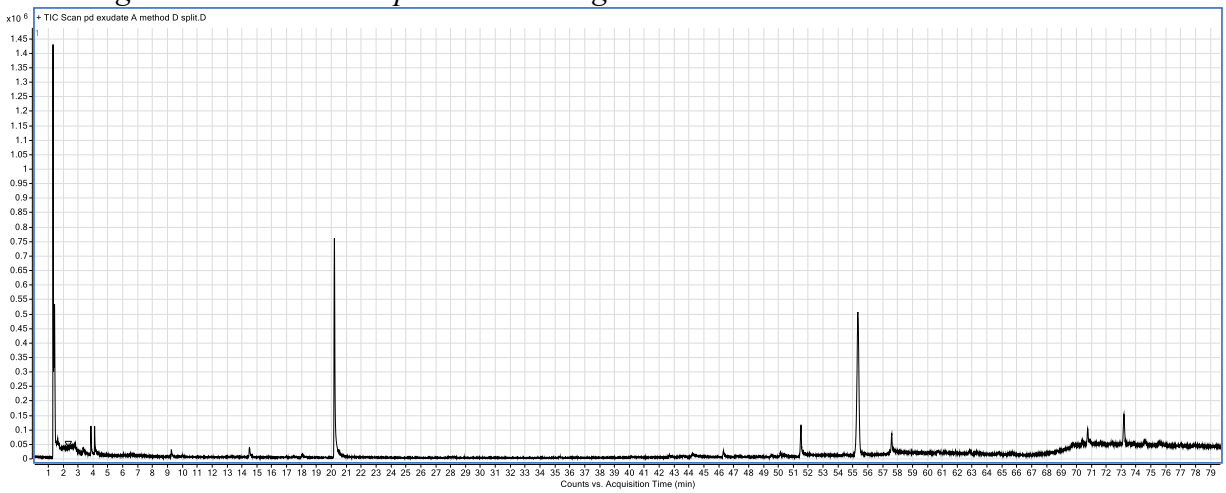

Figure 44 Exudate sample B chromatogram.

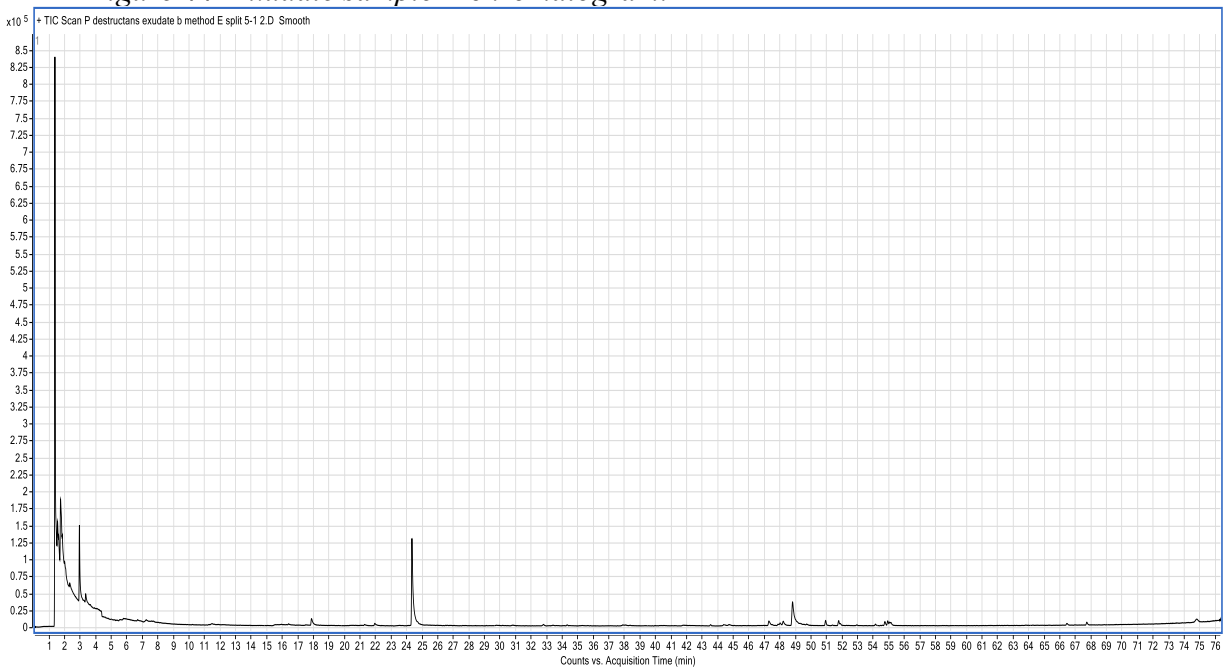

Figure 45 Exudate sample C chromatogram.

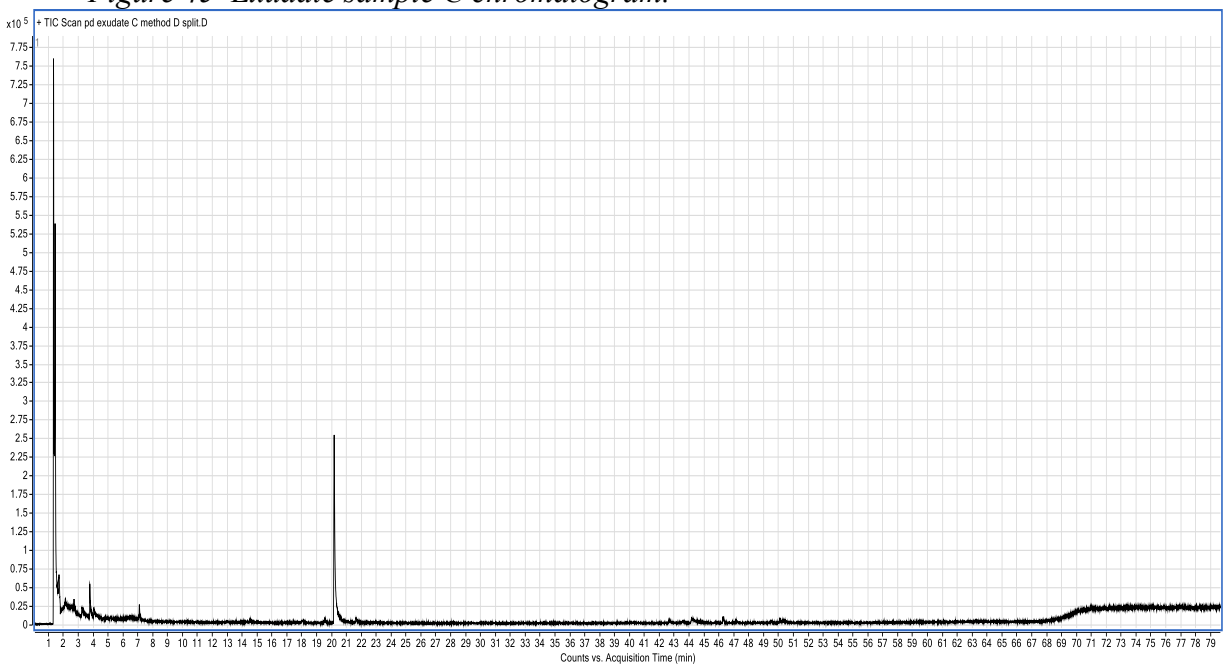

Figure 46 Exudate sample D chromatogram.

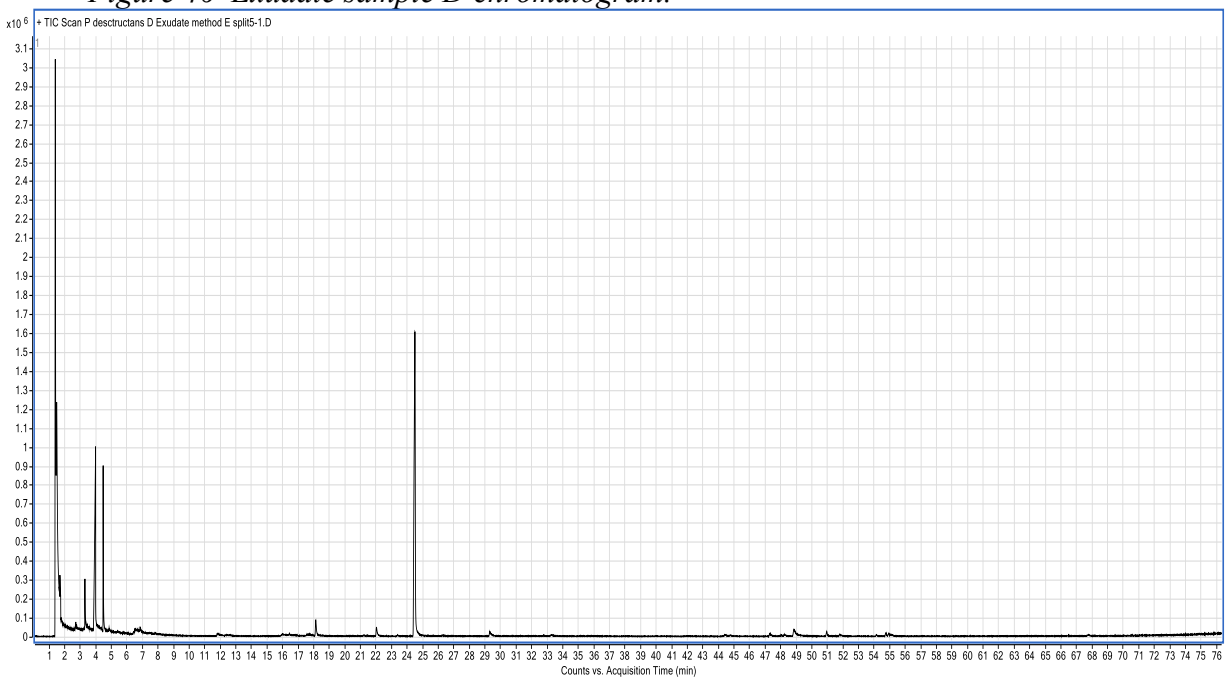

Standards

Figure 47 Acetic acid standard chromatogram.

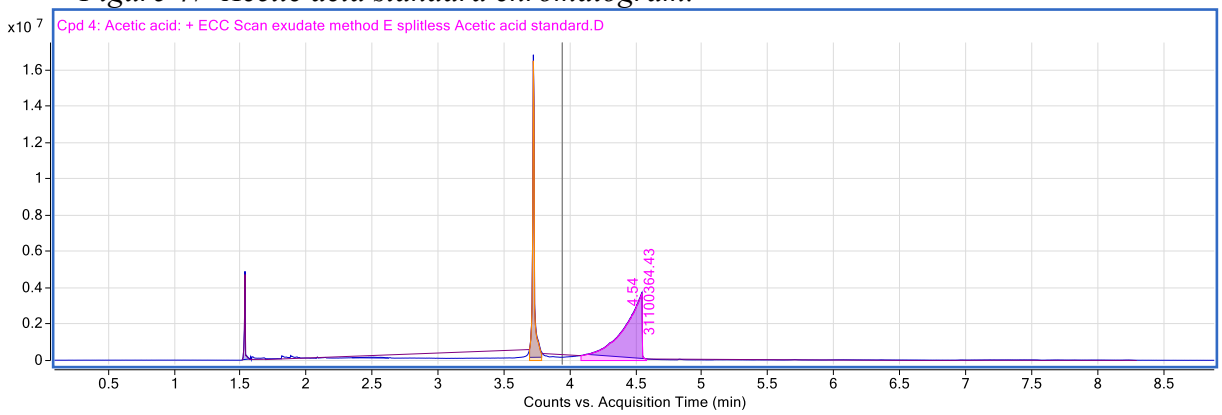

Table 8 Acetic acid standard run.

Compound Identity	Retention time	% identity
Acetic acid	3.69	97.76
Acetic acid, methyl ester	4.08	96.76

Acetic acid was the only standard used against the exudate samples. This was due to the exotic nature of many of the compounds that would require specialty synthesis by outside vendors. As table 8 shows, the retention times of the known standard correspond to the deviation that is seen in the retention times for acetic acid in the exudate (3.12-4.47, table 6). The deviation seen in retention times in the exudate samples, from those of the acetic acid standard, stems from human variability introduced by performing direct injection.

3.8 Compounds identified from SPME GC-MS analysis.

Table 9 Compounds identified from SPME GC-MS analysis.

Empty Vial.	**Big Brown Wing Control.**	***P. destructans* on Big Brown Bat wing.**	***P. destructans* producing exudate on SDA.**	***P. destructans* conidiation on SDA.**
Compound - RT	**Compound - RT**	**Compound - RT**	**Compound - RT**	**Compound – RT**
Oxime, methoxy-phenyl – 10.23	Isopropyl Alcohol – 1.51	N-methyltaurine – 1.32	2-Butanone, 3-methyl- - 2.22	Formamide – 1.43
1-Hexanol, 2-ethyl- - 16.92	1-butanol – 2.66	Methylamine, N,N-dimethyl- - 1.38	2,3-Butanedione – 2.38	Methylamine, N,N-dimethyl- - 1.45
Benzaldehyde, 2,5-bis(trimethylsily)oxy) – 22.13	Hexanal – 5.45	Toluene – 4.45	p-Menth-8-ene, 3-methylene- - 14.67	2-Butanone, 3-methyl- - 2.61
	Styrene – 8.99	2-Pentanone, 4-hydroxy-4-methyl- - 6.94	2-Methylenebornane – 15.59	Toluene – 4.51
	Nonanal – 20.96	Benzaldehyde – 12.67	Benzene, 1,3-dimethoxy- - 26.7	2-Pentanone, 3-methylene- - 19.97
	Decanal – 30.9.	Benzoic acid, 2-formyl-4,6-dimethoxy-, 8,8-dimethoxyoct-2-yl ester – 13.22	Phenol, 2,6-bis(1,1-dimethylethyl)-4-methyl-, methylcarbamate – 48.62	Benzene, 1,3-dimethoxy- - 26.44

	Butylated Hydroxytoluene – 41.0	Benzyl alcohol – 17.05		Hexane, 3,3-dimethyl- - 53.8
		Hexane, 3,3-dimethyl- - 40.49		

The compounds listed in the control columns are not comprehensive of all compounds identified. However, they are the compounds that were also detected in experiments with *P. destructans* present thereby giving the ability to discern between true mVOCs and substrate background.

Table 10 Classification and structure of VOC compounds identified from SPME GC-MS.

Compound Name	Compound Classification	Structure
N-methyltaurine		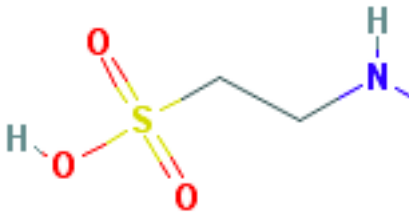
Methylamine, N,N-dimethyl- -		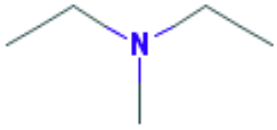

Toluene	Benzenoids	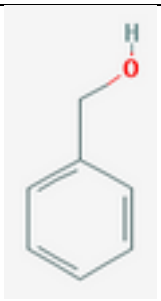
2-Pentanone, 4-hydroxy-4-methyl-		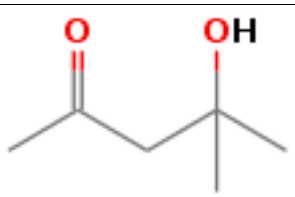
Benzaldehyde	Benzenoids	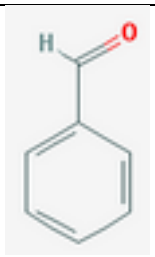
Benzoic acid, 2-formyl-4,6-dimethoxy-, 8,8-dimethoxyoct-2-yl ester		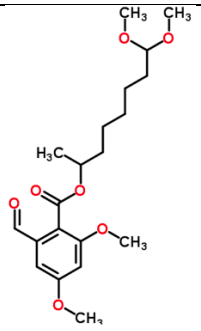
Benzyl alcohol	Benzoids	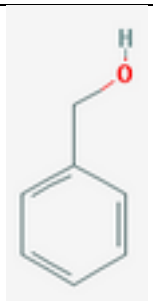
Hexane, 3,3-dimethyl-	Alkane	

		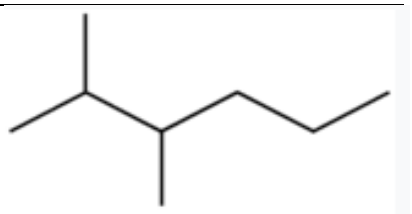
2-Butanone, 3-methyl	Ketones	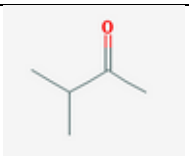
2,3-Butanedione	Ketones	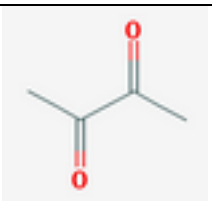
p-Menth-8-ene, 3-methylene		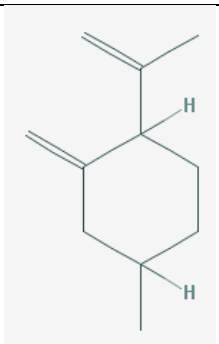
2-Methylenebornane		
Benzene, 1,3-dimethoxy	Benzenoids, ethers	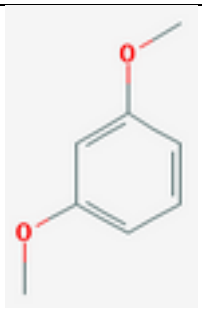

Phenol, 2,6-bis(1,1-dimethylethyl)-4-methyl-, methylcarbamate (Carbamic acid)	Thiocarbamides	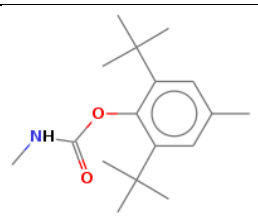
Formamide	Amides	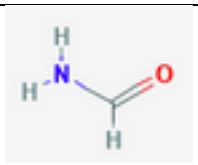
2-Pentanone, 3-methylene	Ketone	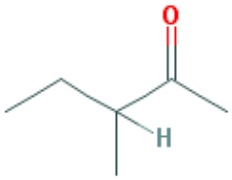

Figure 48 Chromatogram for empty vial control, SPME.

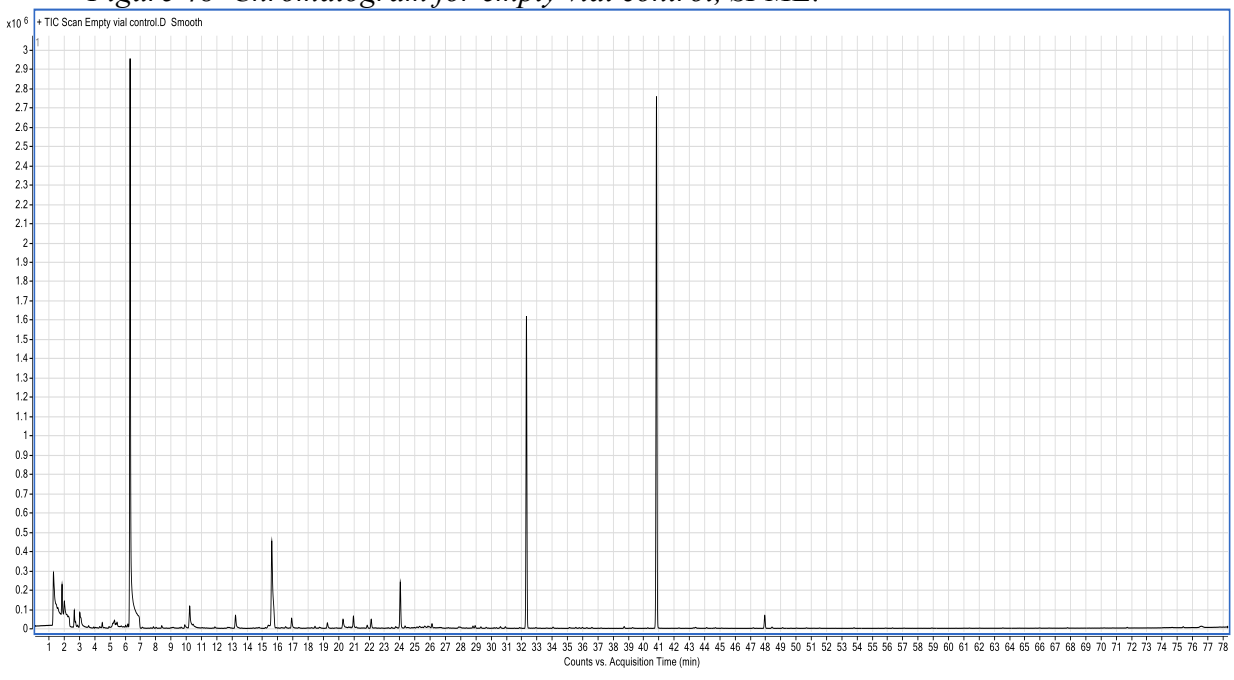

Figure 49 Chromatogram for wing tissue control, SPME.

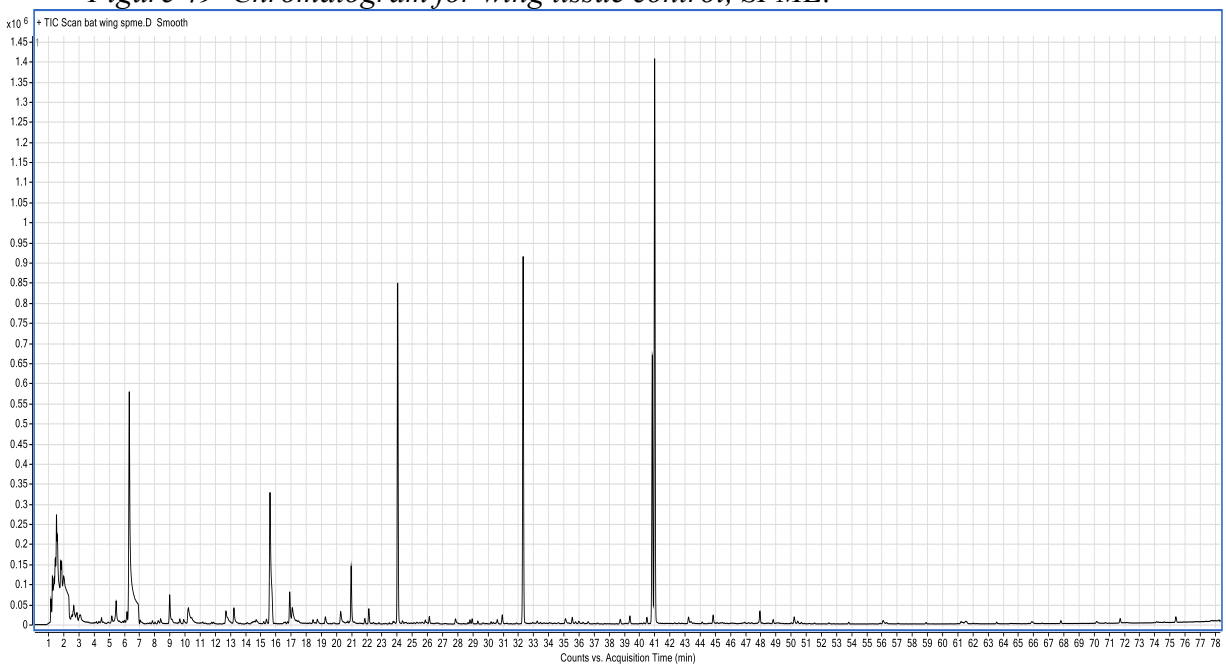

Figure 50 Chromatogram for P. destructans on Big Brown Bat wing, SPME.

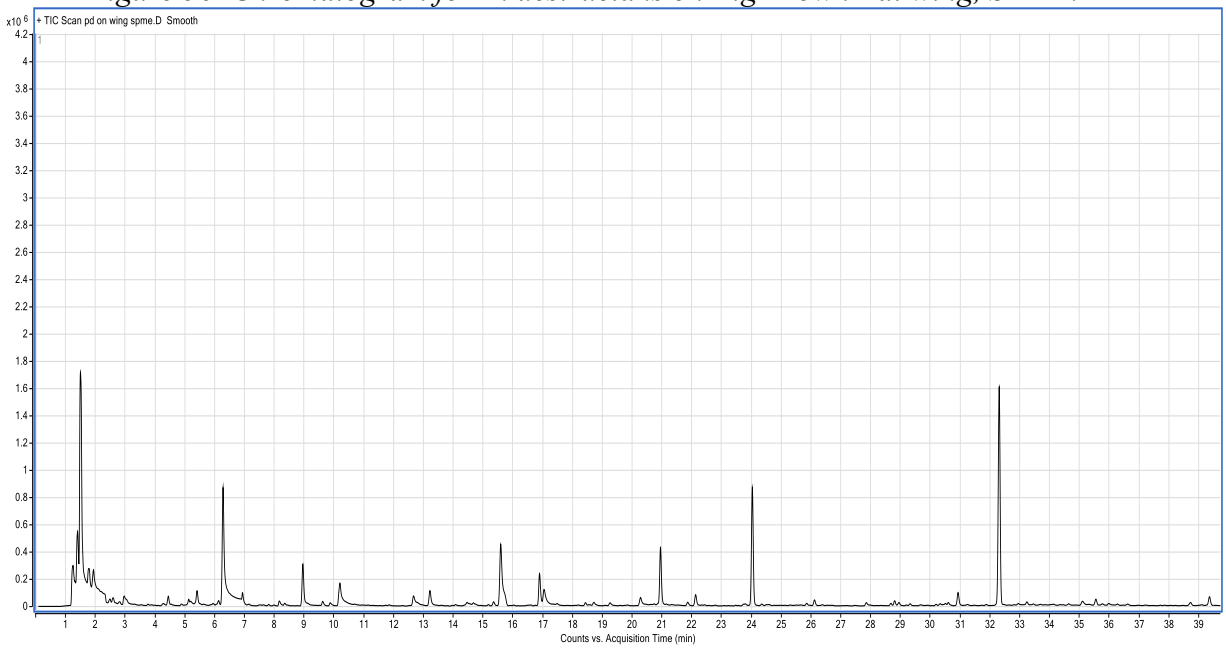

Figure 51 Chromatogram for P. destructans producing exudate (sample B) on SDA, SPME.

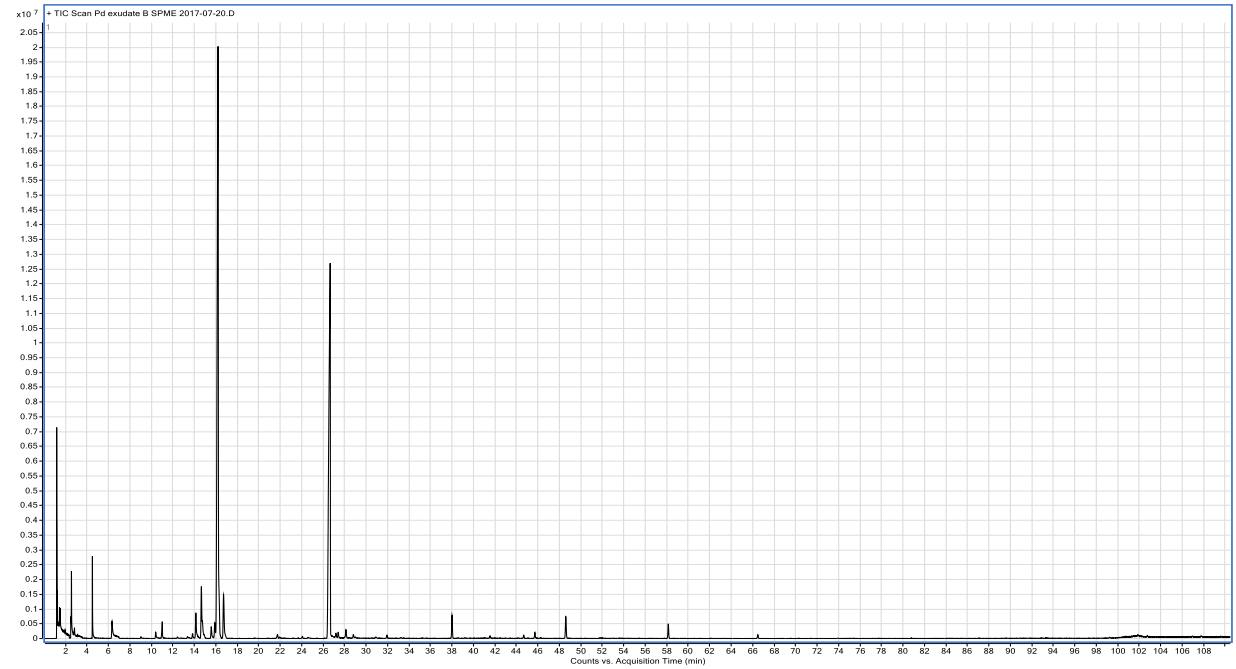

Figure 52 Chromatogram for P. destructans *heavy conidiation, SPME.*

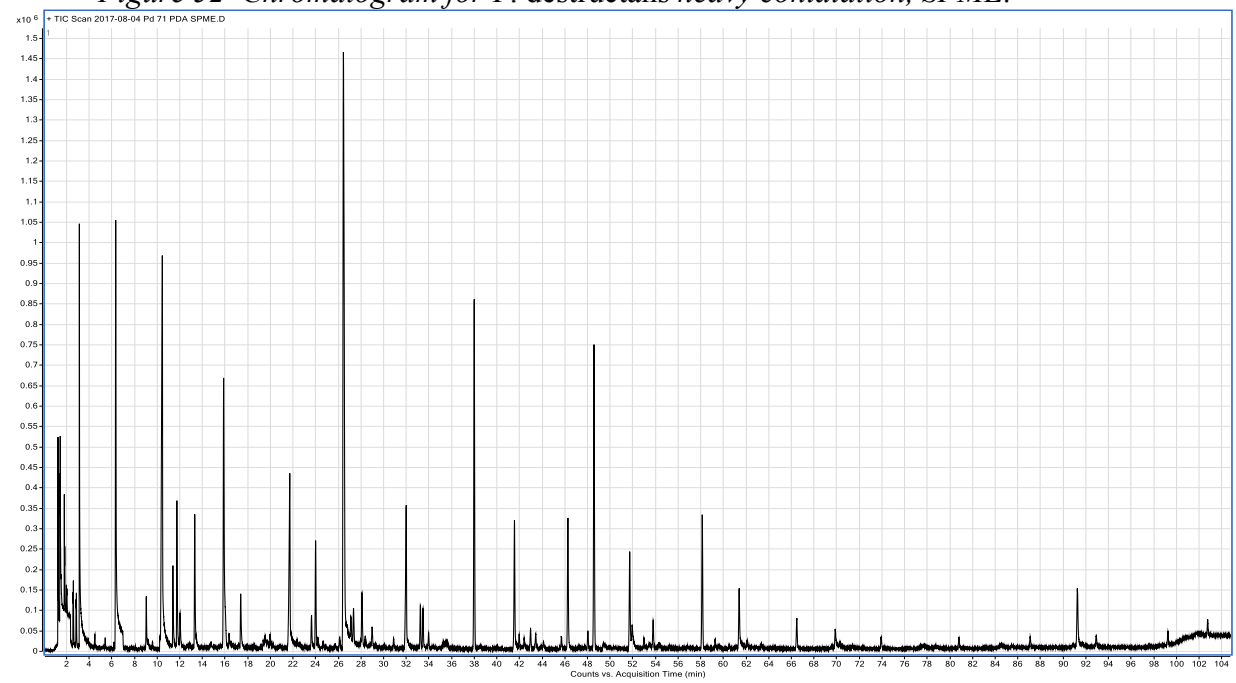

Chromatograms correspond to the data in table 9. Large peaks that are not listed in the data tables are siloxanes that are associated with material that is part of either the SPME fiber or the column.

Figure 53 Section of Big Brown Bat wing with P. destructans *growth used for GC-MS experiment.*

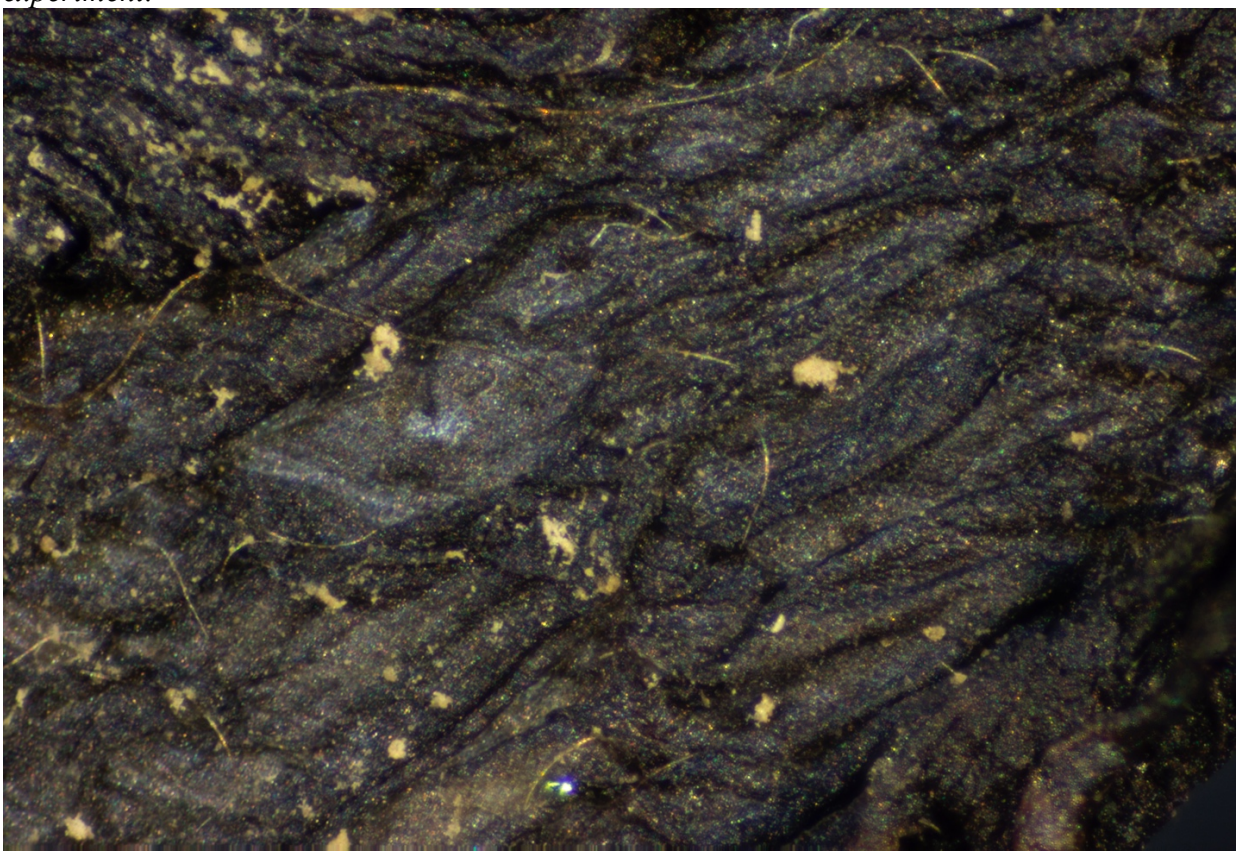

4 DISCUSSION

4.1 in vitro lipid growth experiments

The three most prevalent fatty acids in bat wing sebum were used as sole carbon sources for *in vitro* growth experiments. Using a defined media formulated for *Aspergillus* sp. growth experiments, the optimum carbon concentration for *in vitro* growth was determined using glucose and was determined to be 5 grams per Liter. An equivalent carbon quantity was determined for oleic, palmitic and stearic acids. Radial growth from plugs of *P. destructans* in each of the fatty acid media formulations was tracked for 70 days while incubated at 14°C.

The final mean area of radial growth from each media type was compared using a one way ANOVA and Tukeys test. None of the groups exhibited significantly different growth from the control group on SDA. The implication of this growth experiment is that *P. destructans* can utilize any of the three most common fatty acids in sebum as well as it can an enriched media source.

The article by Frank et al. in 2016 proposed that myristic acid and stearic acid significantly reduced the growth of *P. destructans* at 10.5 ^{0}C but not at 4-5 ^{0}C. Additionally, they claim that oleic and palmitoleic acids greatly reduced the growth of *P. destructans* at both temperatures. There are fundamental flaws in the methodology used in their growth experiments that invalidate their claims. The most critical flaw is that the fatty acids were added to an enriched media source (SDA) to test inhibition of growth. Utilization of sugars and lipids are two different pathways in fungi. Uptake of lipids through beta-oxidation into the glyoxylate pathway is slower than sugars through glycolysis. However, lipids once broken down provide much more energy than sugars. As this research has shown, the nutrient rich SDA plates have a faster initial growth but the lipid plates will eventually have greater growth (Fig. 23).

Combining the nutrient sources will split the organism's resources and reduce the growth rate. In a direct comparison of growth it may appear the addition of fatty acids provide an inhibitory effect however this view lacks an understanding of the complicated metabolic processes that are in effect in *P. destructans*.

Furthermore, experimental plates were inoculated from growth plates incubated at a higher temperature (12 ^{0}C) than any of the experimental groups (5 and 10.5^{0}C). It has been established that the optimal growth of *P. destructans* occurs between 12.5 and 15.8 ^{0}C (Verant et al., 2012). Utilization of lower temperatures, while in line with those seen during field conditions, will have an impact upon growth rates and possibly on physiological abilities. Additionally, inoculation was accomplished using loops that were then streaked on experimental plates. Using a streak method introduces significant variability from one inoculation area to another by way of an unknown number of conidia or quantity of mycelia being transferred. These factors that contribute an unknown level of variability into their experiments are important to point out due to it being a published and cited work that directly contradicts this work.

It is clear that the main components of sebum do not contain any compounds that may be inhibitory host factors that can slow the growth of *P. destructans*. Unfortunately, from the in vitro growth experiments it appears that sebum may contribute heavily to growth. Additionally, as the confocal images show C-16 and C-18 fatty acids are a predominant component of the bat wing membrane thus providing even more substrate to *P. destructans* while it has an active glyoxylate cycle.

4.2 LSCM of bat wing tissue

Wing punches from tri-color bats located in Osbourne Cave and Paulding mine were taken for examination of C-16 and C-18 fatty acid distribution using LSCM. Bodipy FL fluorescent stain co-localizes with C-16 fatty acids while Bodipy 500 localizes with C-18. The stains could not be used in conjunction due to overlapping spectra thereby requiring analysis of separate samples with the understanding that there is minor variability from one individual to another. A clear pattern is visible from the Bodipy FL to 500 stained samples. At the center of the wing membrane cells there is a large spot of unstained tissue on the Bodipy 500 samples indicating a lack of C-18 fatty acids in these locations. Granted, these are not quantitative measurements of the fatty acids present. However, they do suggest a pattern of distribution in wing membrane cells.

The presence of C-16 and C-18 fatty acids is highly dispersed across wing membranes providing an excellent substrate for *P. destructans* growth and reproduction. As figures 21 and 22 show, from the in vitro experiments, both of these fatty acid types provide enough carbon for growth. In fact, the growth rate on these fatty acids is as high if not higher than with an enriched source such as SDA. Furthermore, the tissue used for these images as part of the staining process went through multiple wash steps that would have removed most if not all of the surface lipids present in the sebum. The living host would be producing sebum rich in fatty acids that *P. destructans* can utilize for growth. Once *P. destructans* has penetrated the tissue, as these images show, there is still a large area of fatty acids that can be utilized. Furthermore, once death of the host occurs the fatty acids in the wing tissue can provide energy for the fungi to persist.

4.3 Bat fur

As part of the Big Brown Bat wings samples provided there was a portion of the forearm that was covered in fur. A portion of the forearm was removed from the rest of the wing inoculated with *P. destructans* and subjected to the same incubation conditions as the wing membrane. The fur of the forearm was examined using wide-field, scanning electron, and laser scanning confocal microscopy for growth of *P. destructans*.

All images showed heavy mycelial growth over tufts of hair and curled along the length of the individual hairs. The bat had never been exposed to *P. destructans* prior to *in vitro* inoculation. Therefore, resulting growth indicates a suitable substrate for growth and energy is present. The widefield images at 1000x magnification (Figure 34) show conidia formation with no penetration into the hair. Previous research into *P. destructans* exo-enzymes is inconclusive on keratinase production. (Raudabaugh and Miller, 2013). The ability to penetrate into the individual hairs would be a strong indicator that a keratinase enzyme is being used to degrade the hair into a usable substrate for growth. While these images do not provide conclusive evidence that *P. destructions* does not produce keratinase they do suggest that if production is present the activity is extremely weak and cannot transform the bat hair into a usable substrate.

None of the wide-field or SEM images (Figures 35 and 36) show penetration into the hair or the hair being degraded in any way. They do show a pattern of the mycelia coiling around the hair as mycelial extension occurs. Both image types show a significant amount of conidiation present. The ability of *P. destructans* to propagate on just fur has serious impact on disease transmission and infection testing. Therefore, a subsample of the inoculated hair was fluorescently stained to test for viability. Fluorescent viability staining was performed on a hair sample with visible mycelial and conidia growth. The images (Figures 37 and 38) indicated,

through green fluorescence, that the mycelia that was wrapped around hair and the conidia were viable. This provides more evidence that without utilization of the hair as a substrate the sebum present on the hair is providing the needed nutrients for *P. destructans* growth and reproduction.

Utilization of the sebum present on hair for growth and reproduction has implications for transmission of WNS. Growth on hair does not have any direct health impact upon the host. However, as the images show growth can be quite heavy thereby providing a substantial amount fungal mass that can be shed into hibernacula or directly onto another bat. This allows for bats that do not have penetrative infections into delicate wing tissue to be a vector and contribute to the continuation of the WNS disease cycle.

4.4 Exudate

During the course of fatty acid growth experiments the noticeable phenomena of exudate production was observed on the SDA control plates (Figure 17). These were the only plates that were seen to have exudate production leading to the idea that with all other growth variables being the same across the experimental groups that it is the enriched nutrient source that allowed for this production. Upon further investigation of the exudate it was determined that this is an important time point in *P. destructans* life cycle and the WNS disease cycle due to the fluorescence of the exudate and the associated VOCs produced.

Figure 54 Comparison of UV trans-illumination and in vitro *imaging.*

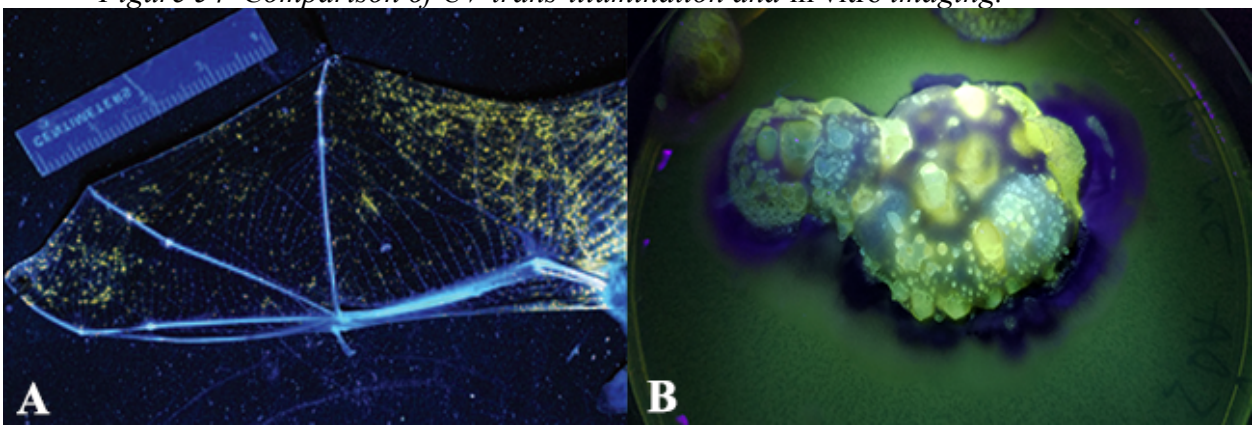

In the paper by Turner et al. in 2014 the diagnostic method of using UV light to detect fluorescence from a WNS infection was proposed. This became a standard methodology among ecologists and wildlife biologists working with WNS infected bats. However, from our investigation it can be shown that this is an ineffective diagnostic method due to the high number of false negative results. The fluorescence seen in Figure 53A, as Turner describes, emits orange-yellow (600-650nm) fluorescence. This is the same region of the light spectrum that the exudate produced by our *P. destructans* cultures grown *in vitro* exhibited fluorescence (Figure 53). Additionally, as seen in the images where *P. destructans* was grown *in vitro* and was exposed to UV illumination the mycelia had a purple hue whereas *P. destructans* photographed *in vivo* on a bat wing was not visible in images. This supports the idea that the *in vitro* images exhibit the color purple due to the UV light reflecting back from the mycelia with energy loss expanding the wavelengths into the 425-450nm range and is not fluorescent.

Further evidence supporting the ineffectiveness of UV trans-illumination as a diagnostic method comes from a direct comparison to qPCR. In the paper by McGuire et al. *in vitro* infected bat wing samples were subjected to UV detection and qPCR. The UV illumination only

had a 73% to 83% success rate of identifying *P. destructans* infected tissue whereas qPCR correctly identified all samples.

With the *in vitro* growth experiments suggesting a higher quantity of nutrients being needed or possibly a specific combination that is not always present for exudate production to occur there is a significant portion of the WNS disease cycle in which an infection cannot be detected. During initial infection and even during reproduction it is unlikely the exudate will be produced. As it was seen in the growth experiments, even with ideal nutrient conditions it was 26 days after being transferred on to SDA before there was visible exudate production.

4.5 GC-MS exudate

The production of an exudate observed during *in vitro* growth presented the opportunity for examination in to physiological phenomena that can be attributed to a high nutrient content substrate. As it has already been established, the exudate is the compound that fluoresces under UV excitation and has been inaccurately used for WNS infection diagnosis. Being a known marker of the disease makes it a critical time point in the overall disease cycle to investigate. Therefore, the exudate was analyzed using GC-MS to identify VOCs associated with exudate production (table 6).

The GC-MS results showed acetic acid and methyl ester-acetic acid as being a component of the exudate. This is not an unexpected result based upon *P. destructans* saprophytic nature. Many filamentous fungi are known to have the capability to adjust the pH of their environment to aid in utilization of a substrate. This is particularly true for organisms that can degrade cellulosic materials (Liaud et al., 2014). Furthermore, the alteration of pH on the bat wing may be one of the direct reasons for the changes seen in the composition of the wing

microbiome. A recent study characterized the microbiome of wings with and without having a WNS infection showing there is an alteration in the microbes present (Lemieux-Labonte et al., 2017).

The last two identified compounds were the fatty acids, n-hexadecanoic acid and octadecanoic acid. While the body of this research focuses on accumulation of free fatty acids to fuel growth and provide energy *de novo* production of free fatty acids on a glucose rich substrate can be an accompanying trait often seen in fungi. As the exudate production was seen to occur on enriched substrate of SDA it is not an unexpected result to see free fatty acids in the exudate.

The compound N,N-dimethylamine has no identifiable association to mVOCs produced by other fungi.

The compounds identified through direct injection GC-MS are not comprehensive of the components of *P. destructans* exudate. Alternative methods of analysis are required to make an exhaustive profile. Alternative columns and LC-MS profiling would be excellent methods to further this research.

4.6 GC-MS SPME

Profiling of microbial VOCs has been gaining attention and is becoming a more widespread research technique. It already has a solid foundation in food research where aromas associated with products are of the utmost importance for commercializing a product. Some research groups have used characterization of an organisms VOC production as means of identification. Also, the health impact of indoor air quality and VOCs associated with mold is a major area of research in human health. However, the studies that have the potential to have the

greatest impact on WNS research are the recognition and investigation into the role VOCs play on cell signaling.

This research provides an introductory profile of the mVOCs produced by *P. destructans* at significant time points in the growth cycle. The VOC sampling was conducted using a SPME fiber in a controlled headspace with a section of a Big Brown Bat wing, A Big Brown Bat wing with *P. destructans* growth, *P. destructans* on SDA while producing an exudate, and *P. destructans* on SDA with heavy conidiation. The VOCs identified at these time points are high confidence identifications based upon their spectra match in the NIST database.

GC-MS headspace analysis was conducted on a uninnoculated section of Big Brown bat tissue as a control to isolate volatiles produced by *P. destructans* from those associated with decomposing wing tissue. In the work by Cablk et al. tissue from cows, chickens, pigs and humans were analyzed for VOCs. Volatiles that were associated with the bat tissue and also identified in the Cablk study were Hexanal, Nonanal, and Decanal. The literature also showed many tissues produced Toluene during decomposition. Toluene was detected only on the bat tissue inoculated with *P. destructans*. Research has associated Toluene with mVOC production by *Stachybotrys chartarum* during indoor air quality studies (Betancourt et al., 2013). Further experiments will be needed to determine if toluene is being produced by the substrate or organism.

Not all compounds listed in table 9 can be identified in the literature as being a microbally produced VOC. This could be due to its rarity as a mVOC and there has not been a published study on the topic to date. However, the most likely reason is due to changes in the compound during thermal deabsorption in the inlet, which is 250^0C. High temperatures can sheer functional groups or degrade a compound. Lastly, the identifications are based upon the

NIST spectral database where isomers and slightly differing bond structures cannot always be properly associated with a compound identification leading to a best possible identification that isn't always correct.

During the headspace analysis of the sample of *P destructans* growing on the Big Brown bat wing the compound benzaldehyde was identified. It is known as an aroma compound that is similar to bitter almonds and is known to be produced by *Bjerkandera adusta* (Lapadatescu et al., 1997). Another aroma volatile, Benzoic acid, 2-formyl-4,6-dimethoxy-, 8,8-dimethoxyoct-2-yl ester, has not been previously associated with microbial production but with the freshness of cabbage (Barry-Ryan et al., 2009).

For the *P. destructans* sample on SDA that was actively producing exudate 3-methyl- 2-Butanone was identified in the headspace and is a compound that has been identified as an aroma extract (Micheluz et al., 2016). Additionally, it has been identified in VOC profiling from *A. flavis* aflotoxin positive and negative strains (Jurjevic et al., 2008)

Furthermore, 3-methyl-2-butanone, a ketone, has been previously identified as a mVOC produced by the species *Aspergillus Versicolor, Chaetomium Globosum, Eurotium Amstelodami,* and *Penicillium Brevicompactum* and associated with indoor air quality studies (Schleibinger et al., 2005). Additionally, 3-methyl-2-butanone has been shown in studies as a VOC compound that can induce SOS activity in prokaryotic cells (Nakajima et al., 2006). The *umu* tests used to make this determination are a precursor to a modified version that determines genotoxicity in humans from VOCs. This may have health implications for WNS infected bats not only due to the possibility of genotoxicity, especially when large clusters of bats hibernate packed together, but also to the possible damage that may occur to their natural skin microflora. Lastly, the

compound has also been identified as being produced by a number of *Trichoderma* species that exhibit a complex VOC profile that can promote plant growth (Lee et al., 2016)

The compound 2-Methylenebornane is a mVOC that has been associated with *Penicillium crustosum* in studies of delineating species specific volatile profiles in a compost facility (Fisher et al., 1998). Benzene, according to the mVOC database is produced by *Penecillium* sp.. Additionally, it was reported that *Aspergillus versicolor* produced benzene as VOC when utilizing wall paper as a growth substrate (Matysik et al., 2008)

The majority of VOCs identified in this study have previously been associated with either poor quality air or an aroma. This leaves the topic of cell signaling by *P. destructans* untouched. Of the known purposes of VOC production by fungi this topic is the one that may have the greatest impact upon WNS by giving targets for treatment.

REFERENCES

Barry-Ryan, C., M. Devereux, and J. Lonchamp. 2009. Identification of volatile quality markers of ready-to-use lettuce and cabbage. Food Research International. 42:1077-1086.

Bat Conservation International. 2017. http://www.batcon.org/our-work/regions/contact-bci/usa-canada/white-nose-syndrome.

Betancourt, D., T. Dean, M. Menetrez, and S. Moore. 2013. Characterization of Microbial Volatile Organic Compounds (MVOC) Emitted by Stachybotrys chartarum. BMC Microbiology. 13:1-10.

Bolker, M., and R. Kahmann. 1993. Sexual Pheromones and Mating Responses in Fungi. The Plant Cell. 5:1461-1469.

Chaturvedi V., D. Springer, M. Behr, R. Ramani, X. Li, M. Peck, P. Ren, D. Bopp, B. Wood, W. Samsonoff, C. Butchkoski, A. Hicks, W. Stone, R. Rudd, S. Chaturvedi. 2010. Morphological and Molecular Characterizations of Psychrophilic Fungus Geomyces destructans from New York Bats with White Nose Syndrome (WNS). PLOS ONE. 5:1-12.

Ding, Z., L. Li, Q. Che, D. Li, Q. Gu, and T. Zhu. 2016. Richness and bioactivity of culturable soil fungi from the Fildes Peninsula, Antarctica. Extremophiles. 20:425-435.

Eskew, E. and B. Todd. 2013. Parallels in amphibian bat declines from pathogenic fungi. Emerging infectious diseases. 19:379-385.

Fenton, M. 2012. Bats and white-nose syndrome. PNAS. 109:6794-6795.

Fischer, G., R. Schwalbe, M. Moller, R. Ostrowski, and W. Dott. 1998. Species-specific production of microbial volatile organic compounds (MVOC) by airborne fungi from a compost facility. Chemosphere. 39: 795-810.

Frank, C., M. Ingala, R. Ravenelle, K. Dougherty-Howard, S. Wicks, C. Herzog, and R. Rudd. 2016. The Effects of Cutaneous Fatty Acids on the Growth of Pseudogymnoascus destructans, the Etiological Agent of White-Nose Syndrome (WNS). PLOSone. 11:1-15.

Gabriel, K. 2017. Biomimicry of Volatile-based microbial control for mitigating fungal pathogenicity. Dissertation, Georgia State University.

Johnson, I., H. Kang, and R. Haugland. 1991. Fluorescent membrane probes incorporating dipyrrometheneboron difluoride fluorphores. Anal. Biochem.198:228–237.

Jurjevic, Z., G. Rains, D. Wilson, and W. Lewis. 2008. Volatile metabolites associated with one aflatoxigenic and one nontoxigenic Aspergillus flavus strain grown on two different substrates. Phytopathologia Mediterranea. 47:266-271.

Kafer, E.. 1977. Meiotic and mitotic recombination an Aspergillus and its chromosomal aberrations. Advances in Genetics. 19:33-131.

Zukal, J., H. Bandouchova, J. Brichta, A. Cmokova, K. Jaron, M. Kolarik, V. Kovacova, A. Kubatova, A. Novakova, O. Orlov, J. Pikula, P. Presetnik, J. Suba, A. Zahradnikova, and N. Martinkova. 2016. White-nose syndrome without borders: Pseudogymnoascus destructansinfection tolerated in Europe and Palearctic Asia but not in North America. Nature/Scientific Reports. 6:1-18.

Lapadatescu, C., G. Feron, C. Vergoignan, A. Dijian, A. Durand, and P. Bonnarme. 1997. Influence of cell immobilization on the production of benzaldehyde and benzyl alcohol by the white-rot fungi Bjerkandera adusta, Ischnoderma benzoinum and Dichomitus squalens. Applied Microbiology and Biotechnology. 47:708-714.

Lee, S., M. Yap, G. Behringer, R. Hung, and J. Bennett. 2016. Volatile organic compounds emitted by *Trichoderma* species mediate plant growth. Fungal Biology and Biotechnology. 3:1-14.

Lemieux-Labonte, V. A. Simard, C. Willis, F. Lapointe. 2017. Enrichment of beneficial bacteria in the skin microbiota of bats persisting with white-nose syndrome. Microbiome. 5:1-14.

Liaud, N., C. Ginies, D. Navarro, N. Fabre, S. Crapart, I. Herpoel-Gimbert, A. Levasseur, S. Raouche, and J. Sigoillot. 2014. Exploring fungal biodiversity: organic acid production by 66 strains of filamentous fungi. Fungal Biology and Biotechnology. 1:1-10.

Lucan, R., H. bandouchova, T. Bartonicka, J. Pikula, A. Zahradnikova, J. Zukal, and N. Martinkova. 2016. Ectoparasites may serve as vectors for the white-nose syndrome fungus. Parasites & Vectors. 9:1-5.

Matysik, S., O. Herbarth, and A. Mueller. 2008. Determination of volatile metabolites originating from mould growth on wall paper and synthetic media. Journal of Microbiological methods. 75:182-187.

McGuire, L., J. Turner , L. Warnecke, G. McGregor, T. Bollinger, V. Misra, J. Foster, W. Frick, A. Kilpatrick, and C. Willis. 2016. White-Nose Syndrome Disease Severity and a Comparison of Diagnostic Methods. EcoHealth. 13:60-71.

Mendes-Giannini, M., M. Taylor, J. Bouchara, E. Burger, V. Calich, E. Escalante, S. Hanna, H. Lenzi, M. Machado, M. Miyaji, J. Monteiro da Silva, E. Mota, A. Restrepo, S. Restrepo, G. Tronchin, L. Vincenzi, C. Xidieh, and E. Zenteno. 2010. Pathogenesis II: fungal responses to host responses: interaction of host cells with fungi. Medial Mycology. 38:113-123.

Micheluz, A., S. Manente, M. Rovea, D. Slanzi, G. Varese, G. Ravagnan, and G. Formenton. 2016. Detection of volatile metabolites of moulds isolated from a contaminated library. Journal

of Microbiological Methods. 128:34-41.

Muller, L., J. Lorch, D. Lindner, M. O'Connor, A. Gargas, D. Blehert. 2013. Bat white-nose syndrome: a real-time TaqMan polymerase chain reaction test targeting the intergenic spacer region of Geomyces destructans. Mycologia. 105:253–259.

Nakajima, D., R. Ishii, S. Kageyama, Y. Onji, S. Mineki, N. Morooka, K. Takatori, S. Goto. 2006. Genotoxicity of Microbial Volatile Organic Compounds. Journal of Health Science. 52:148-153.

Paiva-Cardoso, M., F. Morinha, P. Barros, H. Vale-Goncalves, A. Coelho, L. Fernandes, P. Travassos, A. Faria, E. Bastos, M. Santos, and J. Cabral. 2014. First isolation of *Pseudogymnoascus destructans* in bats from Portugal. European Journal of Wildlife Resaerch. 60:645-649.

Palmer, J. A. Kubatova, A. Novakova, A. Minnis, M. Kolarik, and D. Lindner. 2014. Molecular characterization of a heterothallic mating system in *Pseudogymnoascus destructans*, the fungus causing white-nose syndrome. G3. 4:1755-1763.

Pannkuk, E., L. Mcguire, L. Warnecke, J. Turner, C. Willis, and T. Risch. 2016. Glycerophospholipid profiles of bats with whit nose syndrome. Physiol Biochem Zool. 88:425-432.

Park, M., E. Do, and W. Jung. 2013. Lipolytic enzymes involved in the virulence of human pathogenic fungi. Mycobiology. 41:67-72.

Pavlinic, I., M. Dakovic, and I. Lojikic. 2015. Pseudogymnoascus destructans in Croatia confirmed. European Journal of Wildlife Research. 61:325-328.

Pollock, T., C. Moreno, L. Sanchez, A. Ceballos-Vasquez, P. Faure, and E. Mora. 2015. Wound healing in the flight membranes of wild big brown bats. Wildlife Management. 80:19-26.

Puechmaille, S., G. Wibbelt, V. Korn, H. Fuller, F. Forget, K. Muhldorfer, A. Kurth, W. Bogdanowicz, C. Borel, T. Bosch, T. Cherezy, M. Drebet, T. Gorfol, A. Haarsma, F. Herhaus, G. Hallart, M. Hammer, C. Jungmann, Y. Le Bris, L. Lutsar, M. <assing, B. Mulkens, K. Passior, M. Starrach, A. Wojtaszewski, U. Zophel, and E. Teeling. 2011. Pan-European Distribution of White-Nose Syndrome Fungus (Geomyces destructans) Not Associated with Mass Mortality. PLOSone.

Rajkumar, S., X. Li, R. Rudd, J. Okoniewski, J. Xu, S. Chaturvedi, and V. Chaturvedi. 2011. Clonal genotype of Geomyces destructans among bats with white nose syndrome, New York, USA. Emerging Infectious Diseases. 17:1273-1276.

Raudabaugh, D., and A. Miller. 2013. Nutritional Capability of and Substrate Suitability for Pseudogymnoascus destructans, the Causal Agent of Bat White-Nose Syndrome. PLOS ONE. 8:1-9.

Reynolds, H., and H. Barton. 2014. Comparison of the white-nose syndrome agent Pseudogymnoascus destructans to cave-dwelling relatives suggests reduced saprotrophic enzyme activity. Plos One. 9:1-11.

Rollins-smith, L., L. Reinert, C. O'Leary, L. Houston, and D. Woodhams. 2005. Antimicrobial peptide defenses in amphibian skin. Integr Comp Biol. 45:137-142.

Santiago, I., M. Soares, C. Rosa, and L. Rosa. 2015. Lichensphere: a protected natural microhabitat of the non-lichenised fungal communities living in extreme environments of Antarctica. Extremophiles. 19:1087-1097.

Scheleibinger, H., D. Laubmann, C. Brattig, M. Mangler, D. Eis, nad H. Ruden. 2005. Emission patterns and emission rates of MVOC and the possibility for predicting hidden mold damage? Indoor Air. 15:98-104.

ThermoFisher. 2004. LIVE/DEAD Baclight bacterial viability kits. Molecular Probes Inc. 1-8.

ThermoFisher. 2017. https://www.thermofisher.com/us/en/home/life-science/cell-analysis/labeling-chemistry/fluorescence spectraviewer.html?gclid=EAIaIQobChMIvdXh_5qg1wIVRIF-Ch3chQDcEAAYASAAEgL32PD_BwE&s_kwcid=AL!3652!3!211105705082!p!!g!!spectraviewer&ef_id=WPTHMQAAAdSwUrCU:20171102153155:s

ThermoFisher. 2017. The molecular probes handbook.

Turner, G., C. Meteyer, H. Barton, J. Gumbs, D. Reeder, B. Overton, H. Bandouchova, T. Bartonicka, N. Martinkova, J. Pikula, J. Zukal, and D. Blehert. 2014. Nonlethal screening of bat-wing skin with the use of ultraviolet fluorescence to detect lesions indicative of white-nose syndrome. Journal of Wildlife Diseases. 50:566-573.

U.S. Fish and Wildlife Service. 2016. https://www.whitenosesyndrome.org/national-plan/elements-national-plan.

Verant, M., J. Boyles, W. Waldrep, G. Wibbelt, and D. Blehert. 2012. Temperature-Dependent Growth of Geomyces destructans, the Fungus That Causes Bat White-Nose Syndrome. PLOS ONE. 7:1-7.

Voigt, C. 2103. Bat flight with bad wings: is flight metabolism affected by damaged wings. Journal of Experimental Biology. 216:1516-1521.

Wang. S., X. Zuo, X. Zhao, Y. Li, X. Zhou, P. Lv, Y. Luo, and J. Yun. 2015. Responses of soil fungal community to the sandy grassland restoration in Horqin Sandy Land, northern China. Environmental Monitoring and Assessment. 188:1-13.

Zukal, J., H. Bandouchova, J. Brichta, A. Cmokova, K. Jaron, M. Kolarik, V. Kovacova, A. Kubatova, A. Novakova, O. Orlov, J. Pikula, P. Presetnik, J. Suba, A. Zahradnikova, and N.

Martinkova. 2016. White-nose syndrome without borders: Pseudogymnoascus destructansinfection tolerated in Europe and Palearctic Asia but not in North America. Nature/Scientific Reports. 6:1-18.

APPENDICES

Appendix A

Compounds that are not identified in table are either a siloxane based compound that originated from the column or are of an extremely low percentage identity score and cannot be listed with any margin of confidence.

Direct Injection of exudate full compound lists.

Exudate A deconvolution	NIST Score	Score	RT
Cpd 1: 1.32			1.32
Cpd 2: 1.37			1.37
Cpd 3: Carbon dioxide		87.31	1.42
Cpd 4: Methylamine, N,N-dimethyl-		87.65	1.63
Cpd 5: Nitrosyl chloride	0.686	100	2.45
Cpd 6: Benzenemethanol, a-(1-aminoethyl)- , (R*,S*)-(+)-	0.211	100	2.83
Cpd 7: Acetic acid		95.57	3.33
Cpd 8: 3.78/ 61.8		81.38	3.86
Cpd 9: Silanediol, dimethyl-		91.01	4.11
Cpd 10: Oxime, methoxy-phenyl-_	0.843	100	9.26
Cpd 11: 13.08			13.08
Cpd 12: Butane, 2,2-dimethyl-		86.84	14.5
Cpd 13: Cyclohexanone, 3-methyl-	0.253	100	18.03
Cpd 14: Dehydromevalonic lactone		91.14	20.2
Cpd 15: 46.31			46.31
Cpd 16: n-Hexadecanoic acid		83.23	51.51
Cpd 17: Hexanedioic acid, bis(2-ethylhexyl) ester	0.662	100	55.33
Cpd 18: a-methylfentanyl	0.688	100	55.35
Cpd 19: Octadecanoic acid	0.639	100	57.6
Cpd 20: Pyrrolo[1,2-a]pyrazine-1,4-dione, heahydro-3-(phenylmethyl)-	0.974	100	63.27
Cpd 21: cyclononasiloxane	0.842	100	70.38
Cpd 22: 1,3-Benzenedicarboxylic acid, bis(2-ethylhexyl) ester		81.24	70.76
Cpd 23: Supraene	0.353	100	73.19
Cpd 24: 2-methyl-2-butyl-1,3-benzodioxole	0.882	100	73.22

Exudate A integration	NIST Score	Score	RT
Cpd 1: Carbon dioxide		87.94	1.32
Cpd 2: Carbon dioxide		87.36	1.37
Cpd 3: Carbon dioxide		92.05	1.42
Cpd 4: Benzenemethanol, 2-(2-aminopropoxy)-3-methyl-	0.299	100	1.63
Cpd 5: 2.82			2.82
Cpd 6: 3.33			3.33
Cpd 7: 2-Propanone, 1-hydroxy-	0.531	100	3.86
Cpd 8: Silanediol, dimethyl	0.963	100	4.11
Cpd 9: 1,2,4-Benzenetricarboxylic acid, 1,2-dimethyl ester	0.498	100	6.53
Cpd 10: Oxime-, methoxy-phenyl-_	0.689	100	9.26
Cpd 11: Pantolactone		83.54	14.5
Cpd 12: Butane, 2,3-dimethyl-2nitro-	0.203	100	18.03
Cpd 13: Dehydromevalonic lactone		95.06	20.2
Cpd 14: 42.69			42.69
Cpd 15: Pyrrolo[1,2-a]pyrazine-1,4-dione, hexahydro-	0.349	100	44.23
Cpd 16: Pyrrolo[1,2-a]pyrazine-1,4-dione, hexahydro-3-(2-methylpropyl)-	0.406	100	46.31
Cpd 17: Pyrrolo[1,2-a]pyrazine-1,4-dione, hexahydro-3-(2-methylpropyl)-	0.523	100	50.13
Cpd 18: 50.33			50.33
Cpd 19: n-Hexadecanoic acid		84.82	51.52
Cpd 20: Hexanedioic acid, bis(2-ethylhexyl) ester		96	55.33
Cpd 21: Octadecanoic acid	0.724	100	57.6
Cpd 22: 60.18			60.18
Cpd 23: 62.86			62.86
Cpd 24: 63.28			63.28
Cpd 25: heptasiloxane	0.406	100	64.75
Cpd 26: 65.71			65.71
Cpd 27: heptasiloxane	0.451	100	69.69
Cpd 28: octasiloxane	0.432	100	70.39
Cpd 29: octasiloxane	0.332	100	70.76
Cpd 30: heptasiloxane	0.454	100	70.9
Cpd 31: heptasiloxane	0.442	100	71.59
Cpd 32: heptasiloxane	0.451	100	72.4
Cpd 33: 73.19			73.19
Cpd 34: octasiloxane	0.436	100	74.6
Cpd 35: heptasiloxane	0.433	100	75.54

Exudate B deconvolution	NIST Score	Score	RT
Cpd 1: 1.32			1.32
Cpd 2: Carbon dioxide		87.31	1.39
Cpd 3: Methylamine, N,N-dimethyl-		86.64	1.57
Cpd 4: cyanopyrazine	0.5	100	2.37
Cpd 5: Methylamine, N,N-dimethyl-		82.37	2.62
Cpd 6: 3.25/ 84.6		93.66	3.12
Cpd 7: Acetic acid, methyl ester		86.41	3.66
Cpd 8: 2,3-Hexanedione		86.21	3.82
Cpd 9: Silanediol, dimethyl-		90.85	3.95
Cpd 10: Acetic acid	0.579	100	4.22
Cpd 11: Cyclobutanol	0.215	100	5.28
Cpd 12: Propanoic acid, 2-hydroxy-2-methyl-, ethyl ester	0.382	100	6.33
Cpd 13: 1,2,4,5-Tetrazine	0.356	100	6.47
Cpd 14: Acetamide, oxime	0.951	100	9.91
Cpd 15: 12.39			12.39
Cpd 16: 2-Hydroxy-gamma-butyrolactone	0.376	100	12.62
Cpd 17: Thiophene, 3,4-dimethyl	0.541	100	13.87
Cpd 18: 2(3H)-Furanone, dihydro-3-hydroxy-4,4-dimethyl-, (.+/-.)-		86.67	14.45
Cpd 19: 17.99			17.99
Cpd 20: Dehydromevalonic lactone		90.2	20.19
Cpd 21: 2,3-Furandione, dihydro-4,4-dimethyl	0.841	100	43.59
Cpd 22: 6,6-Dimethyl-1,5-diazabicyclo[3.1.0]hexane	0.278	100	44.2
Cpd 23: 46.30			46.3
Cpd 24: n-Hexadecanoic acid	0.581	100	51.5
Cpd 25: Octadecanoic acid	0.693	100	57.61
Cpd 26: 70.33			70.33
Cpd 27: 1,3-Dioxolane-4-methanol, 2-pentadecyl-, acetate, trans-	0.984	100	71.99
Cpd 28: 1-Triethylsilyloxyheptadecane	0.595	100	75.24

Exudate B integration	NIST Score	Score	RT
Cpd 1: Carbon dioxide		87.93	1.32
Cpd 2: Carbon dioxide		92.1	1.39
Cpd 3: 2-Propanamine		82.47	1.58
Cpd 4: Benzenemethanol, 2-(2-aminopropoxy)-3-methyl-	0.323	100	2.06
Cpd 5: Ethanamine, 2-(2,6-dimethylphenoxy)-N-methyl-	0.312	100	2.62
Cpd 6: Acetic acid, anhydride with formic acid		81.29	3.12
Cpd 7: 2-Propanone, 1-hydroxy-		84.77	3.66
Cpd 8: silanediol, dimethyl	0.957	100	3.95
Cpd 9: 6.33			6.33
Cpd 10: Pentanal	0.376	100	12.65
Cpd 11: 13.86			13.86
Cpd 12: Pantolactone		89.44	14.45
Cpd 13: 17.98			17.98
Cpd 14: Dehydromevalonic lactone		95.53	20.19
Cpd 15: Octadrine	0.275	100	40.1
Cpd 16: 3-Methyl-1,4-diazabicyclo[4.3.0]nonan-2,5-dione, N-acetyl-	0.272	100	42.68
Cpd 17: dl-alanyl-dl-norleucine	0.35	100	43.62
Cpd 18: Pyrrolo[1,2-a]pyrazine-1,4-dione, hexahydro-	0.611	100	44.2
Cpd 19: Pyrrolo[1,2-a]pyrazine-1,4-dione, hexahydro-3-(2-methylpropyl)-	0.37	100	46.31
Cpd 20: Pyrrolo[1,2-a]pyrazine-1,4-dione, hexahydro-3-(2-methylpropyl)-	0.388	100	50.12
Cpd 21: Pyrrolo[1,2-a]pyrazine-1,4-dione, hexahydro-3-(2-methylpropyl)-	0.439	100	50.3
Cpd 22: n-Hexadecanoic acid		82.94	51.52
Cpd 23: Octadecanoic acid	0.692	100	57.61
Cpd 24: 63.24			63.24
Cpd 25: Heptasiloxane	0.535	100	72.07

Exudate C deconvolution	NIST Score	Score	RT
Cpd 1: hydrogen azide	0.182	100	1.34
Cpd 2: hydrogen azide	0.182	100	1.45
Cpd 3: Acetone		89.02	1.71
Cpd 4: trans-1-chloropropene	0.0637	100	1.89
Cpd 5: 2-propanamine	0.895	100	2.72
Cpd 6: Acetic acid		84.6	3.25
Cpd 7: acitic acid, methyl ester	0.618	100	3.78
Cpd 8: acetimide, 2-fluoro-	0.811	100	4.05
Cpd 9: 2-Pentanone, 4-hydroxy-4-methyl-		80.28	7.1
Cpd 10: Dehydromevalonic lactone		92.6	20.18
Cpd 11: 2,3-Dimethyloxirane-2-carboxylic acid, methyl ester	0.8	100	21.66
Cpd 12: 5-Isopropylidene-3,3-dimethyl-dihydrofuran-2-one	0.328	100	46.27

Exudate C integration	NIST Score	Score	RT
Cpd 1: Carbon dioxide		87.82	1.34
Cpd 2: Carbon dioxide		94.8	1.45
Cpd 3: 2-Propanamine		83.14	1.6
Cpd 4: 2-Propanamine		83.31	1.71
Cpd 5: 1-(5-Bicyclo[2.2.1]heptyl)ethylamine	0.356	100	2.13
Cpd 6: 1-(5-Bicyclo[2.2.1]heptyl)ethylamine	0.272	100	2.72
Cpd 7: Dimethylamine		80.7	3.25
Cpd 8: Acetaldehyde		81.39	3.78
Cpd 9: Acetamide, 2-fluoro-		81.8	4.06
Cpd 10: 2-Pentanone, 4-hydroxy-4-methyl-		80.48	7.1
Cpd 11: Propane		89.02	18.02
Cpd 12: Imidazole-5-carboxylic acid, 2-amino-	0.309	100	19.56
Cpd 13: Dehydromevalonic lactone		95.15	20.18
Cpd 14: Acetamide	0.325	100	21.65
Cpd 15: Tuaminoheptane	0.235	100	42.66
Cpd 16: octodrine	0.17	100	43.6
Cpd 17: Pyrrolo[1,2-a]pyrazine-1,4-dione, hexahydro-	0.517	100	44.2
Cpd 18: Pyrrolo[1,2-a]pyrazine-1,4-dione, hexahydro-3-(2-methylpropyl)-	0.474	100	46.3
Cpd 19: 1-methyldecylamine	0.116	100	47.17
Cpd 20: Pyrrolo[1,2-a]pyrazine-1,4-dione, hexahydro-3-(2-methylpropyl)-	0.546	100	50.11

Exudate D deconvolution		
Label	Score	RT
Cpd 1: Hydrogen azide	100	1.4
Cpd 2: Hydrogen azide	100	1.49
Cpd 3: Methylamine, N,N-dimethyl-	92.39	1.7
Cpd 4: Acetic acid	100	2.72
Cpd 5: Methylamine, N,N-dimethyl-	92.32	3.3
Cpd 6: Acetic acid	96.72	3.99
Cpd 7: Acetic acid, methyl ester	86.44	4.47
Cpd 8: Ethanone, 1-(2-methylcyclopropyl)	100	6.53
Cpd 9: 6.85		6.85
Cpd 10: Succindialdehyde	100	16.01
Cpd 11: Pantolactone	90.69	18.14
Cpd 12: Cyclohexanone, 2-methyl	100	22.03
Cpd 13: Dehydromevalonic lactone	92.26	24.5
Cpd 14: dl-mevalonic acid lactone	100	29.31
Cpd 15: Pyrrolo[1,2-a]pyrazine-1,4-dione, hexahydro-	81.75	48.86
Cpd 16: Pyrrolo[1,2-a]pyrazine-1,4-dione, hexahydro-3-(2-methylpropyl)-	100	50.96

Exudate D intergaration		
Label	Score	RT
Cpd 1: Carbon dioxide	87.94	1.32
Cpd 2: Carbon dioxide	87.36	1.37
Cpd 3: Carbon dioxide	92.05	1.42
Cpd 4: Benzenemethanol, 2-(2-aminopropoxy)-3-methyl-	100	1.63
Cpd 5: 2.82		2.82
Cpd 6: 3.33		3.33
Cpd 7: 2-Propanone, 1-hydroxy-	100	3.86
Cpd 8: Silanediol, dimethyl	100	4.11
Cpd 9: 1,2,4-Benzenetricarboxylic acid, 1,2-dimethyl ester	100	6.53
Cpd 10: Oxime-, methoxy-phenyl-_	100	9.26
Cpd 11: Pantolactone	83.54	14.5
Cpd 12: Butane, 2,3-dimethyl-2nitro-	100	18.03
Cpd 13: Dehydromevalonic lactone	95.06	20.2
Cpd 14: 42.69		42.69
Cpd 15: Pyrrolo[1,2-a]pyrazine-1,4-dione, hexahydro-	100	44.23
Cpd 16: Pyrrolo[1,2-a]pyrazine-1,4-dione, hexahydro-3-(2-methylpropyl)-	100	46.31
Cpd 17: Pyrrolo[1,2-a]pyrazine-1,4-dione, hexahydro-3-(2-methylpropyl)-	100	50.13
Cpd 18: 50.33		50.33
Cpd 19: n-Hexadecanoic acid	84.82	51.52
Cpd 20: Hexanedioic acid, bis(2-ethylhexyl) ester	96	55.33
Cpd 21: Octadecanoic acid	100	57.6
Cpd 22: 60.18		60.18
Cpd 23: 62.86		62.86
Cpd 24: 63.28		63.28
Cpd 25: heptasiloxane	100	64.75
Cpd 26: 65.71		65.71
Cpd 27: heptasiloxane	100	69.69
Cpd 28: octasiloxane	100	70.39
Cpd 29: octasiloxane	100	70.76
Cpd 30: heptasiloxane	100	70.9
Cpd 31: heptasiloxane	100	71.59
Cpd 32: heptasiloxane	100	72.4
Cpd 33: 73.19		73.19
Cpd 34: octasiloxane	100	74.6
Cpd 35: heptasiloxane	100	75.54

Appendix A.1 SPME full compound lists.

Vial control deconvolution

Label	NIST Score	Score	RT
Cpd 1: 1.29			1.29
Cpd 2: 1.32			1.32
Cpd 3: Silanol, trimethyl-		93.21	1.86
Cpd 4: Acetic acid		85.02	2
Cpd 5: Acetaldehyde		86.98	2.28
Cpd 6: Oxetane, 2,3,4-trimethyl-, (2.alpha.,3.alpha.,4.beta.)-		88.92	2.66
Cpd 7: Silanediol, dimethyl-		91	3.02
Cpd 8: Butanoic acid		82.08	5.3
Cpd 9: Cyclotrisiloxane, hexamethyl-		89	6.32
Cpd 10: Oxime, methoxy-phenyl	0.652	100	10.23
Cpd 11: Phenyl-pentamethyl-disiloxane	0.267	100	13.23
Cpd 12: Cyclotetrasiloxane, octamethyl-		84.83	15.61
Cpd 13: 1-Hexanol, 2-ethyl-		87.95	16.92
Cpd 14: Cyclotrisiloxane, hexamethyl-		82.21	20.28
Cpd 15: Benzaldehyde, 2,5-bis(trimethylsily)oxy)	0.457	100	22.13
Cpd 16: Cyclopentasiloxane, decamethyl	0.924	100	24.04
Cpd 17: 5H,13H-Dibenzo[c,h]dipyrrolo[3,2-e:3',2'-j][2,6]naphthyridine, 6,7,7a,8,14	0.82	100	32.3
Cpd 18: Cyclohexasiloxane, dodecamethyl-		91.3	32.31
Cpd 19: Cycloheptasiloxane, tetradecamethyl	0.389	100	40.84
Cpd 20: Cyclooctasiloxane, hexadecamethyl-		81.9	47.95

Vial Control Integration			
Label	NIST Score	Score	RT
Cpd 1: (2-aziridinylethyl)amine	0.768	100	1.29
Cpd 2: Silanol, trimethyl	0.7	100	1.86
Cpd 3: 2,3-Epoxybutane	0.152	100	2
Cpd 4: Butane, 1-chloro-		81.95	2.65
Cpd 5: Silanediol, dimethyl-	0.941	100	3.02
Cpd 6: Butanoic acid		80.8	5.3
Cpd 7: Cyclotrisiloxane, hexamethyl-		96.86	6.32
Cpd 8: Oxime-, methoxy-phenyl-_		82.1	10.23
Cpd 9: Phenyl-pentamethyl-disiloxane	0.462	100	13.23
Cpd 10: Cyclotetrasiloxane, octamethyl-		97.78	15.61
Cpd 11: 1-Hexanol, 2-ethyl-		84.31	16.92
Cpd 12: 2-Octanol, 2-methyl-6-methylene	0.625	100	19.26
Cpd 13: Cyclotrisiloxane, hexamethyl-		85.19	20.29
Cpd 14: Nonanal		89.42	20.96
Cpd 15: Benzaldehyde, 2,5-bis[(trimethylsily)oxy]	0.556	100	22.13
Cpd 16: Cyclopentasiloxane, decamethyl-		94.68	24.04
Cpd 17: Cyclohexasiloxane, dodecamethyl-		93.85	32.31
Cpd 18: Cycloheptasiloxane, tetradecamethyl-	0.752	100	40.84
Cpd 19: Cyclooctasiloxane, hexadecamethyl-		88.53	47.95

Wing control deconvolution			
Label	NIST Score	Score	RT
Cpd 1: Argon	0.649	100	1.14
Cpd 2: (2-aziridinylethyl)amine	0.877	100	1.24
Cpd 3: (2-aziridinylethyl)amine	0.877	100	1.31
Cpd 4: (2-aziridinylethyl)amine	0.877	100	1.36
Cpd 5: Ethanol	0.654	100	1.42
Cpd 6: Isopropyl Alcohol		81.07	1.51
Cpd 7: tert-butyldimethylsilanol	0.404	100	1.78
Cpd 8: methane, trimethoxy-	0.329	100	1.85
Cpd 9: argon	0.412	100	1.94
Cpd 10: 1-butanol	0.548	100	2.66
Cpd 11: disiloxane, hexamethyl-	0.636	100	2.88
Cpd 12: Cyclopropane, butyl-	0.231	100	5.17
Cpd 13: Hexanal		85.71	5.45
Cpd 14: Hexane, 2,3,4-trimethyl-		91.53	6.17
Cpd 15: Cyclotrisiloxane, hexamethyl-		80.5	6.32
Cpd 16: Styrene		93.18	8.99
Cpd 17: oxime, -methyl-phenyl-_	0.902	100	10.19
Cpd 18: Ethanone, 2-(formyloxy)-1-phenyl-		87.4	12.69
Cpd 19: Trisiloxane, 1,1,3,3,5,5-hexamethyl-	0.161	100	13.23
Cpd 20: 3,4-Dihydroisoquinolin-7-ol, 1-[4-hydroxybenzyl]-6-methoxy-	0.394	100	15.6
Cpd 21: Cycloteterasiloxane, octamethyl-	0.843	100	15.61
Cpd 22: 1-Hexanol, 2-ethyl-		90.4	16.91
Cpd 23: 1,2-Ethanediol, 1,2-diphenyl-, (R*,R*)-(.+/-.)-		84.73	17.09
Cpd 24: Cyclotrisiloxane, hexamethyl-		82.75	20.27
Cpd 25: Nonanal		92.59	20.96
Cpd 26: Benzaldehyde, 2,5-bis[(trimethylsilyl)oxy]-	0.478	100	22.13
Cpd 27: Cyclopentasiloxane, decamethyl-		88.07	24.04
Cpd 28: Decanal	0.12	100	30.93
Cpd 29: Cyclohexasiloxane, dodecamethyl-		92.98	32.31
Cpd 30: 3-Isopropoxy-1,1,1,7,7,7-hexamethyl-3,5,5-tris(trimethylsiloxy)tetrasilc	0.483	100	40.84
Cpd 31: Butylated Hydroxytoluene		85.73	41
Cpd 32: Butane, 2,2-dimethyl-		84.84	44.88
Cpd 33: Benzoic acid, 2,4-bis[(trimethylsilyl)oxy]-, trimethylsilyl ester	0.257	100	47.94

Wing control integration			
Label	Notes	Score	RT
Cpd 1: (2-aziridinylethyl)amine	0.864	100	1.15
Cpd 2: (2-aziridinylethyl)amine	0.688	100	1.24
Cpd 3: (2-aziridinylethyl)amine	0.86	100	1.31
Cpd 4: Topotecan	0.904	100	1.43
Cpd 5: Topotecan	0.723	100	1.51
Cpd 6: Dimethylamine		81.41	1.58
Cpd 7: Propanoic acid, 2,3-dihydroxy-	0.293	100	1.78
Cpd 8: Glycine	0.261	100	1.85
Cpd 9: O-Methylisourea	0.144	100	1.98
Cpd 10: 1-Butanol	0.262	100	2.65
Cpd 11: Silanediol, dimethyl	0.81	100	3.05
Cpd 12: Hexanal		80.62	5.45
Cpd 13: Heptane, 2,4-dimethyl-		82.45	6.17
Cpd 14: Cyclotrisiloxane, hexamethyl-		93.93	6.31
Cpd 15: Styrene		89.01	8.99
Cpd 16: Oxime-, methoxy-phenyl-_	0.85	100	10.22
Cpd 17: Benzaldehyde		84.83	12.69
Cpd 18: Phenyl-pentamethyl-disiloxane	0.554	100	13.23
Cpd 19: Cyclotetrasiloxane, octamethyl-		95.81	15.61
Cpd 20: 1-Hexanol, 2-ethyl-		90.56	16.91
Cpd 21: L-Arginine, N2-[(phenylmethoxy)carbonyl]-		83.59	17.09
Cpd 22: 2-octanol, 2-methyl-6-methylene	0.323	100	19.26
Cpd 23: Cyclotrisiloxane, hexamethyl-		81.15	20.27
Cpd 24: Nonanal		94.33	20.96
Cpd 25: Benzaldehyde, 2,5-bis(trimethylsilyl)oxy)-	0.498	100	22.12
Cpd 26: Cyclopentasiloxane, decamethyl-		95.5	24.04
Cpd 27: Decanal		83.27	26.12
Cpd 28: 1-[2,4-Bis(trimethylsiloxy)phenyl]-2-[(4-trime	0.386	100	27.85
Cpd 29: Decanal		80.75	30.93
Cpd 30: Cyclohexasiloxane, dodecamethyl-		93.27	32.31
Cpd 31: Cyclopentasiloxane	0.43	100	35.11
Cpd 32: 35.55			35.55
Cpd 33: 1s,4R,7R,11R-1,3,4,7-Tetramethyltricyclo[5.3.	0.366	100	39.36
Cpd 34: Oxalic acid, allyl nonyl ester		80.04	40.48
Cpd 35: Cycloheptasiloxane	0.697	100	40.84
Cpd 36: Butylated Hydroxytoluene		95.72	40.99
Cpd 37: Cycloheptasiloxane	0.749	100	43.23
Cpd 38: Dodecane, 2,7,10-trimethyl-	0.0369	100	44.85
Cpd 39: Cyclooctasiloxane, hexadecamethyl-		82.58	47.94
Cpd 40: Benzoic acid, 3-methyl-2-trimethylsilyloxy-, tr	0.246	100	50.2
Cpd 41: Hexanedoic acid, bis(2-ethylhexyl) ester	0.219	100	61.52
Cpd 42: Cyclononasiloxane	0.502	100	75.39

P destructans on wing deconvolution			
Label	Score	NoIST Score	RT
Cpd 1: (2-Aziridinylethyl)amine	100	0.877	1.26
Cpd 2: N-methyltaurine	100	0.544	1.32
Cpd 3: Methylamine, N,N-dimethyl-	100	0.928	1.38
Cpd 4: Methylamine, N,N-dimethyl-	80.24		1.41
Cpd 5: Isopropyl Alcohol	92.74		1.5
Cpd 6: Isopropyl Alcohol	84.75		1.53
Cpd 7: Silanol, trimethyl-	100	0.465	1.78
Cpd 8: Silanol, trimethyl-	82		1.8
Cpd 9: Acetic acid	93.46		1.94
Cpd 10: 1-Butanol	100	0.104	2.61
Cpd 11: Silanediol, dimethyl-	88.63		2.97
Cpd 12: Toluene	91.92		4.45
Cpd 13: Hexanal	92.03		5.41
Cpd 14: Cyclotrisiloxane, hexamethyl-	87.94		6.28
Cpd 15: 2-Pentanone, 4-hydroxy-4-methyl-	92.91		6.94
Cpd 16: Styrene	95.25		8.96
Cpd 17: Oxime-, methoxy-phenyl-_	100	0.935	10.21
Cpd 18: Benzaldehyde	94.64		12.67
Cpd 19: Benzoic acid, 2-formyl-4,6-dimethoxy-, 8,8-dimethoxyoct-2-yl ester	100	0.542	13.22
Cpd 20: Cyclotetrasiloxane, octamethyl-	100	0.173	15.6
Cpd 21: 1-Hexanol, 2-ethyl-	91.77		16.9
Cpd 22: Benzyl alcohol	90.13		17.05
Cpd 23: Cyclotrisiloxane, hexamethyl-	85.55		20.29
Cpd 24: Nonanal	83.05		20.96
Cpd 25: Benzaldehyde, 2,5-bis[(trimethylsily)oxy]	100	0.406	22.13
Cpd 26: Cyclopentasiloxane, decamethyl-	87.9		24.03
Cpd 27: Undecanal	93.61		30.93
Cpd 28: Cyclohexasiloxane, dodecamethyl-	93.08		32.31
Cpd 29: 1s,4R,7R,11R-1,3,4,7-Tetramethyltricyclo[5.3.1.0(4,11)]undec-2-en-8-one	100	0.558	39.37
Cpd 30: Hexane, 3,3-dimethyl-	88.94		40.49
Cpd 31: 3-Isopropoxy-1,1,1,7,7,7-hexamethyl-3,5,5-tris(trimethylsiloxy)tetrasiloxane	100	0.499	40.84
Cpd 32: Butylated Hydroxytoluene	86.63		41.01
Cpd 33: Benzoic acid, 4-ethoxy-, ethyl ester	93.09		41.55
Cpd 34: cyclohexasiloxane, dodecamethyl-	100	0.912	43.23
Cpd 35: Hexane, 3,3-dimethyl-	87.78		44.84
Cpd 36: Cyclooctasiloxane, hexadecamethyl-	88.57		47.95

P destructans on wing integration			
Label	Score	NIST Score	RT
Cpd 1: (Aziridinylethyl)amine	0	0.747	1.23
Cpd 2: (Aziridinylethyl)amine	0	0.732	1.26
Cpd 3: Methylamine, N,N-dimethyl-	80.9		1.39
Cpd 4: Topotecan	0	0.426	1.41
Cpd 5: Isopropyl Alcohol	91.54		1.5
Cpd 6: Isopropyl Alcohol	89.53		1.53
Cpd 7: Glycine	0	0.446	1.78
Cpd 8: Silanol, trimethyl	0	0.446	1.8
Cpd 9: Ethanamine, 2-propoxy-	0	0.183	1.94
Cpd 10: Silanediol, dimethyl	0	0.956	2.96
Cpd 11: Toluene	92.41		4.45
Cpd 12: Hexanal	88.09		5.41
Cpd 13: Cyclotrisiloxane, hexamethyl-	95.62		6.28
Cpd 14: Cyclotrisiloxane, hexamethyl-	0	0.452	6.93
Cpd 15: Styrene	97.51		8.96
Cpd 16: Oxime-, methoxy-phenyl-_	82.82		10.21
Cpd 17: Benzaldehyde	90.75		12.67
Cpd 18: vanillin, tert-butyldimethylsily ether	0	0.237	13.22
Cpd 19: Cyclotetrasiloxane, octamethyl-	97.01		15.59
Cpd 20: 1-Hexanol, 2-ethyl-	94.18		16.9
Cpd 21: Benzyl alcohol	91.79		17.05
Cpd 22: Cyclotrisiloxane, hexamethyl-	81.32		20.29
Cpd 23: Nonanal	96.56		20.96
Cpd 24: Benzaldehyde, 2,5-bis[(trimethylsily)oxy]-	0	0.297	22.13
Cpd 25: Cyclopentasiloxane, decamethyl-	95.85		24.03
Cpd 26: Undecanal	94.58		30.93
Cpd 27: Cyclohexasiloxane, dodecamethyl-	94.26		32.31
Cpd 28: cyclopentasiloxane, decamethyl-	0	0.385	35.11
Cpd 29: 1s,4R,7R,11R-1,3,4,7-Tetramethyltricyclo[5.3.1.0(4,11)]undec-2-en-8-one	0	0.156	39.37
Cpd 30: Dodecane, 2,6,11-trimethyl-	88.1		40.49
Cpd 31: cycloheptasiloxane, tetradecamethyl	0	0.763	40.84
Cpd 32: Butylated Hydroxytoluene	96.51		41.01
Cpd 33: Benzoic acid, 4-ethoxy-, ethyl ester	90.64		41.56
Cpd 34: cyclohexasiloxane,dodecamethyl	0	0.369	43.23
Cpd 35: Tridecane, 6-methyl-	87		44.85
Cpd 36: Cyclooctasiloxane, hexadecamethyl-	82.05		47.95
Cpd 37: tetracosamethyl-cyclododecasiloxane	0	0.279	75.4

P destructans producing exudate on SDA SPME, deconvolution		
Label	Score	RT
Cpd 1: 0.87		0.87
Cpd 2: 1.05		1.05
Cpd 3: Acetone	96	1.16
Cpd 4: 2-Butanone, 3-methyl-	91.84	2.22
Cpd 5: 2,3-Butanedione	88.63	2.38
Cpd 6: 2-Butanone, 3-methyl-	83.52	2.46
Cpd 7: 2-Butanol, 3-methyl-	82.17	2.49
Cpd 8: 2-Methylenebornane	80.71	14.16
Cpd 9: p-Menth-8-ene, 3-methylene-	82.75	14.67
Cpd 10: 2-Methylenebornane	84.83	15.59
Cpd 11: 15.90		15.9
Cpd 12: p-Menth-8-ene, 3-methylene-	88.56	16.12
Cpd 13: 16.71		16.71
Cpd 14: 26.67		26.67
Cpd 15: Benzene, 1,3-dimethoxy-	89.46	26.7
Cpd 16: 28.12		28.12
Cpd 17: Cyclohexasiloxane, dodecamethyl-	86.74	38.01
Cpd 18: 48.60		48.6
Cpd 19: 48.61		48.61
Cpd 20: Phenol, 2,6-bis(1,1-dimethylethyl)-4-methyl-, methylcarbamate	83.31	48.62

P destructans producing exudate on SDA SPME, integration		
Label	Score	RT
Cpd 1: Carbon dioxide	81.56	0.87
Cpd 2: 1.05		1.05
Cpd 3: Acetone	88.31	1.16
Cpd 4: 2-Butanone, 3-methyl-	93.93	2.22
Cpd 5: 2-Butanone, 3-methyl-	94.22	2.37
Cpd 6: 2-Pentanol	83.83	2.5
Cpd 7: Cyclotrisiloxane, hexamethyl-	93.86	6.35
Cpd 8: 1,3-Cyclopentadiene, 1,3-bis(1-methylethyl)-	88.49	13.84
Cpd 9: 2,4-Cycloheptadien-1-one, 2,6,6-trimethyl-	89.16	14.07
Cpd 10: 2,4-Cycloheptadien-1-one, 2,6,6-trimethyl-	89.6	14.16
Cpd 11: p-Menth-8-ene, 3-methylene-	91.38	14.57
Cpd 12: p-Menth-8-ene, 3-methylene-	91.56	14.67
Cpd 13: p-Menth-8-ene, 3-methylene-	89.71	15.59
Cpd 14: p-Menth-8-ene, 3-methylene-	93.58	16.12
Cpd 15: 5-Undecen-3-yne, (Z)-	86.26	16.71
Cpd 16: Benzene, 1,3-dimethoxy-	98.04	26.69
Cpd 17: Bicyclo[2.2.1]heptan-2-one, 1,4,7,7-tetramethyl-	97.58	28.12
Cpd 18: Cyclohexasiloxane, dodecamethyl-	94.32	38.01
Cpd 19: 48.60		48.6

P destructans heavy conidiation SPME, deconvolution

Label	Score	RT
Cpd 1: 1.24		1.24
Cpd 2: Methylamine, N,N-dimethyl-	86.68	1.4
Cpd 3: Formamide	81.26	1.43
Cpd 4: Methylamine, N,N-dimethyl-	87.18	1.45
Cpd 5: Silanol, trimethyl-	93.41	1.81
Cpd 6: 1.85		1.85
Cpd 7: 2.00		2
Cpd 8: 2-Butanone, 3-methyl-	91.67	2.61
Cpd 9: Disiloxane, hexamethyl-	88.71	2.84
Cpd 10: 2.87 2-propenoic acid, 2-(trimethyylsilyl)oxy)- trimethyl ester	NIST (26.5)	2.87
Cpd 11: Silanediol, dimethyl-	91.01	3.13
Cpd 12: Toluene	87.97	4.51
Cpd 13: Cyclotrisiloxane, hexamethyl-	80.14	6.35
Cpd 14: 6.61		6.61
Cpd 15: Styrene	95.17	9.05
Cpd 16: 2,5-Dimethylpyrimidine	87.7	10.23
Cpd 17: 10.46		10.46
Cpd 18: Cyclohexanol, 2-methyl-, cis-	95.49	11.39
Cpd 19: Cyclohexanol, 2-methyl-, cis-	97.47	11.74
Cpd 20: Cyclohexanone, 2-methyl-	84.32	12.02
Cpd 21: 13.32		13.32
Cpd 22: 15.88		15.88
Cpd 23: 4-Cyanocyclohexene	83.53	16.34
Cpd 24: 1-Hexanol, 2-ethyl-	91.26	17.38
Cpd 25: 19.37		19.37
Cpd 26: 19.54		19.54
Cpd 27: 2-Pentanone, 3-methylene-	80.72	19.97
Cpd 28: Cyclotrisiloxane, hexamethyl-	81.32	21.71
Cpd 29: 23.64		23.64
Cpd 30: 23.99		23.99
Cpd 31: 26.11		26.11
Cpd 32: Benzene, 1,3-dimethoxy-	85.57	26.44
Cpd 33: Cyclopentasiloxane, decamethyl-	85.03	26.51
Cpd 34: 27.12 2-methylisoborneol	NIST (74.1)	27.12
Cpd 35: 27.34		27.34
Cpd 36: Bicyclo[2.2.1]heptan-2-one, 1,4,7,7-tetramethyl-	91.06	28.09
Cpd 37: 29.00		29
Cpd 38: 30.89		30.89
Cpd 39: 31.99		31.99
Cpd 40: 33.25		33.25
Cpd 41: 33.48		33.48
Cpd 42: 33.97		33.97
Cpd 43: 35.63		35.63
Cpd 44: 38.00		38

Cpd 45: Cyclohexasiloxane, dodecamethyl-	86.24	38
Cpd 46: Cyclopentasiloxane, decamethyl-	81.27	41.55
Cpd 47: 41.97		41.97
Cpd 48: 42.41		42.41
Cpd 49: 42.97		42.97
Cpd 50: 43.43		43.43
Cpd 51: 46.27		46.27
Cpd 52: Hexane, 3,3-dimethyl-	84.32	48.05
Cpd 53: 48.56		48.56
Cpd 54: 48.58		48.58
Cpd 55: 49.42		49.42
Cpd 56: 51.73		51.73
Cpd 57: 51.97		51.97
Cpd 58: 52.98		52.98
Cpd 59: Hexane, 3,3-dimethyl-	86.04	53.8
Cpd 60: 58.13		58.13
Cpd 61: 59.26		59.26
Cpd 62: 61.40		61.4
Cpd 63: 66.48		66.48
Cpd 64: 69.88		69.88
Cpd 65: 73.93		73.93
Cpd 66: 80.80		80.8
Cpd 67: 87.09		87.09
Cpd 68: 91.25		91.25
Cpd 69: 92.92		92.92
Cpd 70: 99.24		99.24
Cpd 71: 102.76		102.76